Dissertation ETH Nr. 15906

PGSE Diffusion and Multidimensional NMR studies on Late Transition Metal Complexes. Applications in Homogeneous Catalysis

A Dissertation submitted to the

SWISS FEDERAL INSTITUTE OF TECHNOLOGY ZURICH

For the degree of

Doctor of Natural Sciences

Presented by

Anil Kumar Payyadi Govardhan

M.Sc., Bangalore University, India

Born February 26th 1977

Citizen of India

Accepted on the recommendation of

Prof. Dr. P. S. Pregosin, examiner

Prof. Dr. A. Togni, Co-examiner

Zurich, 2005

In Memory of my beloved Parents

Acknowledgements

First of all to my supervisor, Professor Paul S Pregosin, for guiding me through the past three years, for his critical and prolific discussions on Chemistry and NMR. Further, his willingness and accessibility to discussion not only limited to NMR.

Secondly to Dr. Heinz Rüegger, for his excellent co-operation, thoroughness and expert opinion on some of my research problems. He was always enthusiastic and approachable for discussions ranging from microcosmic atom to the macrocosmic world culture. He also took me for several hiking spots which I would have never dreamed of.

Professor Antonio Togni for having accepted to be my co-examiner.

Professors Mike Whittlesey, Consiglio Giambattista, Ernst P. Kuendig, Antonio Mezzetti and their coworkers for their fruitful collaborations.

A special acknowledgement to Dr. Pascal Dotta, who kept coming up with novel compounds of interesting structures, without which my NMR assignment interest would have faded away.

To all my lab members: Drs. Eloisa, Tilmann, Nacho, Daniele, Eric and soon-to-be-Drs. Rene and Deva, for maintaining a lively working atmosphere.

To all my Indian friends, specifically, Ravi, Shiva, Srinivas, Vishwa, Shailesh, Vikas, the Cricket group and other InSaZ members, who made my stay homely.

To all members of the Inorganic and Technical Chemistry department of ETH who made a comforting and pleasant atmosphere to work with.

To my family members and friends, for their understanding and support throughout these years, without them I would have never accomplished this degree. Lastly to my late beloved parents whose inputs in my childhood has brought me this far.

Parts of this thesis can be found in the following publications:

- A [Pd(η^3-PhCHCHCHPh)(phosphino-oxazoline)]$^+$ complex with almost identical P-and N-trans influences. ^{13}C chemical shifts and allylic alkylation chemistry.
P. Dotta, P. G. A. Kumar and P. S. Pregosin, *Magn. Reson. Chem.* **2002**, *40*, 653-658.

- PGSE Diffusion Studies on Chelating Phosphine Complexes of Ru(II). Solvent Dependence and Ion pairing
P. G. A. Kumar, P. S. Pregosin, J. M. Goicoechea and M. K. Whittlesey, *Organometallics* **2003**, *22*, 2956-2960.

- Diffusion and NOE NMR Spectroscopy. Applications to Problems Related to Coordination Chemistry and Homogeneous Catalysis
P. S. Pregosin, E. Martinez-Viviente and P. G. A. Kumar, *Dalt. Trans.* **2003**, 4007-4014.

- Pd-(MOP) Chemistry: Novel Bonding Modes and Interesting Charge Distribution
P. Dotta, P. G. A. Kumar, P. S. Pregosin, A. Albinati and S. Rizzato, *Organometallics* **2003**, *22*, 5345-5349.

- Palladium-MOP Chemistry: Pseudo-cis allyl MOP Complexes and Flexible Olefin Bonding
P. Dotta, P. G. A. Kumar, P. S. Pregosin and A. Albinati, *Helv.Chim. Acta* **2004**, *87*, 272-278.

- X-Ray diffraction and NMR studies on a series of Binap-based Ruthenium(II) hydroxyphosphine π-arene complexes.
T. J. Geldbach, F. Breher, V. Gramlich, P. G. A. Kumar and P. S. Pregosin, *Inorg. Chem.* **2004**, *43*, 1920-1928.

- The 3,5-dialkyl effect on enantioselectivity in Pd chemistry: Applications involving both bidentate and monodentate auxiliaries
P. Dotta, P. G. A. Kumar, P. S. Pregosin, A. Albinati and S. Rizzato, *Organometallics* **2004**, *23*, 2295-2304.

- PGSE Diffusion, ^{1}H-^{19}F HOESY and NMR studies on several [Rh(1,5-COD)(Biphemp)]X complexes: Detecting positional anion effects.
P. G. A. Kumar, P. S. Pregosin, T. M. Schmid and G. Consiglio, *Magn. Reson. Chem.* **2004**, *42*, 795-800.

- Structural and ^{13}C NMR Studies on Palladium MOP Compounds: A New Weak C-Pd σ-Bond Plus MOP as a Bridging Diene Ligand
P. Dotta, P. G. A. Kumar, P. S. Pregosin, A. Albinati and S. Rizzato, *Organometallics* **2004**, *23*, 4247-4254.

- Towards an Understanding of the Anion Effect in CpRu-Based Diels-Alder Catalysts via PGSE-NMR Measurements.
P. G. A. Kumar, P. S. Pregosin, M. Vallet, G. Bernardinelli, R. F. Jazzar, F. Viton, E. P. Kundig, *Organometallics* **2004**, *23*, 5410-5418.

- ^{195}Pt, ^{1}H and ^{31}P PGSE Diffusion Studies on Platinum Complexes.
D. Nama, P. G. A. Kumar, P. S. Pregosin, *Magn. Reson. Chem.* **2005**, *43*, 246-250.

- Mononuclear and Dinuclear Complexes with a $[Ru(^{t}Bu_2PCH_2CH_2P^{t}Bu_2)(CO)]$ Core
J. M. Goicoechea, M. F. Mahon, M. K. Whittlesey, P. G. A. Kumar, P. S. Pregosin, *Dalton Trans.* **2005**, *3*, 588-597.

- Palladium complexes with *meso*-bis(oxazoline) ligands for alternating styrene/CO copolymerization: Counterion effect
D. Sirbu, G. Consiglio, B. Milani, P. G. A. Kumar, P. S. Pregosin, S. Gischig, *J. Organomet. Chem.*, **2005**, Accepted.

- Bonding in Pd(II) and Pt(II) Allyl MeO-and H-MOP Complexes. Subtle Differences via ^{13}C NMR.
P. G. A. Kumar, P. Dotta, R. Hermatschweiler, P. S. Pregosin, A. Albinati and S. Rizzato, *Organometallics* **2005**, Accepted.

- PGSE Diffusion and ^{1}H, ^{19}F- HOESY Studies on Ionic Liquids: The Effect of Co-solvent on the Aggregation States
P. G. A. Kumar, P. S. Pregosin, T. J. Geldbach, P. J. Dyson, **2005**, Submitted.

- [RuCl(*p*-cymene)(phosphoramidite)]$^{+}$, a 16-Electron Fragment Stabilized by an η^2-Aryl-Metal Interaction, and Its Use in the Asymmetric Catalytic Cyclopropanation of Olefins
D. Huber, P. G. A. Kumar, P. S. Pregosin, A. Mezzetti, **2005**, In preparation.

Contents

Summary

Applications of NMR, in homogeneous catalysis, using multinuclear and multidimensional techniques plus PGSE diffusion studies on late transition metal complexes are described in this thesis.

Chapter 1 deals with the fundamental features and the basic principles involved in successfully carrying out the described NMR techniques. The subject of discussion will be relevant to the field of inorganic/coordination chemistry.

After a brief introduction to ion-pairing and heteronuclear NOESY, chapter 2 focuses firstly on PGSE NMR diffusion studies on a few Ru(II)-model complexes and then extended to the study of other metals as well. Further, the effect of the solvent on ion-pairing, hydrogen bonding and aggregation is portrayed.

For example, the rate dependence of the [Ru(η^5-C_5H_5)(BIPHOP-F)(acetone)][Y] catalyzed Diels-Alder reaction of cyclopentadiene with acrolein, on the anion, Y, is shown to be due to selective ion-pairing (Section 2.4). Pulsed gradient spin-echo (PGSE) diffusion measurements on the model Cp and indenyl complexes, [Ru(η^5-C_5H_5)(CH_2=CH-CN)(BIPHOP-F)][Y], Y = BF_4 and BArF and [Ru(η^5-C_9H_7)(CH_2=CH-CN)(BIPHOP-F)][Y], Y = BF_4 and BArF, respectively, combined with ^1H,^{19}F HOESY NMR data can be used to understand how the ion-pairing for the BF_4 anion differs relative to that of the BArF anion.

Chapter 3 concentrates on the unusual and unexpected bonding modes exhibited by the monodentate phosphine complexes. The subject is rounded on MOP (and/or their analogues) and

phosphoramidite ligands, both ligands shown that given an opportunity they tend to chelate in a surprising fashion. Further, restricted rotation of the phosphines due to 3,5-meta dialkyl substitution is discussed based on multidimensional NMR studies.

For instance, the scheme presented below illustrates the various binding modes exhibited by the MOP auxiliary.

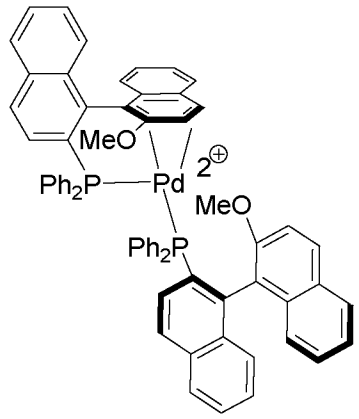

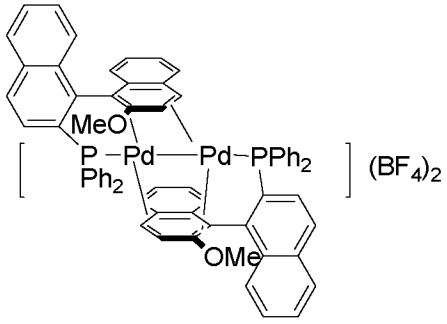

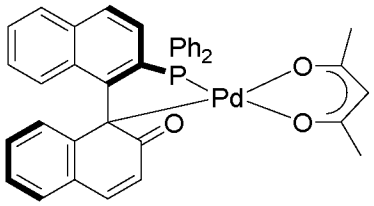

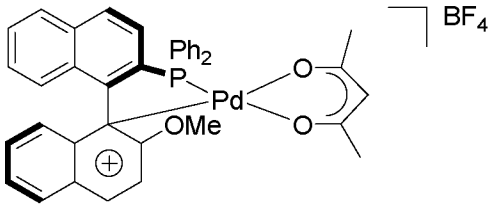

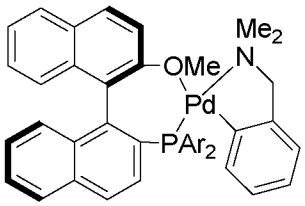

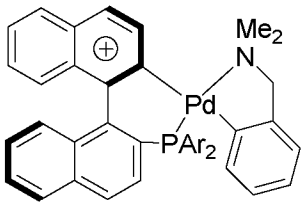

The Appendices, at the end, serve as a support to the above chapters describing some of the additional complexes applicable.

Zusammenfassung

In dieser Dissertation werden Anwendungen der NMR-Spektroskopie in homogener Katalyse durch Anwendung multinuklearer und multidimensionaler Techniken und PGSE Diffusions Studien an späten Übergangsmetallekomplexen beschrieben.

Kapitel 1 befasst sich mit den wesentlichen Experimenten und den grundlegenden Prinzipien, die für eine erfolgreiche Durchführung der beschriebenen Techniken verantwortlich sind.

Nach einer kurzen Einführung in die Ionen-Paarung und die heteronukleare NOE-Spektroskopie, konzentriert sich Kapitel 2 zunächst auf PGSE NMR Diffusions Studien an einigen Ru(II)-Modellkomplexen und dann auch ausgeweitet auf die Studie an anderen Metallen. Des Weiteren ist die Auswirkung des Lösungsmittels auf die Ionen-Paarung, Wasserstoffbrücken und Aggregation beschrieben.

Zum Beispiel, die Geschwindigkeitsabhängigkeit der [Ru(η^5-C_5H_5)(BIPHOP-F)(acetone)][Y] katalysierten Diels-Alder Reaktion von Cyclopentadien mit Acrolein, ist auf das Anion Y zurückzuführen, welches selektiv Ionen-Paarung eingeht (Abschnitt 2.4). PGSE Diffusionsmessungen am Modell von Cp- und Indenyl-Komplexen, [Ru(η^5-C_5H_5)(CH_2=CH-CN)(BIPHOP-F)][Y], Y = BF_4 und BArF und [Ru(η^5-C_9H_7)(CH_2=CH-CN)(BIPHOP-F)][Y], Y = BF_4 und BArF, kombiniert mit ^{1}H,^{19}F HOESY NMR Daten können für das Verständnis, wie sich die Ionen-Paarung für das BF_4 Anion von der Ionen-Paarung für das BarF Anion unterscheidet, verwendet werden.

Kapitel 3 beschreibt die unüblichen und unerwarteten Bindungsmodi von monodentaten Phosphinekomplexen. Dabei werden MOP- (und/oder Analogon davon) und Phosphoramidit-Liganden behandelt. Beide Liganden zeigen eine Tendenz zur Chelatbildung in einer überraschenden Art, wenn eine Gelegenheit gegeben wird. Des Weitern wird die beschränkte Rotation der Phosphine aufgrund der 3,5-meta Dialkylsubstituenten diskutiert basiert auf multidimensionalen NMR Messungen.

Das unten gezeigte Schema illustriert die verschiedenen Bindungsmodi, die mit MOP-Liganden möglich sind.

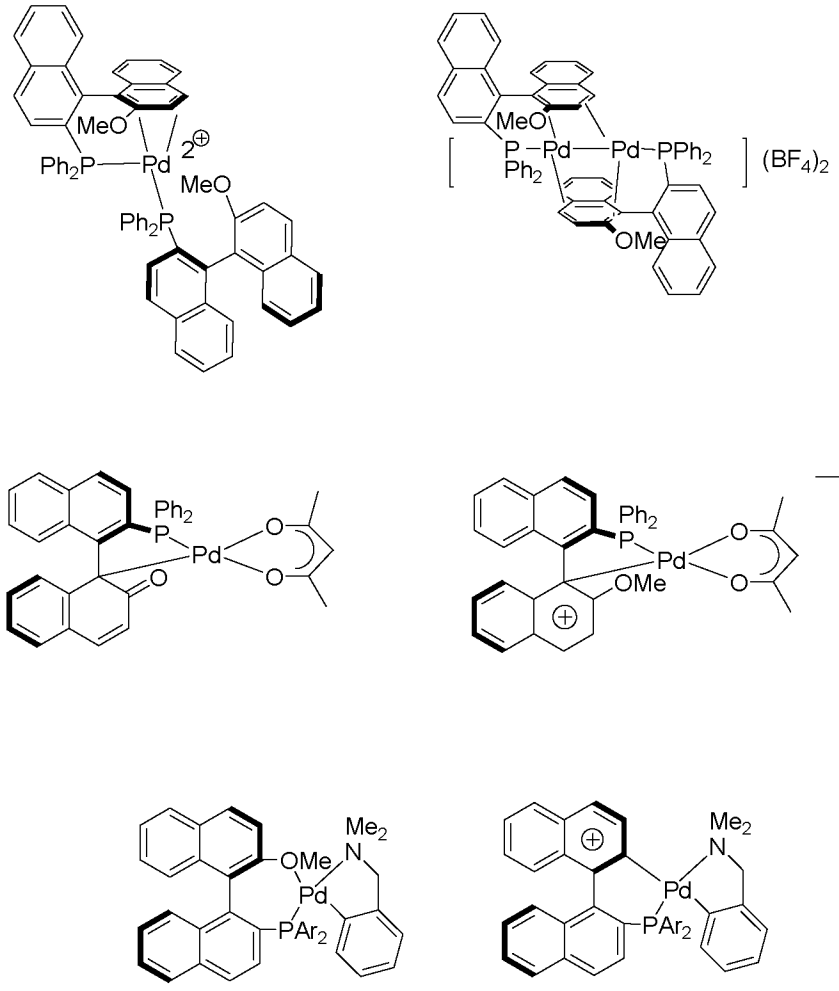

Der Anhang dient als Unterstützung zu den vorhandenen Kapiteln und beschreibt einige der zusätzlichen Komplexe.

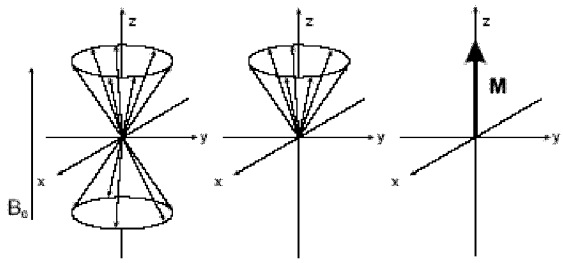

Chapter 1

NMR Spectroscopy- A tool for Organometallic Chemists

1.1 Preface

The aim of this chapter is to provide a background for the NMR Spectroscopy, which is used as a main analytical tool in solving several of the chemical structures discussed. The normal strategy used to solve the structure is in the order of

Measurements- Assignment

- 1D ^{31}P, ^{1}H and ^{13}C measurements - chemical shifts and coupling constants
- 2D ^{31}P, ^{1}H correlation (HMQC or COSY) - heteronuclear coupling to the protons
- 2D ^{1}H, ^{1}H correlation (COSY or TOCSY)- Proton J-coupling over 2 or 3 bonds
- 2D ^{13}C, ^{1}H correlation (HMQC and HMBC) – heteronuclear coupling to protons via one bond and long-range
- 2D ^{1}H, ^{1}H correlation (NOESY or ROESY) – Through space correlation and exchange
- 2D ^{19}F, ^{1}H correlation (HOESY) - Through space correlation

PGSE NMR diffusion studies on the complexes arose due to the ability of using a multinuclear approach, e.g., ^{1}H (and sometimes ^{31}P) data for the cation and ^{19}F results for the anion. PGSE is used in solving problems related to ion-pairing, molecular volumes and hydrogen bonding in organometallic chemistry. Occasionally one can use this method to explain the anion effects in homogeneous catalysis.

The following section starts with a history of NMR, followed by a discussion on the application of NMR in the field of organometallic chemistry and then ends with an outline of PGSE diffusion NMR.

1.2 Introduction to NMR Spectroscopy

The initial observation of proton magnetic resonance in water by Bloch[1] and in paraffin by Purcell[2] has led to the discipline of Nuclear Magnetic Resonance (NMR) Spectroscopy. This technique has seen an unparalleled growth as an analytical method and now, in numerous disguises, finds application in chemistry, biology, medicine, material science and geology. Although the first observations were made by physicists, a few pioneering chemists immediately realized the significance of the chemical shifts and spin-spin coupling constants within the context of structural chemistry.

Nuclear spin systems possess unique properties that predestinate them for molecular studies[3]:

(i) The nuclear sensors provided by nature are extremely well localized, with a diameter of a few femtometers, and can report on local affairs in their immediate vicinity. It is thus possible to explore molecules and matter in great detail.

(ii) The interaction energy of the sensors with the environment is extremely small, with less than 0.2 J/mol, corresponding to the thermal energy at 30 mK, and the monitoring of molecular properties is virtually perturbation-free. Nevertheless, the interaction is highly sensitive to the local environment.

(iii) Geometrical information can be obtained from nuclear pair interactions. Magnetic dipolar interactions provide distance information, while scalar J-coupling interactions allow one to determine dihedral bond angles.

Inorganic chemists still profoundly rely on X-ray crystallography. Spectroscopic techniques like IR, UV are far superior to NMR; however, a planned approach using NMR can lead to a plethora of applications in organometallic/coordination chemistry which will be discussed in the subsequent chapters.

1.3 NMR in organometallic chemistry

NMR spectroscopy has a history of more than 50 years and has provided a major aid in solution structure analysis. Starting from modest 40 MHz machines, one can now measure on instruments approaching the GHz range. Coordination chemists have been rather slow in profiting from this method, as many of the metal complexes of the first transition series are paramagnetic, and thus only sometimes suitable for this methodology. Further, sensitivity was initially a problem, i.e., many metal complexes are only sparingly soluble; however, the advent of polarization transfer methods, high field magnets and improved probe head technology have more or less eliminated this difficulty. This technique has now grown into one of the fastest ways to screen reactions and, at the same time, provide insights into molecular structure and solution dynamics. Measurements of ^{1}H, ^{13}C, ^{19}F and ^{31}P spins on ca 1-2 mg of sample with molecular weights in the range 500-1000 Dalton are now a fairly routine matter.

In the recent years, an ETHZ research group has advocated a simple 2-D NMR approach to confront structural questions and problems related to enantioselective homogeneous catalysis[4]. The usual tactics in handling the problems are shown below

(**1**) Assign the ^{1}H resonances by correlating these to other spins, *e.g.* ^{31}P, ^{13}C, metals (such as ^{195}Pt or ^{103}Rh), or other protons. (**2**) Determine the solution 3-D structure, using ^{1}H NOE spectroscopy. (**3**) Check the flexibility of the chiral pocket *via* NOE (or ROE) results and (**4**) determine if and which exchange processes occur (phase sensitive NOESY or ROESY data).

In addition to (1)–(4), there are always the usual empirical couplings constant and chemical shift correlations which function as complementary aids.

The spin I = ½, nuclei with the largest magnetic moments and natural abundance are still favored in the inorganic community, e.g., ^{1}H, ^{13}C, ^{19}F, ^{31}P, $^{111,113}Cd$, ^{195}Pt and ^{199}Hg; however, ^{15}N, ^{29}Si, ^{77}Se, ^{103}Rh, $^{107,109}Ag$ and ^{183}W (see **table 1.1**)are now all practically routine candidates[5-7].

Table 1.1. Relative intensities for selected nuclei of common interest[8]

Nucleus	Abund (%)	Rel Sens.	Comment[a]
^{1}H	99.9	1	
^{29}Si	4.7	7.84×10^{-3}	both[b]
^{57}Fe	2.2	3.37×10^{-5}	indirect
^{59}Co	100	0.28	direct[c]
^{95}Mo	15.7	3.23 x 10–3	direct[c]
^{103}Rh	100	3.11×10^{-5}	indirect
^{109}Ag	48.2	1.01×10^{-4}	indirect
^{119}Sn	8.58	5.18×10^{-2}	both[b]
^{183}W	14.4	7.20×10^{-4}	indirect
^{187}Os	1.6	1.22×10^{-5}	
^{195}Pt	33.7	9.94×10^{-3}	both
^{199}Hg	16.8	5.67×10^{-3}	both

[a] Both direct and indirect methods (INEPT, HMQC … etc) are in use. [b]Most efficient via indirect methods. [c] Lines can be broad due to the quadrupole moment of the metal.

The assignment is often the most tedious job, in that the chemist is, of necessity, immersed in the NMR details; nevertheless, the chemical return is well worth the time investment.

The following sections describe simple applications using the methods mentioned and relate, primarily, to structural problems of chiral complexes. Nevertheless, all of the examples illustrate a structural or dynamic subtlety. Slowly, multi-dimensional methods are increasing in popularity within the inorganic community; however, while several of these may be necessary to properly characterize a specific complex, they are not all equally useful. COSY measurements connect coupled proton spins and are thus useful for assignments. However, NOESY data can provide three-dimensional structure features *and* reveal exchange phenomena, thereby making these much more valuable for the co-ordination chemist.

There are basically two NMR categories: one which uses coupling constants, *i.e.*, an 'X,H'-correlation, and one based on NOE-type measurements, which includes 2-D exchange spectroscopy.

1.3.1 X,H Correlation

Generally called heteronuclear correlation, this technique establishes a connection between a proton and a heteronucleus, e.g., ^{13}C, ^{31}P etc, through one or more bonds. The most sensitive, and now routinely used method for obtaining spin I = 1/2 NMR signals for less sensitive nuclei involves double-polarisation transfer (I→S→I) and uses one of the two-dimensional NMR sequences shown in **Figs 1.1** and **1.2**.

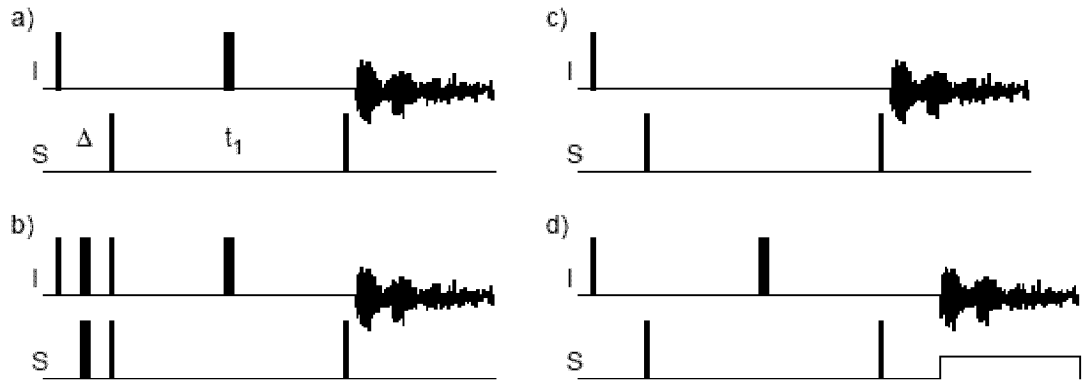

Figure 1.1. Heteronuclear Multiple Quantum Correlation (HMQC) pulse sequences. a) Sequence for small J(I,S) values, b) for larger, resolved J(I,S) values and phase sensitive presentation, c) Zero or Double Quantum variant for the determination of the I-spin multiplicity, and d) with refocussing and optional S-spin decoupling[8].

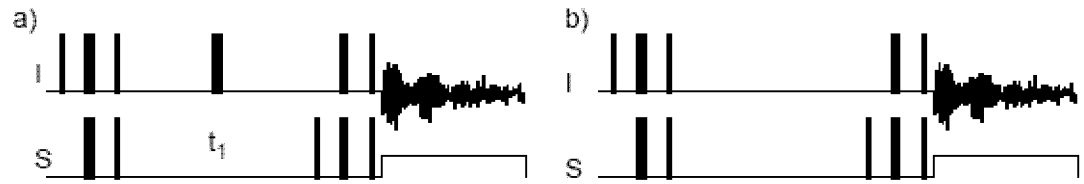

Figure 1.2. Heteronuclear Single Quantum Correlation (HSQC) pulse sequences with optional decoupling of the S-spin. a) Standard sequence and b) modified for the I-spin-multiplicity determination[8].

The I-spins are assumed to be a high receptivity nucleus, most often ^{1}H, i.e., one needs a $^{n}J(X,^{1}H)$ interaction, n= 1-4. The data are detected using the proton signals and the spectra are usually presented as contour plots, as shown in **Figs 1.3** (HMQC) and **1.4** (XH-COSY). Occasionally, ^{31}P or ^{19}F are suitable alternatives to protons. Specifically, for metal complexes containing phosphorus ligands in which the ^{31}P is directly bound to the metal centre, one occasionally has a relatively large $^{1}J(M,P)$ value of the order of 10^{2}-10^{3} Hz[9]. Consequently, one need not be restricted to molecules revealing suitably large proton-metal coupling constants. The time Δ is set to $\leq 1/(2\ J(S,I))$ and the time t_1 represents the time variable for the second dimension. These sequences provide a theoretical enhancement of $(\gamma_I/\gamma_S)^{5/2}$. For nuclei such as ^{57}Fe, ^{103}Rh and ^{183}W this means factors of 5328 and 5689 and 2831, respectively[5].

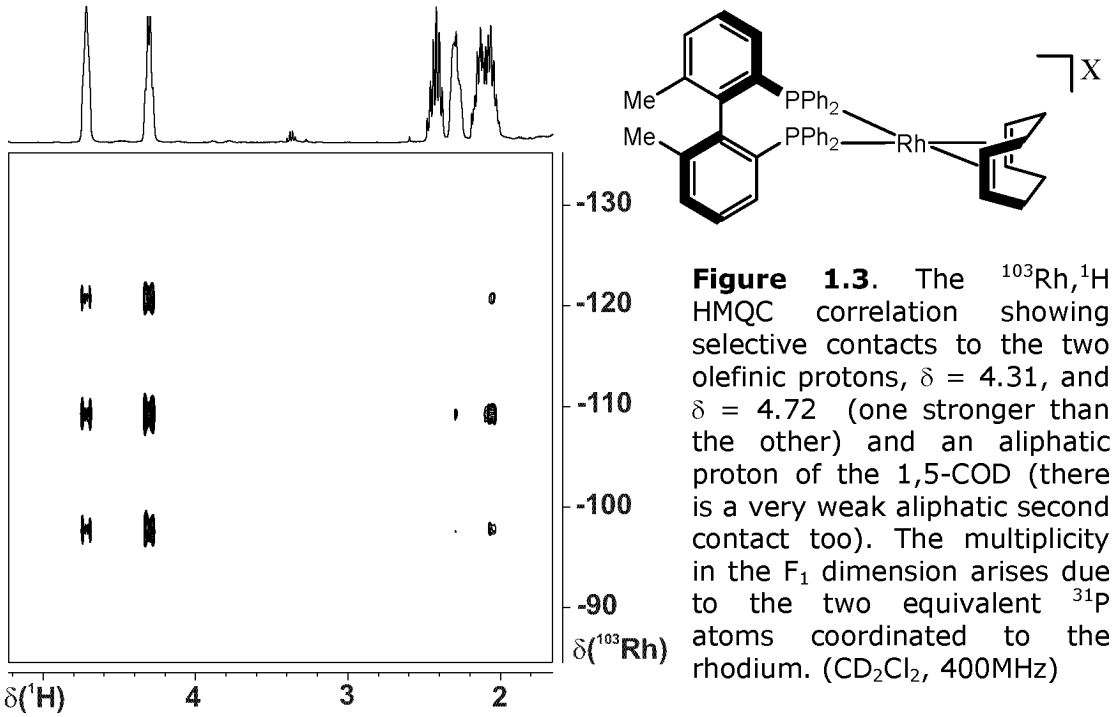

Figure 1.3. The $^{103}Rh,^{1}H$ HMQC correlation showing selective contacts to the two olefinic protons, δ = 4.31, and δ = 4.72 (one stronger than the other) and an aliphatic proton of the 1,5-COD (there is a very weak aliphatic second contact too). The multiplicity in the F_1 dimension arises due to the two equivalent ^{31}P atoms coordinated to the rhodium. (CD_2Cl_2, 400MHz)

HMQC experiment has its own merits and demerits compared to heteronuclear COSY. For example, in $^{31}P,^{1}H$ HMQC, when the

coupling constant $^{3}J(^{31}P,^{1}H)$ is set to 12.5Hz, the resulting spectrum loses selectivity and reveals both *meta* and *para* signals of equal intensity, which can be misleading[10]. Therefore, one needs to have a prior knowledge of the information needed and has been the subject of review in several literatures[4, 6, 8, 10].

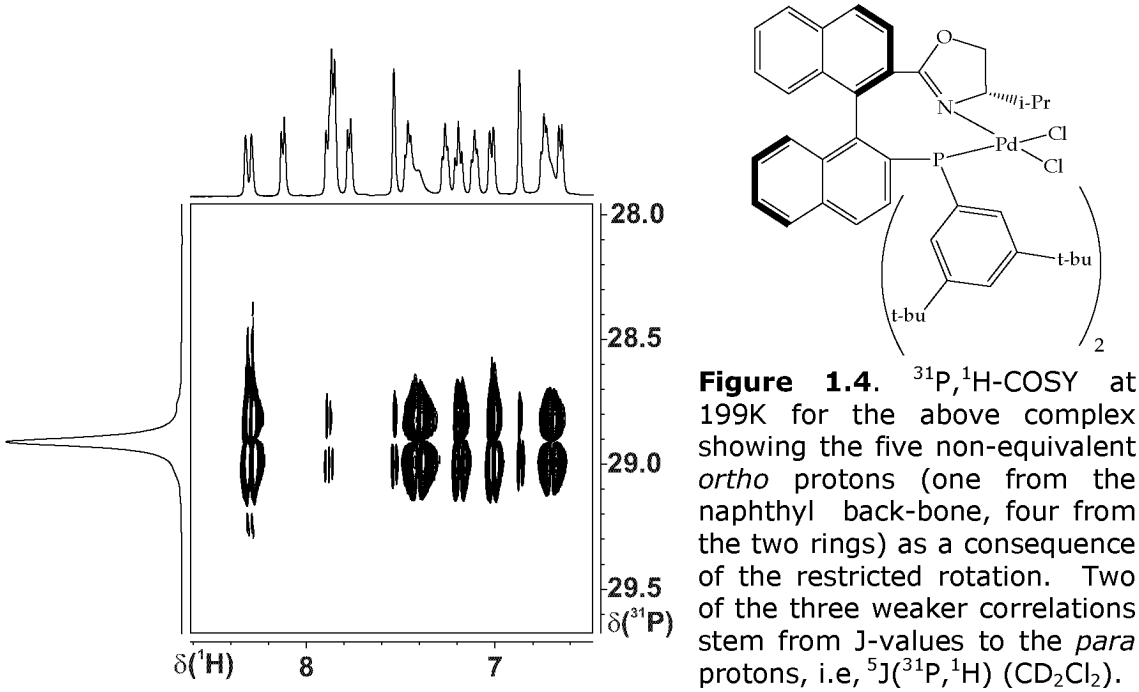

Figure 1.4. $^{31}P,^{1}H$-COSY at 199K for the above complex showing the five non-equivalent *ortho* protons (one from the naphthyl back-bone, four from the two rings) as a consequence of the restricted rotation. Two of the three weaker correlations stem from J-values to the *para* protons, i.e, $^{5}J(^{31}P,^{1}H)$ (CD_2Cl_2).

1.3.2 Nuclear Overhauser and Exchange Spectroscopy

Nuclear Overhauser effects, NOE's, involve dipole-dipole relaxation phenomena which result in signal enhancements[11]. For two interacting protons, the maximum NOE, η_{max} is:

$$\eta_{max} = (5 + \omega^2\tau_c^2 - 4\omega^4\tau_c^4) / (10 + 23\omega^2\tau_c^2 + 4\omega^4\tau_c^4)$$

ω = frequency, τ_c = correlation time

For small molecules with short τ_c values (extreme narrowing limit), this equation reduces to η_{max} = +50%. This is rarely achieved for a single proton in co-ordination compounds as there are often a number of spins contributing to the relaxation of an individual proton and the τ_c values are not always so short.

Clearly, if the quantity

$$(5 + \omega^2\tau_c^2 - 4\omega^4\tau_c^4) = 0,$$

then there is no NOE. It is well known[11] that η_{max} can pass through zero and the limiting value is –100%. This can be the case for biological or other macro-molecules. Further, a negative NOE is also possible for higher molecular weight metal complexes, e.g., MW > 1000, and/or in viscous media (perhaps due to low temperature studies). In these cases ROESY spectra[11] can be useful. Although selective ^{1}H NOE studies and magnetisation transfer experiments are still frequently in use, the simple three-pulse (phase sensitive) 2-D NOESY sequence, given in **Fig. 1.5**, is finding increasing popularity[8, 11].

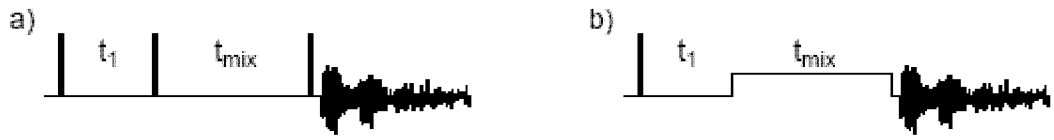

Figure 1.5. Pulse sequences for nuclear Overhauser and chemical exchange spectroscopy. a) NOESY and b) ROESY.

The mixing time should be chosen such that exchange can take place without losing too much signal intensity. Practically, this often means values in the range 0.4-1.0 seconds, although individual T_1's and temperature will require that this parameter be constantly adjusted to suit the co-ordination compound in question. Wherever co-ordination chemistry problems overlap with those of organic chemistry, e.g., conformational analysis, ^{1}H NOE studies will have their classical value. These results allow the determination of the 3-D structure of the complex and thus for enantioselective catalysts, the shape of the chiral pocket offered by a chiral auxiliary to an incoming organic substrate.

Figure 1.6 illustrates an example of a section of NOESY for the cyclometallated Pd-benzyl amine MOP complex, the phosphine being a MOP analog with substitution of 3,5-dimethylphenyl.

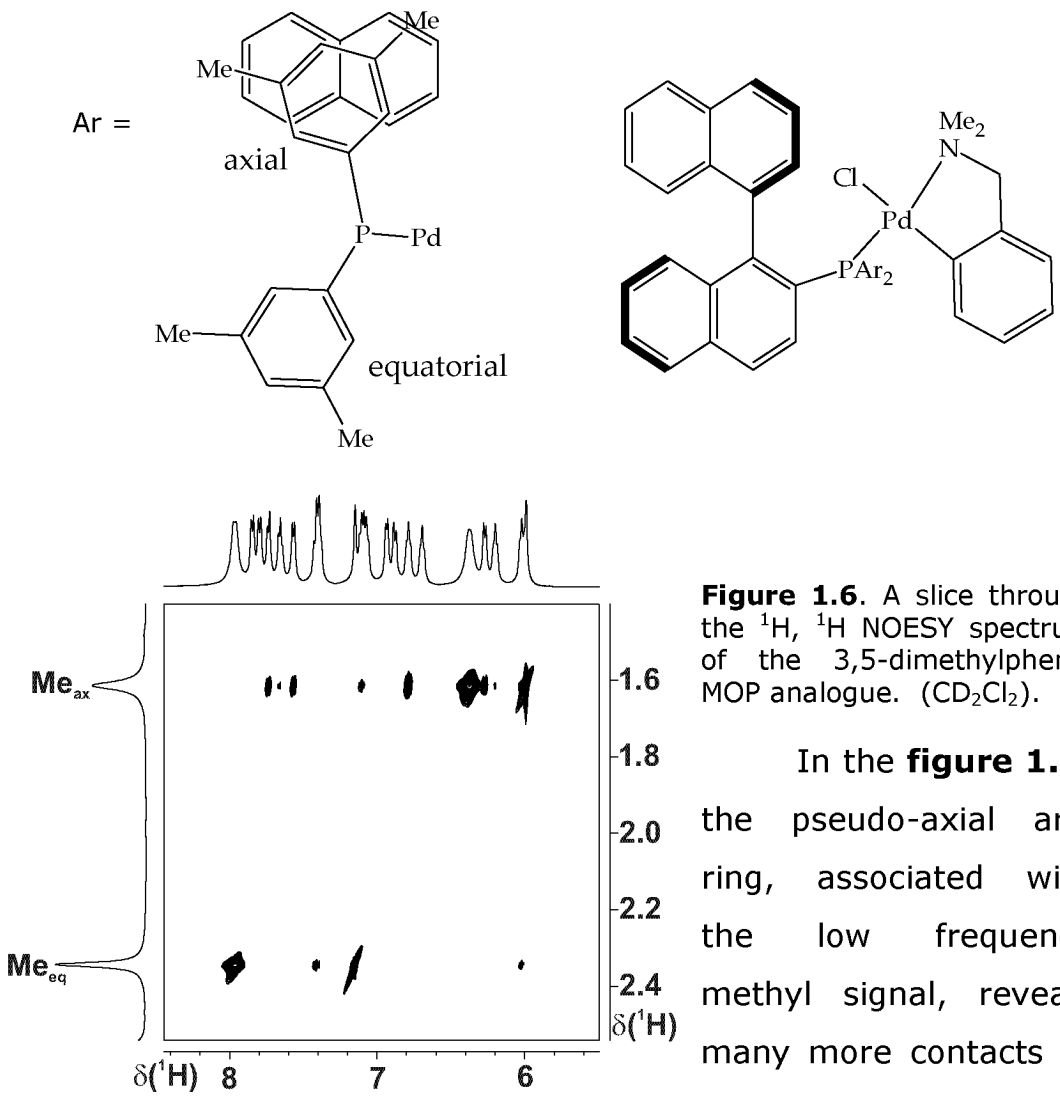

Figure 1.6. A slice through the ^{1}H, ^{1}H NOESY spectrum of the 3,5-dimethylphenyl MOP analogue. (CD_2Cl_2).

In the **figure 1.6**, the pseudo-axial aryl ring, associated with the low frequency methyl signal, reveals many more contacts to the aromatic backbone than does the pseudo-equatorial analogue. Indeed, for the methyl group at higher frequency, the two most intense contacts stem from the adjacent *ortho* and *para* protons of the 3,5-dimethylphenyl moiety and not from the inter-ring NOE's. This brings us to the fact that the axial ring is more restricted than the equatorial aryl ring, thus implying a selective restricted rotation induced by the presence of the 3,5-dialkyl groups(see chap 3.2.3).

The use of phase sensitive NOESY sequence affords exchange information. A unique aspect of this form of exchange spectroscopy concerns the ability to detect species whose concentration is so low, that they escape detection in a conventional 1-dimensional experiment. **Fig. 1.7** shows a section of the ^{1}H NOESY spectrum for

a mixture of isomeric palladium phosphino-oxazoline, 1,3-diphenylallyl complexes[12]. One observes a major component in exchange with a visible (ca 10% of the more abundant isomer). However, there are additional *very broad exchange cross-peaks* from the main isomer to an "invisible" species, which would easily have gone undetected (See Chapter 3.3).

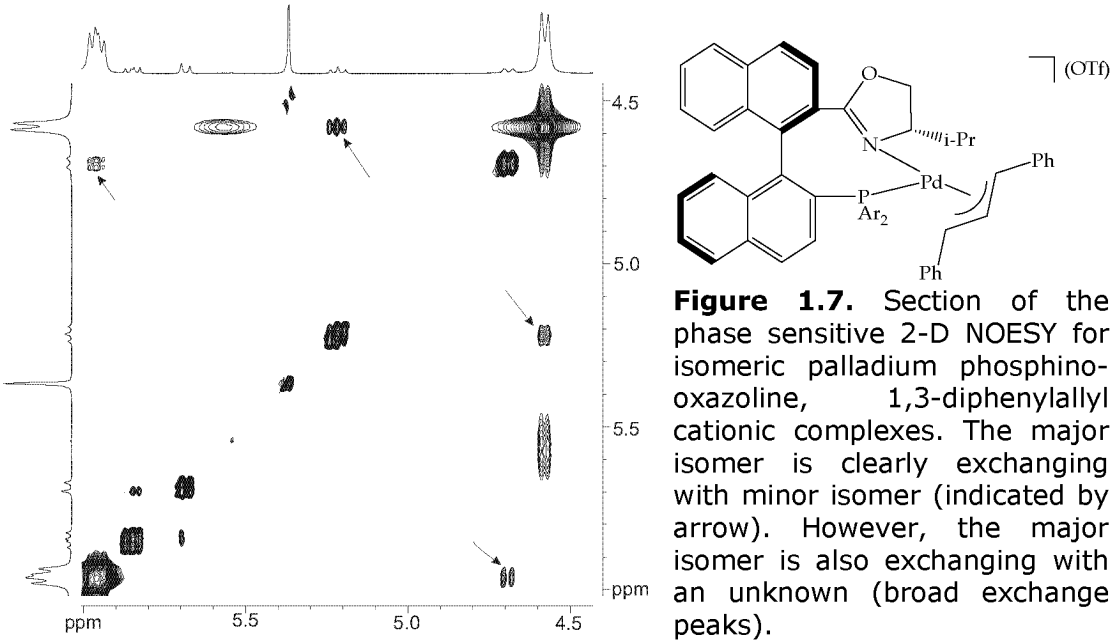

Figure 1.7. Section of the phase sensitive 2-D NOESY for isomeric palladium phosphino-oxazoline, 1,3-diphenylallyl cationic complexes. The major isomer is clearly exchanging with minor isomer (indicated by arrow). However, the major isomer is also exchanging with an unknown (broad exchange peaks).

Apart from $^{1}H,^{1}H$ NOE studies, interest in $^{19}F,^{1}H$ NOE's (see **Fig. 1.8**) in co-ordination chemistry is developing.[13, 14] In the example, the $^{19}F,^{1}H$ HOESY spectra show selective contacts from the BF_4 anion to one of the CHO backbone signals, the vinyl protons of the acrylonitrile, the Cp-ligand and additional contacts to the *ortho* protons of one of the phenyl groups (See Chapter 2.4). Further, several interesting examples of $^{31}P,^{31}P$ exchange spectroscopy have been reported[12].

Slowly, but surely, three-dimensional structures are being solved with NOE- and ROE-NMR methods; nevertheless, there are areas, e.g., determining molecular size, aggregation, and/or the nature of interionic interactions where NMR spectroscopic possibilities have not been sufficiently explored.

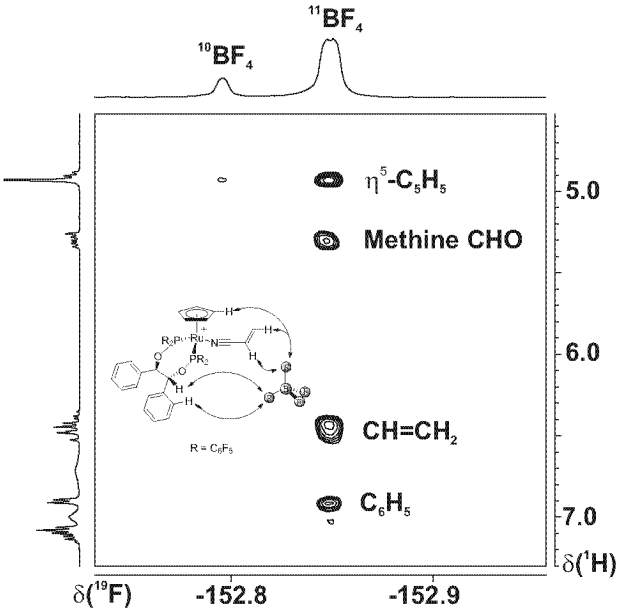

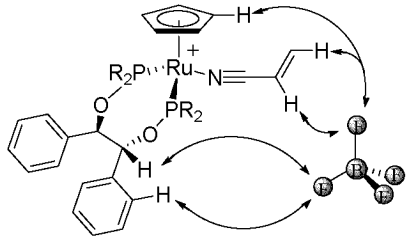

R = C_6F_5

Figure 1.8. The ^{1}H-^{19}F HOESY spectrum of complex [Ru(η^5-C_5H_5)(CH_2=CHCN)(BIPHOP-F)][BF_4].

The following section gives an introduction to the phenomenon of diffusion and how to obtain diffusion coefficients.

1.4 Diffusion NMR- An Overview

1.4.1 Theoretical Synopsis of diffusion

Diffusion is a phenomenon in which matter is transported from one part to another by random molecular motions[15]. Molecules in solution are in constant motion and experience both rotational and translational motion. The process of translational motion in solution is commonly referred to as self-diffusion and is defined with a self-diffusion coefficient D (m^2s^{-1}). The value of D may be approximated by the Stokes-Einstein equation 1.1:

$$D = kT/6\pi\eta r_h \qquad [1.1]$$

where k (JK^{-1}) is the Boltzmann constant, T is the temperature (K), η (P) is the solvent viscosity, and r_h (m) is the hydrodynamic radii. The relationship is strictly valid for a spherical particle with a radius r_h, but it may be used to estimate the size of molecules in solution.

The distance a molecule will travel in a single direction during a defined amount of time t (s) is given by[16]

$$z = (2Dt)^{1/2} \qquad [1.2]$$

Of course, not every molecule will travel the distance defined in equation 1.2 during a specific time period. This is why z (m), a root mean square (RMS) distance is often used and represents an ensemble average of many particles. In the case of unrestricted diffusion a conditional probability function was derived [16],

$$P_s(z,t) = (4\pi Dt)^{-1/2} \exp[-(z-\nu_z t)^2/4Dt] \qquad [1.3]$$

that describes the average probability for any particle to have a dynamic displacement z over a time t. The variable ν_z (ms^{-1}) is the velocity of the particle, and the term is included to illustrate that velocity and diffusion are two separate matters and may be separately analyzed. This function is illustrated in the **Figure 1.9**. Two populations are represented, each having its own characteristic diffusion coefficient. After some time t the probabilities of finding the particles along a single dimension are represented as normalized Gaussian curves. After time passes, t+Δt, the curves broaden. Because a velocity tem is included, the curves shift to the right after Δt. In a typical PGSE NMR experiment, any velocity

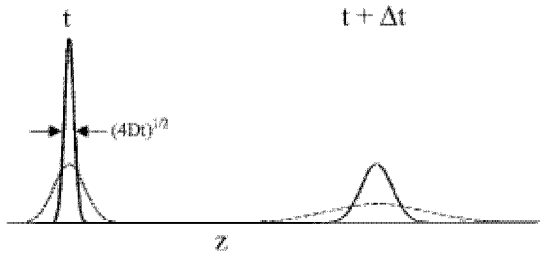

Figure 1.9. Probability curves derived from the average propagator function (Eq. [1.3]) for two populations of molecules and in one dimension. The diffusion coefficient for the molecules represented by the dashed line is greater than that represented by solid line. A velocity component is superimposed upon the diffusion component.

component, brought about by convection, for example, should be strictly avoided or properly compensated.

In order to measure true translation motion, enough time must be allowed to pass in the experiment for *z* to be several times larger than r_h. This point is particularly important for large molecules such as polymers. If the amount of time used is too short, we may actually measure the translation of a chain segment or the rotational diffusion rather than the translation diffusion.

1.4.2 PGSE NMR

Nuclear Magnetic Resonance (NMR) is an attractive technique due to its non-invasive methodology which can yield a vast amount of structural information without destroying the sample. Although inherently insensitive relative to many other analytical techniques, nearly all molecules have NMR-active nuclei, meaning the technique is universal and analyte derivatization is unnecessary. Furthermore, it is a quick technique to analyze a sample without effecting a separation in mixtures[17].

Not many solution-state NMR techniques have been developed to study molecular aggregation, estimate volumes or to study ion-pairing in the field of Organometallic/Coordination Chemistry. In the last decades, the spectroscopists have relied on the traditional methods based on chemical shifts, relaxation[18] and saturation transfer techniques. Recently PGSE-NMR[19-21] (Pulse-Field Gradient Spin-Echo) has emerged as an additional tool for the above problems. The method is advantageous because it is rapid (results can be obtained in seconds to minutes), simple, selective and allows for the facile analysis of mixtures. In addition, it requires no special sample preparation or chromatographic method optimization. Because diffusion coefficients are inversely proportional to hydrodynamic radii, complexed ligands can easily be distinguished

from nonbinding molecules by significant differences in their diffusion coefficients. There are now a number of diffusion NMR methods e.g., PGSE-NMR, DOSY, MOSY some of which are based on two-dimensional experiments. It is indeed interesting to know how the method originated, the way it was improved and how it is applied in the present day. Some of the historical background is discussed below.

1.4.3 Historical Aspects of PGSE-NMR:

Time domain NMR dates from Hahn's observations[22-24] of the free induction decay (FID), the spin echo (SE), and the stimulated echo (STE). The effects of the molecular diffusion, in the presence of magnetic field gradients, on echo amplitudes were evident from the beginning, and Hahn reported a derivation of diffusion dependent signal attenuation, which he attributed to his mentor, C.P.Slitcher[24]. All NMR diffusion measurements are based on the fact that the diffusion coefficient can be calculated from the echo attenuation if the amplitude and duration of the magnetic field gradient are known. The original measurements were carried out with continuous gradients, but the advantages of pulsed gradients were convincingly demonstrated by Stejskal and Tanner[25]. Originally utilized as a technique to measure diffusion coefficients of components in solution and to define domain size in emulsions in the late 1960's and early 1970's, PGSE NMR became more popular as the instrumentation developed and spectral resolution improved. Despite this, it was not until shielded gradients and stable gradient drivers became commercially available in the early 1990's that the method gained widespread use. Furthermore, the studies generally focused on the analysis of known compounds in mixtures, not on the characterization of the unknowns. Reviews on the detailed aspects of the PGSE NMR and its application in various fields can be found in the literature[19-21, 26-28].

1.4.4 Obtaining Diffusion Coefficients (D) by Pulsed Field Gradient Spin-Echo NMR

Diffusion coefficient measurements are possible using pulse sequences that incorporate pulsed-field gradients (PFG). These magnetic field gradients are generated by passing current through a special pair of coils (anti-Helmholtz or Maxwell pair) in the NMR probe. Many modern probes have triple-axis gradients, but the gradient coils aligned along the *z*-axis are the ones utilized in most diffusion measurements. These coils are coaxial with, but physically separate from, the radio frequency (rf) coil, and the turns in the coils are spaced such that the ¨strength¨ of the gradient varies linearly along the sample length[27]. ¨Strength¨ is experimentally defined in terms of gradient amplitude, *G*, duration, δ, and the gyromagnetic ratio, γ, which, when multiplied together, define an applied gradient area. The gradients are used to impose spatially dependent phase angle (ϕ) on the net magnetization of the nuclei in the sample. Although the precession frequencies (ω) of the spins depend on local static magnetic fields, the position from which precession proceeds (i.e., the *xyz* coordinate determined by ϕ) depends on the strength of the applied magnetic field gradient. In effect, the gradient pulses allow the positions of the nuclei to be tracked before (gradient encoding period) and after (gradient decoding period) the experimental diffusion time (Δ). The efficiency of decoding depends on how far on average the molecules diffuse longitudinally through solution with respect to the direction for the magnetic field gradient during Δ. The greater the positional change due to diffusion, the poorer the decoding. For example, a small ligand will on average diffuse a relatively greater distance during Δ compared to a bulkier one. Therefore, the small ligand will more likely receive significantly different encoding and decoding phase angles, leading to attenuation of the resonance intensity because

the magnetization is not entirely refocused. Over the course of the diffusion, the big ligand and small ligand signal intensities (or integrals), I, will decay exponentially with the square of the gradient area according to equation 1.4.

$$I = I_0 \exp[-D(\gamma\delta G)^2(\Delta - \delta/3)] \qquad [1.4]$$

In equation 1.4, I_0 is the signal intensity (or integral) in the absence of an applied magnetic field gradient. The decay rates of the exponential curves for the small and big molecules are proportional to their respective diffusion coefficients (D). By taking the natural log of both sides of equation 1.4, a linear equation results, and D is calculated from the slope.

Figure 1.20 shows an example of a mixture of two sugars (A) and their data fits to the exponential (B) and linear versions (C) of equation 1.4, respectively[28], thus showing both forms of representations (B and C) can be used in finding the D-values. Measurements with high precision allow diffusion coefficients of molecules of similar size and shape to be distinguished when their resonances are resolved in the NMR spectrum. An alternative method is a pseudo two-dimensional (2D) DOSY (diffusion-ordered spectroscopy) spectrum that displays chemical shift along the horizontal axis and the calculated diffusion coefficients along the vertical dimension[29]. The γ^2 –dependence of equation 1.4 means that much larger gradient amplitudes are required to reliably measure diffusion coefficients for nuclei such as ^{13}C compared with more sensitive nuclei such as ^{1}H or ^{19}F. The

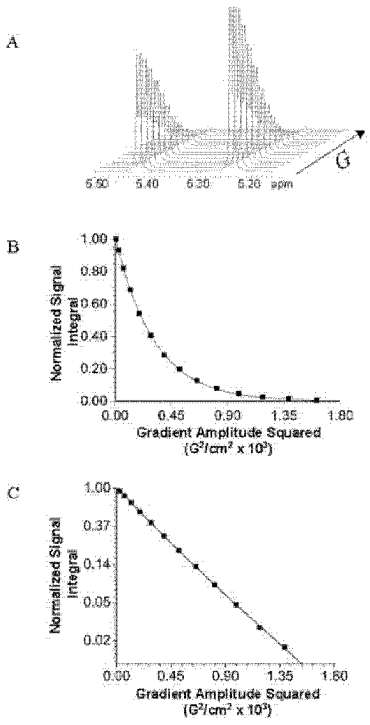

Figure 1.20[27]

experimental parameters δ and Δ (the delay time during which diffusion occurs) are optimized by the user and usually remain fixed throughout the experiment.

As given in Equation 1.4, G is the amplitude for rectangular gradient pulses. Some standard diffusion pulse sequences incorporate shaped gradient pulses (such as sinebell). The more gradual increase in current applied through the gradient coil with shaped gradients is believed to be gentler on the spectrometer hardware and as well prevents phase anomalies in the final spectrum[30, 31]. When sinebell gradient pulses are used, the effective gradient amplitude is scaled by a factor of $2/\pi$ relative to the rectangular pulse[32]. The maximum gradient amplitude of a particular probe should be calibrated regularly using an instrumental algorithm and sample provided by the manufacturer or by performing a diffusion experiment on a sample of known diffusion coefficient such as β-cyclodextrin[33] or water[34]. The article by Price[21] gives further information on gradient calibration and optimization.

Table 1.2 highlights the historical progression of PFG-NMR diffusion methods and illustrates the development of specific and selective techniques used in ligand-protein binding/macromolecular chemistry.

Table 1.2. Development of Pulse Sequences used for PGSE-NMR Diffusion measurements[28]

Pulse sequence	Requirements	Advantages (+) and Limitations (-)	Potential Applications
PGSE	$T_2 > \Delta$	-Analysis of only singlets (not general) -Macromolecules with short T_2 such as proteins cannot be studied	Small organic molecules
STE	$T_1 > \Delta$ $T_2 > \delta + \tau_r$	+J-coupled spins and molecules with short T_2 can be analyzed -Potential eddy current artifacts	Any sample; macromolecules in particular
LED	$T_1 > \Delta$ $T_2 > \delta + \tau_r$	+Eddy current artifacts suppressed -T_e delay increases experimental time	Same as STE
BPPLED, BPPSTE	$T_1 > \Delta$ $T_2 > \delta + \tau_r$	+Eddy current artifacts removed (BPPLED)	Same as STE

		+Static gradients removed +Chemical exchange effects minimized	
CPMG-BPPSTE	Same as BPPSTE, with significant differences in ligand *vs* protein T_2	+Suppression of protein background -Decreased S/N -Elimination of ligand resonances broadened by protein binding	Complex mixtures of small and large molecules
GOSE-BPPSTE	Same as BPPSTE	+Selective for singlet magnetization	Same as CPMG-BPPSTE

Selected PFG-NMR pulse sequences (**Fig.1.21**) used for diffusion measurements are presented below, with radio-frequency (rf) pulses represented by black bars and gradient pulses by gray bars.

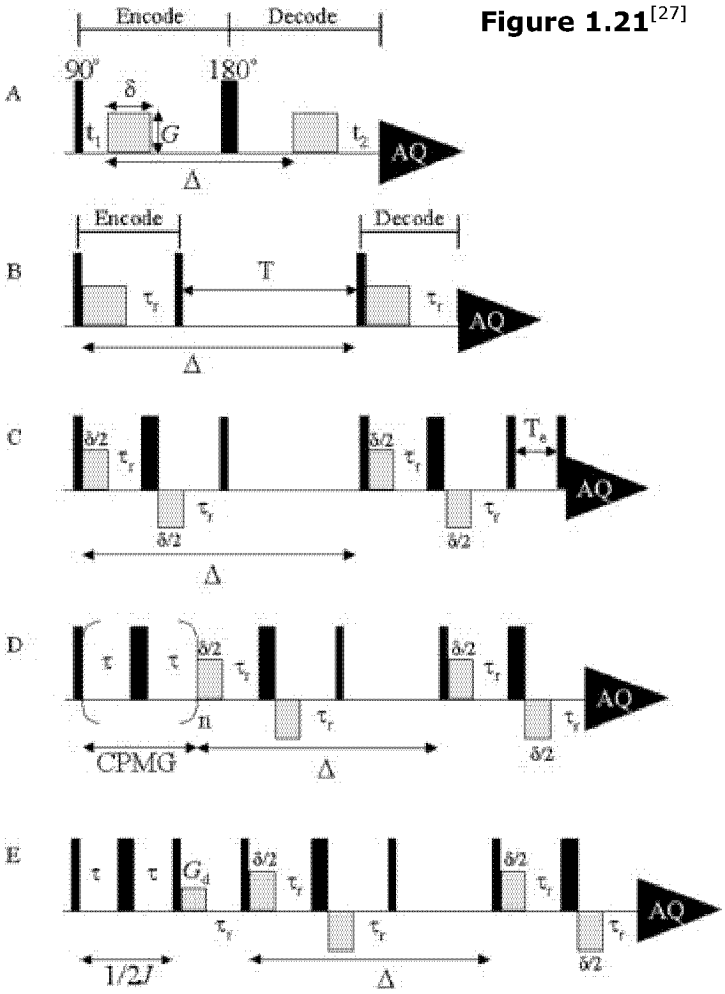

Figure 1.21[27]

(A) Pulsed-Gradient Spin-Echo (PGSE), where the signals begin to decay during t_1 and the echo builds up during t_2.

(B) Pulsed-Field gradient Stimulated Echo (PFG-STE), where τ_r is a gradient recovery delay and T is the effective diffusion time.

(C) Bipolar pulse pair longitudinal eddy current delay (BPPLED).

(D) CPMG-BPPSTE used for reducing the background produced by the protein resonances in ligand-protein studies (where $2\tau n$ is the total CPMG pulse train length).

(E)GOSE-BPPSTE which achieves additional specificity by rejection of J-coupled spins.

Although the PGSE experiment laid the foundation for studying diffusion through PFG-NMR measurements, its utility is limited. Diffusion occurs when the magnetization is in the *xy* plane where signal modulation due to homonuclear spin-spin coupling and

T_2 relaxation occur, making analysis difficult for spin-coupled resonances and relatively large molecules, such as proteins. The pulsed-field gradient stimulated echo (PFG-STE) experiment, originally used by Tanner for diffusion measurements, is more versatile. In this pulse sequence (shown in B), the encode and decode periods are separated by a pair of 90^0 pulses, which allows the majority of the diffusion period (T) to occur in the longitudinal direction. The advantage being that the Echo attenuation occurs because of T_1 relaxation during T, and phase modulation of coupled spins is eliminated. Because the time that the magnetization is held in the transverse plane is short, as long as $T << T_1$, diffusion dominates the measured signal decay rather than the short T_2 relaxation times of big molecules (and, ideally ligands bound to them). The 90^0 pulse after the diffusion time tips the magnetization back into the transverse plane where the magnetizations of all spins (coupled and uncoupled alike) are then decoded.

The PFG-STE experiment served as yet another building block for future experiments. Gibbs and Johnson introduced the longitudinal eddy current (LED) pulse sequence, which incorporates an addition delay period, T_e, after the decoding gradient of the PFG-STE pulse sequence shown in (B). The magnetic fields generated by the gradient pulses induce an electrical current in the NMR rf coil that opposes the gradient magnetic field. This so-called ¨eddy¨ current (discussed below) can interfere with the detection of the free induction delay resulting in distorted line shapes and baselines in the NMR spectrum. By storing the magnetization in the longitudinal plane during T_e, residual eddy currents are allowed to dissipate before detection of the NMR signal. In addition, chemical shift is preserved and modulation from spin-spin coupling is avoided. However, this experiment is not a robust one for measuring molecules where there is effect of chemical exchange.

To successfully carry out a diffusion experiment, one needs to know the procedure, the pulse programme to use, standardization techniques, the problems which might be encountered and how to solve the problems. The next pages will be focused on what are the measures to be taken before the diffusion experiment is carried out on the sample of interest.

1.4.5 Data quality

In order to achieve the most reliable analysis, regardless of the analytical technique, one must reduce or eliminate any experimental artifacts. The PGSE NMR experiment is susceptible to several artifacts, all of which are manageable with proper care and consideration. Before presenting the details of the artifacts, one must identify the constituents of a good data set.

There are five elements of a good data set[27]:

1. Excellent registration of resonances.
2. no gradient-dependent spectral phase distortion or broadening
3. good differentiation in decay among components
4. no baseline artifacts and
5. pure exponential decay

The above elements can be hampered by spectral phase distortions, systematic line broadening, baseline drift etc. Often, many of these problems are present in a single data set.

Proper control of data acquisition is essential for obtaining optimum data quality. The conditions for obtaining such a data set needs the following

1. The NMR Equipment should be sound

2. The two gradient pulses used in the experiment need to be identical, and because of this a stable gradient amplifier is important.
3. The gradient should be a shielded design that allows fast switching, at least on the order of microseconds.

Essentially there are three problems that lead to spectral artifacts in the data set

1. Eddy currents caused by gradient switching
2. Convection currents caused by temperature gradients
3. Non-uniform field gradients inherent in the gradient coil design.

which will be discussed below.

1.4.6 Problems in carrying out NMR diffusion measurements and their solution:

1.4.6.1 Eddy Currents

Eddy currents are electrical currents caused by the fast switching (on and off) of the gradient pulse. Whenever a magnetic field changes, eddy currents simultaneously form within any closely located conductor (like probe body). These currents are set up in a way to oppose the change. The effect produces a magnetic field that can be experienced by the sample and therefore causes distortion in the spectra. To avoid this problem probe manufacturers designed a shielded gradient system. A secondary series of gradient coils outside the primary Maxwell pair is designed and constructed to produce a magnetic field at the inside of the wall of the probe body that is equal and opposite to the one formed by the primary coil. These two fields cancel and the eddy currents that would normally form in the probe body are minimized. No design is perfect and eddy currents, although greatly reduced, are still present[35].

In addition to directly affecting the spectral quality, eddy currents can also have an effect on the locking mechanism. The lock circuitry is designed to compensate for small changes in the main magnetic field. Depending upon the time constants built into the circuitry, it may have a response to the applied gradient pulse and even produce shifts in resonances.

Many articles have been published that discuss ways to minimize this ring down time[35-38]. All deal with either changing the shape of the applied gradient pulse (by changing the current pulse shape delivered to the probe) or using a gradient/RF composite. The different alternatives to the standard square gradient are shown in the **fig. 1.22**. The advantage to changing the shape is that a gentler rise and fall will lessen the intensity of the eddy currents. Use of composite pulse is particularly a better alternative for high resolution work.

Figure 1.22. Alternatives to the standard square gradient. (a) The ramped (or trapezoidal) gradient shape, (b) the half-sine shaped gradient, (c) the bipolar gradient composite, and (d) the CLUB-sandwich gradient composite including tow shaped 180^0 pulses.

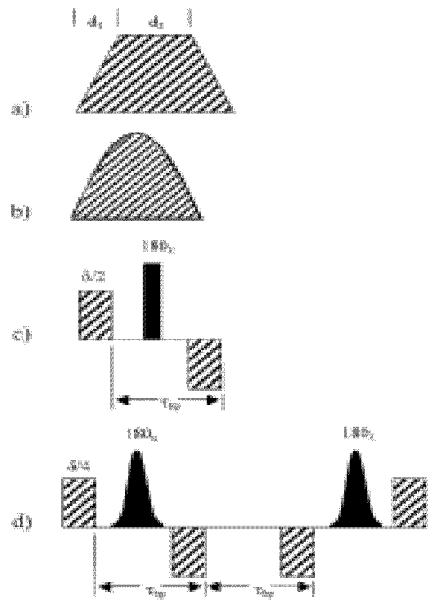

1.4.6.2 Temperature Gradients-Convection

Arguably, the most difficult problem to control is temperature gradients. Most modern NMR systems introduce variable temperature (VT) air through the bottom of the sample region. The VT gas then travels around the side of the tube and exits through a port near the top of the sample region. There is very little room to spare. Because the probe is generally optimized for maximum S/N, the RF coil is as close as possible to the sample tube. This can easily

create a situation where the bottom of the tube experiences warmer gas than the top (or vice versa if cold gas is used to cool the sample). The fact that glass is a good insulator only exacerbates the problem. Although one can achieve an average temperature, there may still be a temperature gradient along the long axis of the tube. Depending on the viscosity of the solvent inside the tube, temperature gradients can cause convection currents to establish and persist.

Several formal methods were presented to measure or visualize thermal convection[39, 40]. To simply observe the effect one needs to allow the signal in the PGSE NMR experiment at the proper temperature to attenuate at least 95% and examine the decay behavior. If there is no effect from the temperature and effects from gradient field nonuniformity are eliminated, the decay should be linear on a semi logarithmic plot.

Most PGSE diffusion experiments have been carried out at ambient temperature. However, for some applications, it is necessary to measure at higher or lower temperatures. The latter would be the case for inorganic or organometallic complexes that are fluxional or unstable in solution at ambient temperature, a common observation. The heating or cooling of the sample may have, potentially, two negative effects on diffusion measurements. First, it can affect the mechanical stability of the experimental set-up, which is obviously detrimental (note: Usually the experiment is carried out at ambient temperature). Second, it may cause the formation of convection currents within the sample, which can be mistaken for

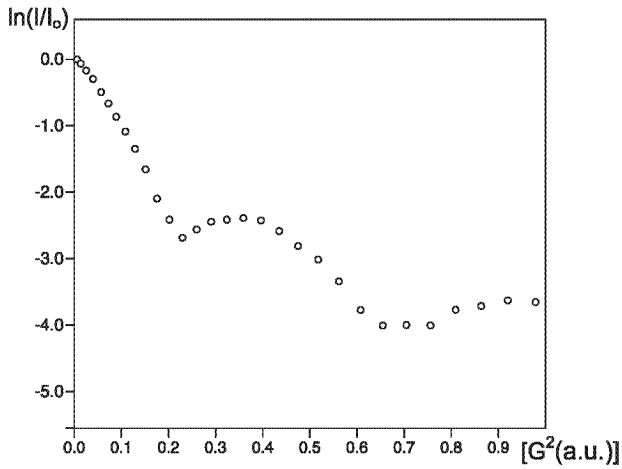

Figure 1.23. A typical plot showing the effect of convection[40].

faster diffusion, or even completely distort the shape of the $\ln(I/I_0)$ vs G^2 plot[41] (See **figure 1.23**).

Convection currents are caused by small temperature gradients within the sample, which are difficult to eliminate even in advanced probe designs. Convection introduces an interfering flow-velocity-dependent phase factor into the amplitude dependence of the signals in PGSE experiments. It has been suggested that convection is especially problematic at high temperatures and sometimes even at low temperatures.

The subject of eliminating convection is discussed in many papers. Solutions such as usage of smaller size NMR tubes[27, 41], sample spinning[42] or convection current compensated pulse sequence[43, 44] purge problems due to convection.

1.4.6.3 Gradient Field Nonuniformity

It is assumed that the gradient is uniform along the *z* direction across the entire sample region. Deviations from a uniform gradient will cause systematic deviations from the ideal decay behavior. Once again, this effect is probe dependent and may vary widely.

Most gradient coil designs have a ¨sweet spot¨ in the very middle of the coil that provides the most uniform gradient. This gradient strength may vary substantially (depending on the specific design) as a function of the distance from the center. Therefore, only a small portion of the sample actually experiences a strong, uniform gradient. Concurrently, most RF coil designs generally excite a region beyond the coil's physical dimensions. This combination produces nonideal signal decay behavior. Antalek has beautifully summarized this effect on a doped water sample[27].

There are two approaches that may be used to obtain a signal from within only the uniform region of gradient: physically constrain

the sample to that region or excite only the spins in that region. It seems like the latter one works better for most cases[27].

1.4.6.4 Other Considerations

Besides the three main concerns previously outlined, there are other minor considerations to bear in mind while obtaining PGSE NMR data. The lock should be well controlled throughout the experiment. Because the gradients temporarily perturb the field, the lock circuit should be blanked during the gradient. If possible, the time constant controlling the response of the lock to field perturbations should be lengthened in order to accommodate the decay of the eddy currents.

Vibrations at the probe should be minimized. The air flow in some probes may cause vibrations and should be optimized to prevent this. It is best to isolate the magnet from building vibrations.

Every gradient probe will have its own characteristic gradient strength for a given current value. The best way to obtain a proper gradient calibration value is to use a solution with a compound having a known diffusion coefficient (D_{known}) e.g. HDO in D_2O, and then estimate their slope by diffusion measurement. The temperature, solvent conditions, and concentration need to be controlled. The slope for the sample of interest is then compared with that of the standard sample using the equation 1.5

$$D = \frac{m_{obs} \times D_{HDO}}{m_{HDO}} \qquad [1.5]$$

The slope of the lines, m, can be obtained by plotting the decrease in signal intensities vs G^2 (equation 1.6).

$$\ln\left(\frac{I}{I_o}\right) = -(\gamma\delta)^2\left(\Delta - \frac{\delta}{3}\right)DG^2 \qquad [1.6]$$

Conclusion: PGSE NMR is nowadays gaining popularity in solving several chemical problems. Optimization of the experimental parameters and a critical analysis of the self-diffusion coefficients has lead to this popularity.

1.5 Concluding Remarks

In summary, modern NMR spectroscopy is now a highly developed and technologically advanced subject. The tremendous growth in available NMR pulse methods can be bewildering and may leave one wondering how best to make use of the new techniques. This chapter will serve as a reference, in the forthcoming chapters, for implementing the NMR techniques to solve some of the structural problems in Organometallic/Coordination Chemistry.

1.6 Bibliography:

[1] F. Bloch, W. W. Hansen and M. Packard, *Phys. Rev.* **1946**, *69*, 127-127.

[2] E. M. Purcell, H. C. Torrey and R. V. Pound, *Phys. Rev.* **1946**, *69*, 37-38.

[3] R. R. Ernst, *Angew. Chem.-Int. Edit. Engl.* **1992**, *31*, 805-823.

[4] P. S. Pregosin and G. Trabesinger, *J. Chem. Soc. Dalton Trans.* **1998**, 727-734.

[5] P. S. Pregosin in *Inorganic Nuclei: Low Sensitivity Transition Metals*, *Vol. 4* ('Ed.' John Wiley & Sons Ltd., **1996**, 2549-2557.

[6] P. S. Pregosin and C. Ammann, *Pure Appl. Chem.* **1989**, *61*, 1771-1776.

[7] P. S. Pregosin and R. W. Kunz, *^{31}P and ^{13}C NMR of Transition Metal Phosphine Complexes*, Springer Verlag, Berlin, **1979**.

[8] P. S. Pregosin and H. Ruegger in *Nuclear Magnetic Resonance (NMR) Spectroscopy*, *Vol.* ('Ed.' J. A. McCleverty and T. Meyer, J.), Elsevier, Amsterdam, **2003**, 1-35.

[9] P. S. Pregosin, *Stereochemistry of Metal Complexes: Unidentate Phosphorus Ligands*, VCH Publishers Inc, Deerfield Beach, Fla., **1987**, 465.

[10] M. Eberstadt, G. Gemmecker, D. F. Mierke and H. Kessler, *Angew. Chem.* **1995**, *107*, 1813-1838.

[11] D. Neuhaus, Williamson, M. P.,, *The Nuclear Overhauser Effect in Structural and Confirmational Analysis*, Wiley-VCH, New York, **2000**.

[12] P. Dotta, P. G. A. Kumar and P. S. Pregosin, *Magn. Reson. Chem.* **2002**, *40*, 653-658.

[13] B. Binotti, A. Macchioni, C. Zuccaccia and D. Zuccaccia, *Comm. Inorg. Chem.* **2002**, *23*, 417-450.

[14] P. S. Pregosin, E. Martinez-Viviente and P. G. A. Kumar, *Dalton Trans.* **2003**, 4007-4014.

[15] H. J. W. Tyrrel, Harris, K.R., *Diffusion in Liquids, Buttersworths, London,* **1984**.

[16] P. T. Callaghan, *Principles of Nuclear Magnetic Resonance Microscopy, Oxford, Clarendon Press.*

[17] B. Meyer and T. Peters, *Angew. Chem.-Int. Edit.* **2003**, *42*, 864-890.

[18] P. J. Hajduk, E. T. Olejniczak and S. W. Fesik, *J.Am. Chem. Soc.* **1997**, *119*, 12257-12261.

[19] W. S. Price, *Concepts Magn. Reson.* **1997**, *9*, 299-336.

[20] P. Stilbs, *Prog. NMR Spectr.* **1987**, *19*, 1.

[21] W. S. Price, *Concepts Magn. Reson.* **1998**, *10*, 197-237.

[22] E. L. Hahn, *Phys. Rev.* **1950**, *77*, 297-299.

[23] E. L. Hahn, *Phys. Rev.* **1950**, *77*, 746-746.

[24] E. L. Hahn, *Phys. Rev.* **1950**, *80*, 580-594.

[25] E. O. Stejskal and J. E. Tanner, *J. Chem. Phys.* **1965**, *42*, 288-&.

[26] C. S. Johnson, *Prog. Nucl. Magn. Reson. Spectrosc.* **1999**, *34*, 203-256.

[27] B. Antalek, *Concepts Magn. Reson.* **2002**, *14*, 225-258.

[28] L. H. Lucas and C. K. Larive, *Concepts Magn. Reson. Part A* **2004**, *20A*, 24-41.

[29] E. J. Cabrita and S. Berger, *Magn. Reson. Chem.* **2002**, *40*, S122-S127.

[30] M. R. Merrill, *J. Magn. Reson. Ser. A* **1993**, *103*, 223-225.

[31] W. S. Price, K. Hayamizu, H. Ide and Y. Arata, *J. Magn. Reson.* **1999**, *139*, 205-212.

[32] O. Kohlmann, W. E. Steinmetz, X. A. Mao, W. P. Wuelfing, A. C. Templeton, R. W. Murray and C. S. Johnson, *J. Phys. Chem. B* **2001**, *105*, 8801-8809.

[33] H. Uedaira, *J. Phys. Chem.* **1970**, *74*, 2211-&.

[34] R. Mills, *J. Phys. Chem.* **1973**, *77*, 685-688.

[35] P. Jehenson, M. Westphal and N. Schuff, *J. Mag. Res.* **1990**, *90*, 264-278.

[36] H. T. Hu and A. J. Shaka, *J. Mag. Res.* **1999**, *136*, 54-62.

[37] W. S. Price and P. W. Kuchel, *J. Mag. Res.* **1991**, *94*, 133-139.

[38] G. Wider, V. Dotsch and K. Wuthrich, *J. Magn. Reson. Ser. A* **1994**, *108*, 255-258.

[39] N. M. Loening and J. Keeler, *J. Mag. Res.* **1999**, *139*, 334-341.

[40] A. Jerschow, *J. Mag. Res.* **2000**, *145*, 125-131.

[41] E. Martinez-Viviente and P. S. Pregosin, *Helv. Chim. Acta* **2003**, *86*, 2364-2378.

[42] J. Lounila, K. Oikarinen, P. Ingman and J. Jokisaari, *J. Magn. Reson. Ser. A* **1996**, *118*, 50-54.

[43] A. Jerschow and N. Muller, *J. Mag. Res.* **1997**, *125*, 372-375.

[44] A. Jerschow and N. Muller, *J. Mag. Res.* **1998**, *132*, 13-18.

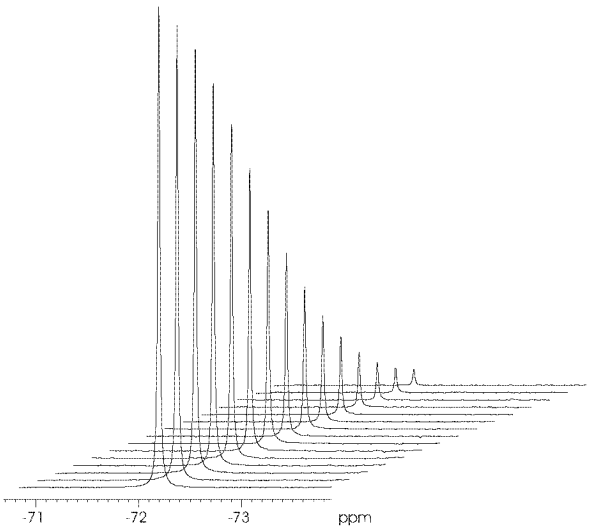

Chapter 2

PGSE Diffusion Studies on late Transition Metal Complexes

2 Diffusion studies

2.1 Introduction

The application of diffusion methodology in Coordination and/or Organometallic Chemistry[1-9] remains sparse but is on the increase. Although the methodology is hardly new[10, 11], finding its way into this field of Chemistry took some time. The diffusion coefficients, D, obtained by the PGSE method provide an indication of molecular volume, and/or aggregation state[12-16], molecule encapsulation[8] and, generally, how the individual charged species translate relative to one another in solution. The ability to use a multinuclear NMR diffusion approach, e.g. ^{1}H data for the cation and ^{19}F results for a suitable anion, combined with ^{1}H,^{19}F HOESY data[5, 17, 18], affords a useful view of how the anions and cations interact. Apart from the high receptivity (^{1}H and ^{19}F), PGSE measurements on Inorganic and Organometallic compounds could be successfully carried out with nuclei such as ^{195}Pt[19], ^{31}P[20], ^{35}Cl[20] or ^{7}Li[21].

The next paragraphs will illustrate some of the applications of diffusion NMR in the field of transition metal chemistry.

The first report of NMR diffusion measurements to determine the aggregation state of a transition metal catalyst concerned the chiral, tetranuclear Cu(I) catalysts (see equation **2.1**) by Seebach[22] *et al.* Such Sulphur-bridged species were interesting since they represent rare examples of chiral chelates functioning as monodentate ligands for a transition metal. These catalysts were used in the conjugate addition reactions of anions to α,β-unsaturated cyclic ketones. Diffusion measurements were shown to be valuable for the determination of the aggregation state of organocopper complexes in solution.

Seebach *et al*[22]

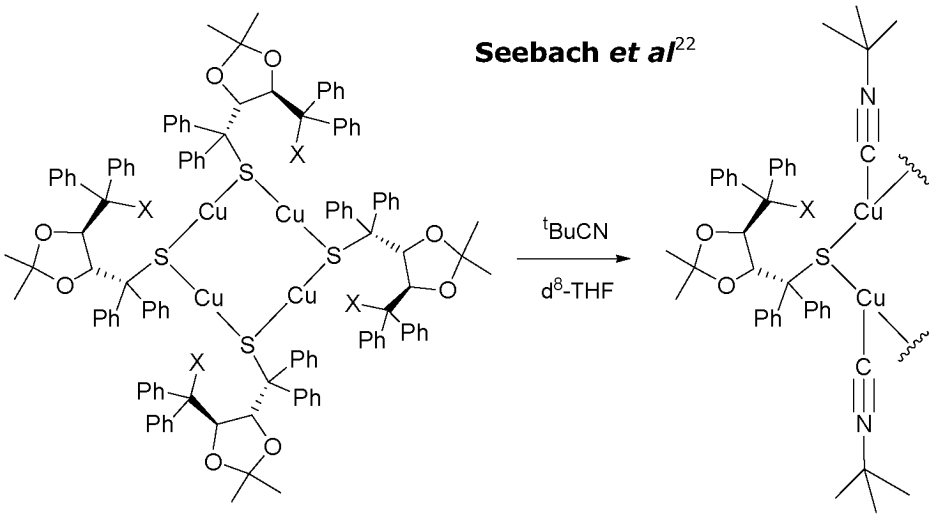

- 2.1

X = OH, OMe, NMe_2

Brintzinger and co-workers[2] have studied the polymerization catalyst MAO/$ZrCp_2Me_2$ in C_6D_6. The calculated effective hydrodynamic radius of 12.2-12.5Å at different zirconocene and MAO concentrations indicated that the ion pair formed in situ (See fragment A) remained associated even at the lowest concentrations studied. At elevated concentrations, aggregation to ion quadrupoles or higher aggregates is indicated by an apparent increase in size.

Fragment A

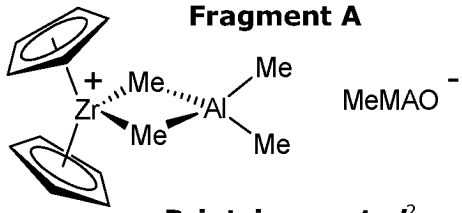

Brintzinger *et al*[2]

Interestingly, for the related series of zirconocene catalysts $[Cp_2ZrMe]^+[MeB(C_6F_5)_3]^-$ Marks and co-workers[15] have found no evidence of significant aggregation to form the ion quadrupoles shown in Equation **2.2**. These authors have found that the tendency to form aggregates of higher nuclearity other than simple ion-pairs is dependent on whether the anion is in the inner or outer coordination sphere of the metallocenium cation.[23]

Marks *et al*[15]

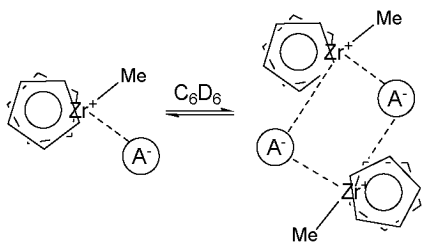

- 2.2

PGSE diffusion measurements have proved very valuable in studying ion-pairs. A relatively large number of cationic compounds are currently in use in homogeneous catalysis and/or organic synthesis. It has been shown that the counterion may influence the rate and/or product distribution of some of these reactions,[24-30] as well as the stability of the compounds.[31] In principle, one can determine the diffusion coefficients for the cation and anion separately and thus gain insight into whether they move together as a single unit (tight ion-pair) or separately. For anions such as PF_6^-, BF_4^-, OTf^- or $BArF^-$, ^{19}F represents both an alternative and a complement to ^1H PGSE methods. HOESY (Heteronuclear Overhauser Spectroscopy), and especially $^1H,^{19}F$ HOESY measurements, also help to localize the position of anions such as PF_6^- or $BArF^-$, relative to a catalytically active transition metal cation.[17, 26, 32-35]

To appreciate the above discussion, some of the recent examples using PGSE and/or $^1H,^{19}F$ HOESY measurements will be presented in the next paragraphs.

Aresta and coworkers[36] recently studied the behavior of [PdH(dppe)2]X (X = BF_4^-, SbF_6^-, OTf^-) as a proton or hydride donor. To explain the ion-pairing between the anions and the PdH moiety, they hypothesized two possible approach of the anion towards the cationic fragment via HOESY measurements (See fragment B).

Fragment B

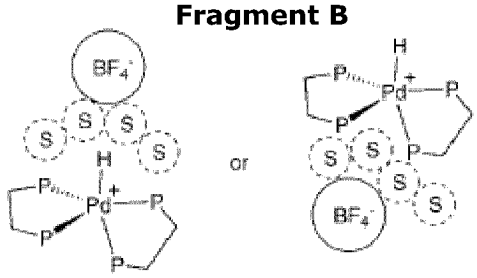

Aresta *et al*[36]

Martinez-Viviente *et al*[37] have obtained diffusion constants for cationic mono- and trinuclear Iridium complexes containing the PHOX chiral P,N-auxiliary with different anions. These data suggest a difference in ion-pairing on varying the solvent. In a study involving mononuclear Ir(I) precursors, the catalytically active species showed good enantioselectivities in the hydrogenation of tri-

substituted olefins, but these mononuclear Ir-complexes reacted with hydrogen, in methanol, to afford a catalytically inactive trinuclear Ir(III) species (shown below), whose presence could be detected via their D-value.

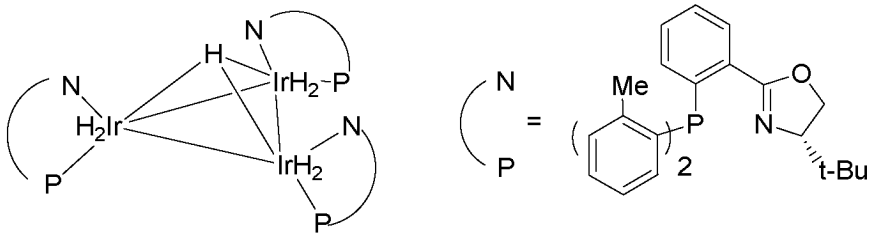

Macchioni and coworkers[4] have recently pointed out that the presence of transition organometallic ion-pairs was not limited to low-polarity solvents but can also be significant in protic solvents with moderate to high relative permittivity.

Martinez-Viviente[38] *et al* have shown that the solvent and concentration has an effect on diffusion values for the chiral organic salts containing TRISPHAT and BINPHAT (see fragment C), and thereby on its diastereomeric structure. Further, the role of temperature on ion-pairing in lithium salts etc, have also been recently reported[21].

Fragment C

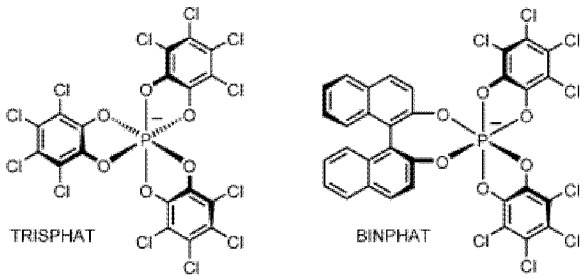

In Conclusion, PGSE NMR diffusion method allows one to rapidly estimate the molecular volume of a metal complex (or a mixture of species). When combined with $^{1}H,^{19}F$ HOESY, it is possible to qualitatively investigate problems involving ion-pairing and aggregation. Thus the PGSE method has emerged as complementary tool in an area of chemistry which remains relatively unexplored.

A quick review concerned with determining D-Values:

Even though this section is a repetition of some of the discussion in Chapter 1, it will serve as a recapitulation.

A PGSE NMR diffusion measurement consists of a spin-echo sequence in combination with the application of pulsed field gradients. The two most common sequences are shown in **Fig. 2.1**.

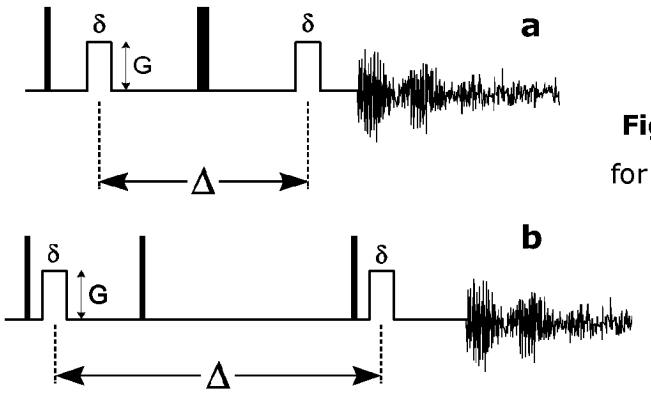

Figure 2.1. Typical pulse sequences for the PGSE experiments: a) the Stejskal-Tanner experiment; b) the Stejskal-Tanner experiment, modified via substitution of two 90° pulses for a single 180° pulse.

The PGSE experiment is usually performed by repeating the sequence while systematically changing either the time allowed for diffusion (Δ), the length (δ) or the strength (G) of the gradient. The diffusion constant, D, can be derived

$$\ln\left(\frac{I}{I_0}\right) = -(\gamma\delta)^2 G^2 \left(\Delta - \frac{\delta}{3}\right) D \qquad \textbf{- 2.3}$$

G = gradient strength, Δ = delay between the midpoints of the gradients, D = diffusion coefficient, δ = gradient length

from equation **2.3**: from the slope of the regression line by plotting $\ln(I/I_0)$ (I/I_o = observed spin echo intensity/intensity without gradients) vs. either Δ-$\delta/3$, δ^2 (Δ-$\delta/3$) or G^2, depending on the parameter varied in the course of the experiment. Compounds with smaller hydrodynamic radii move faster, and reveal larger diffusion coefficients.

The D-value can be related to the hydrodynamic radii of the molecules *via* the Stokes-Einstein equation (**2.4**) and this allows for a viscosity correction.

$$D = \frac{kT}{6\pi\eta r_H} \qquad \textbf{- 2.4}$$

k = Boltzmann constant, T = absolute temperature, η = viscosity, r_H = hydrodynamic radius

Now that it is clear how to determine the diffusion coefficient and thereby the approximate molecular volume of the complex, it would be good to have some model complexes for comparison purposes. The following chapter will focus on some model complexes of Ru(II) and study their behavior in different solvents with respect to the phenomenon of ion-pairing, hydrogen bonding etc.

The complexes presented in the next chapters were available as a consequence of a number of collaborative research projects. The author is highly indebted to the colleagues whose names appear in the table below.

Chapter number	People involved	Place
2.2.2	Theo Zweifel	ETH Diplomarbeit, Switzerland
2.3	Dr. J.M. Goicochea, Prof. M.K. Whittlesey	University of Bath, UK
2.4	M. Vallet, Prof. E.P. Kuendig	University of Geneva, Switzerland
2.5	Dr. T.M. Schmid, Prof. G. Consiglio	D-CHAB, ETH, Switzerland
2.6	Dr. D. Sirbu, Prof. G. Consiglio	D-CHAB, ETH, Switzerland

2.2 Model Complexes: Ru(II) – BINAP

BINAP[39-44] (**1**) complexes of Ru(II) have generated considerable interest in enantioselective homogeneous catalysis. Cationic Ru(II)-Binap systems with different arenes (*p*-cymene, Section **2.2.1** and Cp, Section **2.2.2**) are useful hydrogenation precursors and serve as models for the diffusion studies, where the cation (via ^{1}H) and anion(via ^{19}F) interactions are studied via PGSE measurements.

2.2.1 Ru (II)-p-cymene complexes

The simple model complexes [RuCl(*p*-cymene)(binap)]X (**2a-f** X = BF_4^-, $CF_3SO_3^-$, $BArF^-$, PF_6^-, SbF_6^-, Cl^-) in several different solvents were

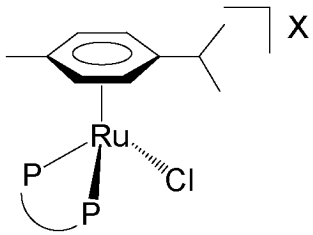

2a-f

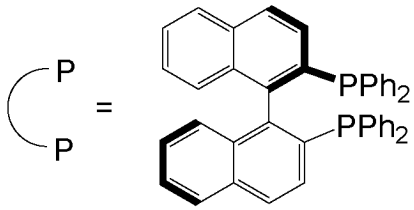

1

chosen for the measurements. The complexed chloride reduces the possibility of a bonding interaction between the anion and the Ru(II) cation. **Table 2.1** shows the diffusion data in different solvents. In methanol, the most strongly solvating and most polar of the three solvents, the observed diffusion values, D, for the cation with several anions are all found to be ca. 6.0×10^{-10} m^2s^{-1}, indicating independent movement of the cation in this solvent. The calculated r_h values (from Stokes- Einstein equation-2.4) assume spherical shapes (crude approximation) and do not consider that the solvent e.g., methanol, may hydrogen bond (especially to the anion). Nevertheless, the estimated r_h values permit a direct comparison between diffusion measurements in variety of solvents, as it corrects for the different solvent viscosities. Since the hydrodynamic radius of the Ru-BINAP cation is found in all three cases to be constant ca. 7.0Å, it is suggested that, for **2a-c** in methanol solution, the cation and anion are well separated.

Table 2.1 Diffusion constants,[a] and hydrodynamic radii[b] and for **2a-f** in several solvents.

	CD_3OD			$CDCl_3$	
	D	r_h (Å)		D	r_h (Å)
		2a (X = BF_4)			
cation	5.98	7.0	cation	5.89	7.0
anion	15.73	2.6	anion	5.99	6.9
		2b (X = CF_3SO_3)			
cation	5.96	7.0	cation	5.93	7.0
anion	12.28	3.4	anion	6.05	6.9
		2c (X = BArF)			
cation	5.98	7.0	cation	4.78	8.6
anion	6.42	6.5	anion	4.88	8.5
		NaBArF			
salt	6.53	6.3			

	CD_2Cl_2			$(CD_3)_2CO$	
	D	r_h (Å)		D	r_h (Å)
		2a (X= BF_4)			
cation	7.89	6.8	cation	10.07	7.2
anion	10.95	4.9	anion	26.85	2.7
		2b (X = CF_3SO_3)			
cation	7.73	6.9	cation	9.95	7.3
anion	10.46	5.1	anion	23.39	3.1
		2c (X = BArF)			
cation	7.71	6.9	cation	9.91	7.3
anion	8.05	6.6	anion	10.83	6.7
		2d (X= PF_6)			
cation	7.87	6.8			
anion	10.99	4.9			
		2e (X = SbF_6)			
cation	7.81	6.8			
		2f (X = Cl)			
cation	7.83	6.8			

[a]All measurements are for 2mM solutions. Anions measured using ^{19}F and cations via ^{1}H. [b]D-values are x 10^{-10} m^2 sec^{-1}.[c]The values for the radii are given to only one significant figure after the period. Consequently different D-values can lead to the same r_h-value. The viscosities used in the calculations (300K) are those of the pure solvents: CH_2Cl_2 = 0.405, $CHCl_3$ = 0.529 (0.542), CH_3OH = 0.526, (0.547), $(CH_3)_2CO$ = 0.303; H_2O = 1.002 (viscosity values from Chemical Properties Handbook, http://www.Knovel.com 1999)

Using ^{19}F PGSE methods for the anions (except for the SbF_6^- case **2e**, whose ^{19}F spectrum is not readily obtained), it is found that the volumes increase (as expected) in the order: BF_4^- < $CF_3SO_3^-$ < $BArF^-$ (see **Fig. 2.2**).

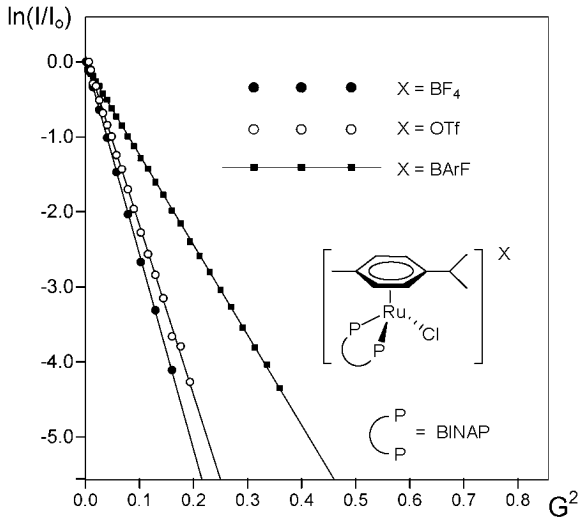

Figure 2.2. PGSE results for several salts of the Ru(II) *p*-cymene Binap complexes **2**. The larger the anion the smaller the absolute value of the slope.

The crystallographically determined value for the BF_4^- bond length[45] is ca 1.35 Å, so that the calculated r_h value of 2.6 Å clearly reflects some degree of solvation. Interestingly, in methanol, the r_h value for the anion in Na(BArF) is only slightly smaller than that found for the BArF anion in the ruthenium salt, **2c** (see **Table 2.1**). As expected, the r_h-values for the BINAP-based cations are found to be larger than those for the BF_4^-, PF_6^- and $CF_3SO_3^-$ anions.

Several PGSE measurements were made in acetone-d_6. These diffusion data, for the BF_4^- and $CF_3SO_3^-$ anions, suggest that this solvent successfully separates these anions from their respective cations; however, as there is some water in the acetone, this reagent may well play a role. The relatively large r_h values for the cations and anions in acetone are likely to result from hydrogen-bonding effects.

In chloroform solution, almost identical D and r_h values for both the cation and anion are observed, thus indicating that fairly tight ion-pairs make a major contribution in this solvent. This conclusion is based primarily on the apparent increase in radius, e.g., r_h = 6.9Å

for the BF_4^- anion. For the BArF analog in this solvent, the calculated radii for the cation and anion are a) much larger than in e.g., methanol and b) almost identical since again the two moieties are moving together. Unexpectedly, for the cation with BF_4^- and $CF_3SO_3^-$ as anions, there seems to be no change in effective radius. This point will be explained following the dichloromethane discussion.

The most comprehensive data set stems from the measurements in CD_2Cl_2. For all six anions the radius of the cation is approximately constant and falls in the range 6.8-7.0Å. However the radii for the anions change significantly relative to the methanol measurements. For the BF_4^- anion the calculated radius is now 4.9Å instead of 2.6Å and for the $CF_3SO_3^-$ anion the value is 5.1Å instead of 3.4Å. For the $BArF^-$ salt, the value is 6.6Å instead of 6.5Å. From previous measurements in methanol, an r_h value of 2.6Å for the PF_6^- anion was found, so that the change to 4.9Å is similar to that observed for the BF_4^- anion.

These increased r_h values for the anions in dichloromethane solution arise due to partial ion pairing effects, i.e., an equilibrium is established between solvent separated and intimate ion pairs. In terms of percentage change, the small BF_4^- and PF_6^- anions will be most affected since, when ion-paired, their D-values will sink drastically and thus their averaged r_h values increase accordingly. The relatively large $BArF^-$ anion will be least effected. On average, a small amount of ion pairing will not significantly change the effective volume of the relatively large Ru-cation, and therefore, these values do not reflect the ion pairing. It is interesting that there is significant ion pairing in CD_2Cl_2, a solvent often used in organometallic reactions.

Having established ion pairing in several solvents, the possibility that the smaller anions might take up a specific shielded position was considered[46]. A ¨tucked-in¨ anion would not significantly increase the effective volume of the cation. To test this idea $^{1}H,^{1}H$ NOESY and $^{1}H,^{19}F$ HOESY spectra for the BF_4^- and $CF_3SO_3^-$ salts were measured. The NOESY results help to assign the ^{1}H NMR spectra of the complexed η^6-arene and thus determine that the *p*-cymene methyl group faces toward the BINAP and the isopropyl group towards the chloride.

The $^{1}H,^{19}F$ HOESY spectra, in both chloroform and dichloromethane (see **Fig. 2.3**), were similar (but not identical) and

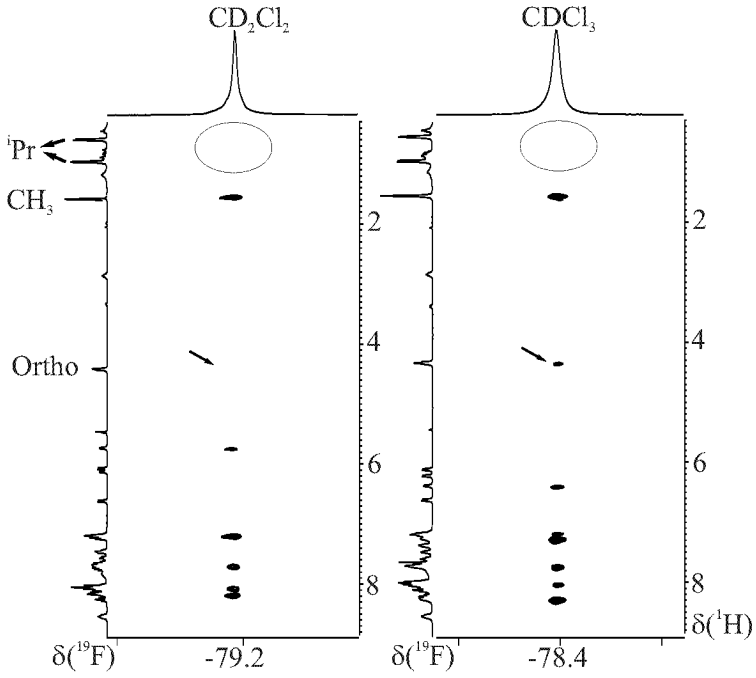

Fig. 2.3. ^{1}H, ^{19}F HOESY spectrum of **2b**, X= $CF_3SO_3^-$ in $CDCl_3$ and CD_2Cl_2. The oval emphasizes that there are no contacts to the *i-propyl* group of the *p*-cymene. However, the anion is closer to the methyl group of the *p*-cymene in both solvents. The arrows indicate the absence and presence of a weak contact to the protons *ortho* to the *p*-cymene methyl group. There are *five selective* contacts to the aromatic protons of the BINAP in $CDCl_3$ but only four in CD_2Cl_2 solvent.

show *no* ^{19}F contacts to the *p*-cymene isopropyl group, a modest contact to the *p*-cymene methyl group, a weak contact to the protons *ortho* to the *p*-cymene methyl group and *four-to- five selective* strong contacts to the aromatic protons of the BINAP. For the triflate case there were fewer contacts in methylene chloride consistent with weaker ion pairing. Consequently, in both solvents, and for both BF_4^- and $CF_3SO_3^-$, the anions approach the ruthenium

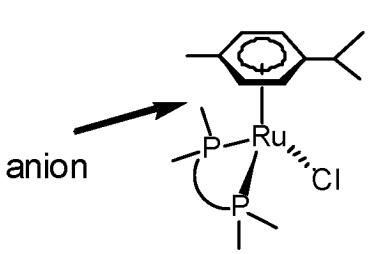

atom from the side of the molecule remote from the chloride and slightly below the complexed arene, i.e., electronic rather than steric control (see fragment).

Given the strong ion pairing in chloroform, and the individual HOESY contacts, it seems reasonable to suggest that these small anions are resting in a position, between the arene and the BINAP ligand, which does not result in any marked increase in the overall volume of the salt.

Conclusions. The PGSE diffusion data, when combined with a suitable ^{1}H, ^{19}F HOESY spectrum, offer a valuable structural aid. These NMR data allow a qualitative estimate of how and where the anions and cations interact which can be monitored individually (assuming a suitable ^{19}F spin is present). For the complexes [RuCl(*p*-cymene)(**1**)]X, **2a-f**, the relatively strong ion pairing in chloroform leads to specific placement of the anion. The ion pairing in dichloromethane is much less pronounced. The chloroform ion pairing (and/or hydrogen-bonding) conclusions stem from anion (^{19}F) NMR diffusion data which indicate a volume for the anion which is almost identical to that found for the much larger cation.

2.2.2 *Ru (II) – Cyclopentadiene complexes:*

Table 2.2. Diffusion Data for the New [Ru(Cp)(CH_3CN)(Binap)]X, **3**

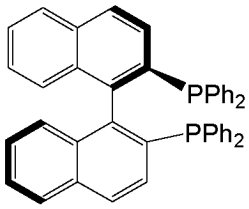

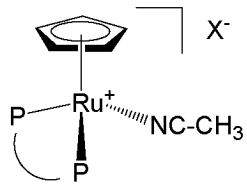

	CD_2Cl_2			*$CDCl_3$*	
	D	r_h (Å)		D	r_h (Å)
		3a (X = BF_4)			
cation	8.26	6.5	cation	6.07	6.8
anion	12.33	4.3	anion	6.14	6.8
		3b (X = CF_3SO_3)			
cation	8.16	6.6	cation	6.00	6.9
anion	12.16	4.4	anion	6.14	6.8
		3c (X= PF_6)			
cation	8.36	6.4	cation	6.13	6.8
anion	12.30	4.4	anion	6.52	6.4
		3d (X = BArF)			
cation	7.76	6.9	cation	4.78	8.6
anion	7.93	6.8	anion	4.97	8.5
		(X = Cl)			
cation	8.51	6.3	cation	6.53	6.4

	$(CD_3)_2CO$			*$CDCl_3$*	
	D	r_h (Å)		D	r_h (Å)
	3a (X= BF_4)			**2a** (X= BF_4)	
cation	10.73	6.8	cation	5.89	7.0
anion	26.84	2.7	anion	5.99	6.9
	3b (X = CF_3SO_3)			**2b**(X= CF_3SO_3)	
cation	10.51	6.9	cation	5.93	7.0
anion	24.63	2.9	anion	6.05	6.9
	3c (X = BArF)			**2c** (X = BArF)	
cation	10.64	6.8	cation	4.78	8.6
anion	26.89	2.7	anion	4.88	8.5
	3d (X= PF_6)				
cation	10.31	7.0			
anion	11.47	6.3			

It would be interesting to study the differences on varying the complexed arene, e.g., p-cymene to cyclopentadiene. **Table 2.2** contains PGSE diffusion data in dichloromethane, chloroform and acetone, for the complexes [Ru(Cp)(CH_3CN)(Binap)](anion), **3**. The values r_h are calculated via the Stokes-Einstein equation (eq. 2.4).

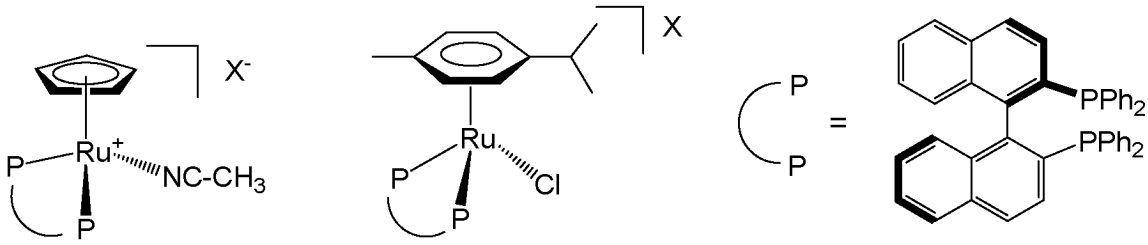

3 **2**

The salts, **3**, are useful since 1) there is very little diffusion data known for Cp-complexes 2) they give us an idea of what to expect for cationic Cp-complexes with large chelating P-donors, 3) they make for an interesting comparison with the previously measured[47] [RuCl(*p*-cymene)(Binap)]X complexes, **2** and 4) they will be good models for the results from the acetonitrile and acrylonitrile complexes which follow (See **Section 2.4**). The complexes **3** were prepared by treating the known complex [Ru(η^5-C_5H_5)(PPh_3)$_2$Cl] with BINAP , **1**, followed by abstraction of the halide using a variety of silver salts in the presence of acetonitrile. The products are [Ru(Cp)(CH_3CN)(Binap)](anion), **3**. anion = **a**, BF_4^-; **b**, $CF_3SO_3^-$; **c**, PF_6^- and **d**, BArF. Data from the neutral complex RuCl(Cp)(Binap), have also been obtained, and provide an indication as to the correct D-value, and hydrodynamic radius for this class (ca 6.3 Å-6.4 Å) in the absence of strong solvation and ion pairing.

It is clear that the chloroform data reveal tight ion pairing, i.e, close to equivalent translation rates for both cation and anion. Due to the ion pairing, these r_h values are much large in chloroform

than, e.g., dichloromethane, especially for the BArF salt. The acetone r_h values for the cations are all on the large side and this might result from adventitious water and/or solvent aggregation in the acetone, thereby strongly solvating both the cation and anion. Note that, in acetone, the BF_4^-, $CF_3SO_3^-$, and PF_6^- all give relatively small r_h values, ca 2.7Å to 2.9Å.

The dichloromethane r_h data for the anions are the most interesting. The values for the BF_4^-, $CF_3SO_3^-$, and PF_6^- anions are all relatively large and suggestive of significant ion pairing. ^1H, ^{19}F HOESY for the X = BF_4^-, $CF_3SO_3^-$ and $BArF^-$ salts have been obtained. **Fig. 2.4** shows NOE contacts from the $CF_3SO_3^-$ anion to the bound acetonitrile and Cp ligands, and some of the aromatic protons. The analogous BF_4^- spectrum shows the same contacts as the $CF_3SO_3^-$ anion; however, the $BArF^-$ anion shows no signals in the ^1H,^{19}F HOESY spectrum.

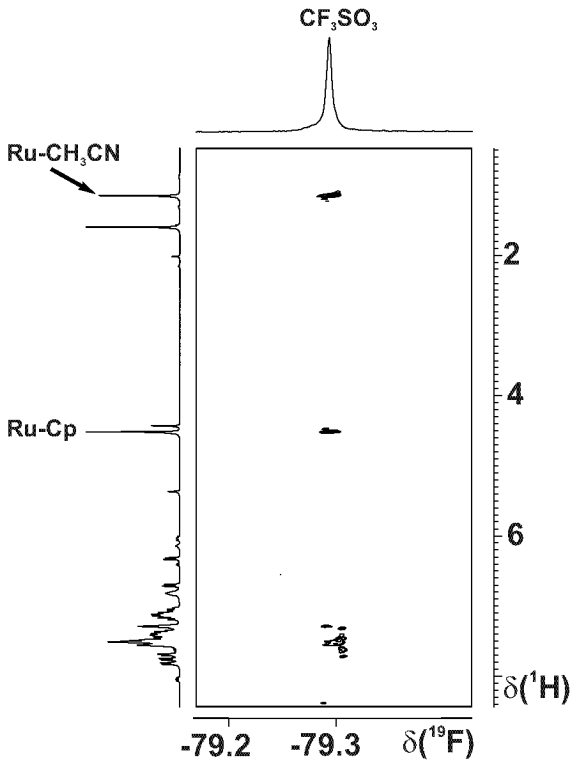

Fig. 2.4. The ^1H,^{19}F HOESY spectrum of complex Ru(Cp)(CH_3CN)(Binap)](CF_3SO_3), **3b**. The small Cp resonance at ca 4.4ppm arises from the Cp-signal for [Ru(Cp)(Binap)](CF_3SO_3)[60] in which the Binap is a 6e donor. The signal at ca 1.6ppm is from the free acetonitrile.

The strong CH_3CN contact suggests that the anion approaches the positive metal centre via the bound nitrile. In the earlier studies[47] on [RuCl(*p*-cymene)(Binap)]X complexes, the anion approaches the Ru-centre from the backside thereby avoiding the negatively charged Cl-ligand. **Table 2.2** also shows some few comparison data for **2** in chloroform. These data reveal that **2** and

3 behave similarly, but that, perhaps, the *p*-cymene complexes for X = BF_4^-, and $CF_3SO_3^-$, possess slightly large volumes (smaller D-values) than the Cp complexes.

In conclusion, this chapter has shown that the PGSE diffusion methodology constitutes a unique, sensitive and flexible tool to study the changes in ion-pairing by varying the solvents. This arises because of the solvent dependences of the observed D-values in the ruthenium salts.

2.3 Ru (II)-dppe complexes:

While water is considered as a very common ligand in coordination chemistry, far fewer examples are known of organometallic aqua complexes, since a metal center wants to be either ¨hard¨ or ¨soft¨, but not usually both at the same time[48]. It is precisely this contradiction which makes organometallic aqua complexes of special interest in terms of their reactivity. It has been proposed that the ruthenium(II) oxidation state is particularly suited for bonding conventional organometallic ligands such as CO and, at the same time, binding to water[48]. In this respect, Whittlesey *et al* reported the synthesis of Ru(II)-aqua complexes $[Ru(H_2O)_3(CO)(dppe)]X_2$[49]; this paucity led to a comparison of the diffusion results from these type of complexes with those from the earlier studied ruthenium(II) models (see **section 2.2.1**).

Results and Discussion:

Table 2.3 shows PGSE diffusion data for the Ru-aqua complexes $[Ru(H_2O)_3(CO)(dppe)]X_2$, X = BF_4^- (**4a**), $CF_3SO_3^-$ (**4b**), SbF_6^- (**4c**), $N(O_2SCF_3)_2^-$ (**4d**), in water, acetone and in one case, for the SbF_6^- anion, dichloromethane solutions.[49, 50]

Table 2.3 Diffusion constants,[a,b] and radii[c] for **4a-d** in several solvents.

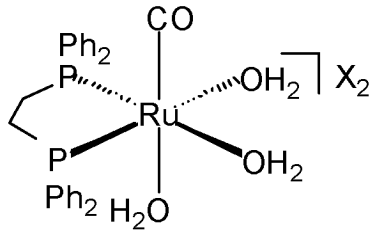

	Solvent		D	r_h (Å)
4a BF_4^-	Acetone	cation	9.36	7.7
		anion	19.88	3.6
	D_2O	cation	3.44	6.2
		anion	15.29	1.4
4b $CF_3SO_3^-$	Acetone	cation	9.24	7.8
		anion	15.58	4.6
	D_2O	cation	3.47	6.1
		anion	9.25	2.3
4c SbF_6^-	Acetone	cation	9.95	7.3
	D_2O	cation	3.30	6.5
	CD_2Cl_2	cation	6.76	7.9
4d $N(O_2SCF_3)_2^-$	Acetone	cation	9.31	7.7
		anion	17.59	4.1
	D_2O	cation	3.43	6.2
		anion	6.74	3.2
5	Acetone	cation	9.31	7.7
		anion	17.70	4.1

[a]All measurements are for 2mM solutions. Anions measured using ^{19}F and cations via ^{1}H. [b]D-values are x 10^{-10} m^2 sec^{-1}.[c]The values for the radii are given to only one number after the period. The viscosities used in the calculations (300K): CH_2Cl_2 = 0.405, $(CH_3)_2CO$ = 0.303, H_2O = 1.002. $[Ru(H_2O)(pyridine)_2(CO)(dppe)](CF_3SO_3)_2$ = **5**

These dicationic dppe complexes are only modestly stable in acetone and CD_2Cl_2 solutions, and then only in the presence of excess water. The dichloromethane data for the SbF_6^- anion, **4c** allow a comparison with [RuCl(*p*-cymene)(BINAP)]SbF_6, **2e**. Interestingly, the diffusion data suggest that the dppe complex, **4c**, is larger than complex **2e**, i.e., r_h =7.9 Å, as opposed to r_h =6.8 Å.

	Solvent		D	r_h (Å)
4c SbF_6^-	CD_2Cl_2	cation	6.76	7.9
2e SbF_6^-	CD_2Cl_2	cation	7.81	6.8

This seems strange; however, two points require further consideration: 1) the naphthyl groups of the BINAP complex may be tucked inside the shell created by the four P-phenyl groups and 2) the complexed water ligands in **4c** may hydrogen bond to anions and/or solvent.

Comparing the D and r_h values for **4a-d** in both water and acetone solutions suggests that the aqueous solutions afford well separated ions, i.e., based on the ^{19}F D and subsequent r_h values, the BF_4^-, $CF_3SO_3^-$ and $N(O_2SCF_3)_2^-$ ions are all much smaller in water than in acetone solutions. Indeed, for these same three salts, the cations in water reveal reduced radii by ca 1.5-1.6 Å. Since strong water solvation of the anions does not reduce their actual volume, the relatively large r_h-values for the cations and anions in acetone are likely to result from hydrogen bonding effects. The three

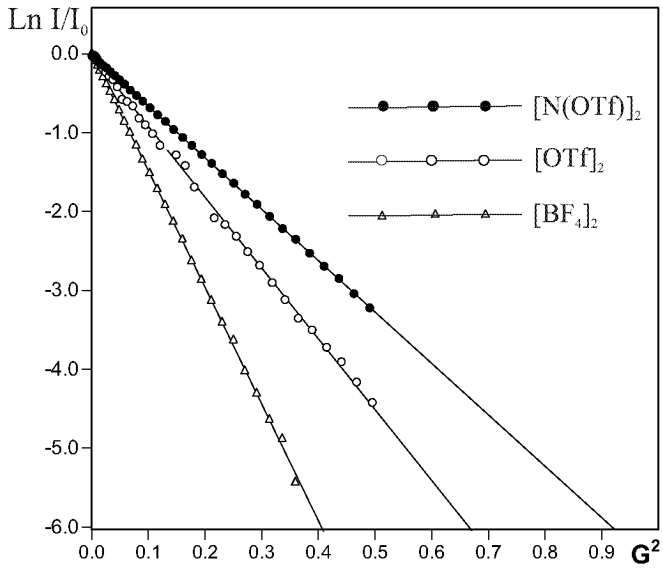

Figure 2.5 shows the translation of different anions in CD_2Cl_2 solutions.

complexed water molecules interact with the anions, thereby significantly increasing their relative averaged volumes, while simultaneously increasing the average size of the cations to a lesser extent. Moreover, the increased positive charge in the dications cannot be overlooked. **Figure 2.5** illustrates the translation of different anions in D_2O solution, the smaller the anion, the faster it diffuses.

The mono-aquo dicationic complex[51] $[Ru(H_2O)(CO)(pyridine)_2(dppe)](CF_3SO_3)_2$, **5**, was measured as a model for **4b**. The two complexed pyridine rings of **5** are expected to add to the observed cationic volume; however, based on a comparison of their D and r_h values in acetone (**Table 2.3**), this is not observed. Indeed, the two are almost identical in size. Moreover, the triflate anion in **5**, r_h = 4.1 Å, is slightly smaller than for **4b**, r_h = 4.6 Å. It is believed that these observed differences arise due to the more efficient hydrogen bonding of the triflate anion to the tris-aqua cation of **4**, relative to the mono-aqua complex **5**.

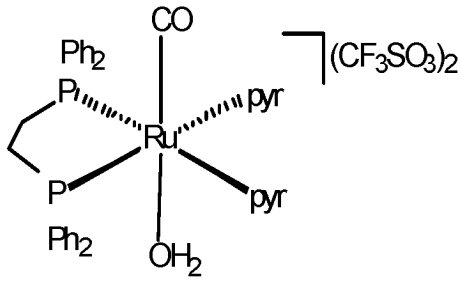

5

Conclusions: Apart from the usual effect of solvents on anions, water of solvent plays a special role. For the compounds $[Ru(H_2O)_3(CO)(dppe)]X_2$ the anion can strongly hydrogen-bond to the complexed water molecules thus creating a species with a much larger volume. This is especially true if the solvent is wet acetone.

2.4 *Ru (II)-BIPHOP complexes. Ion effects in Diels-Alder chemistry:*

Lewis acids can play a key role in organic synthesis and applications are advancing at a rapid pace[52]. The asymmetric Diels-Alder reaction between enals and dienes (see **Scheme 2.1**) has become the test reaction for chiral Lewis acids with single coordination site[53]. In these reactions chiral B, Cu and Ti compounds are often the catalysts of choice[29]. Recently, Ru[54], Rh[55], Ir[55] and Pt[56] complexes have found their way into this exciting field. The main target behind is the development of stable chiral transition metal Lewis acids that activate substrates by single point coordination and that efficiently induce asymmetry in the reaction products.

Results and discussion:

Recently[57, 58], it was found that the rate of the enantioselective Diels-Alder reaction of cyclopentadiene with methacrolein catalyzed by either [Ru(η^5-C_5H_5)(BIPHOP-F)(acetone))][Y] **6**, or [Ru(η^5-C_9H_7)(BIPHOP-F)(acetone)][Y] **7**, is markedly dependent upon the nature of the anion Y (**Scheme 2.1**). The reaction rate increased according to the order Y= BF_4^- < PF_6^- < $BArF^-$ (TFPB in graph). It would be interesting to compare these systems with the model Ru(II) complexes discussed in Chapter 2.2.2, and thus compare anion effect in different solvents.

Scheme 2.1. Ru-BIPHOP complexes in the Diels-Alder catalysis.

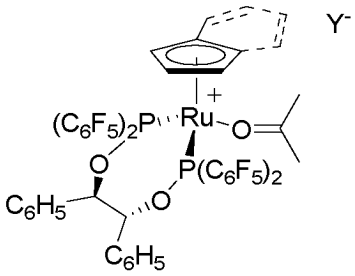

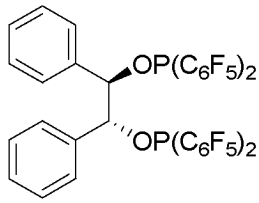

6a : η^5-C_5H_5 ; Y = BF_4^- **7a** : η^5-C_9H_7 ; Y = BF_4^-
6b : η^5-C_5H_5 ; Y = SbF_6^- **7b** : η^5-C_9H_7 ; Y = SbF_6^-
6c : η^5-C_5H_5 ; Y = $BArF^-$ **7c** : η^5-C_9H_7 ; Y = $BArF^-$

(*R*,*R*)-BIPHOP-F

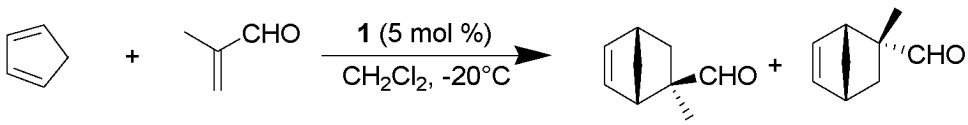

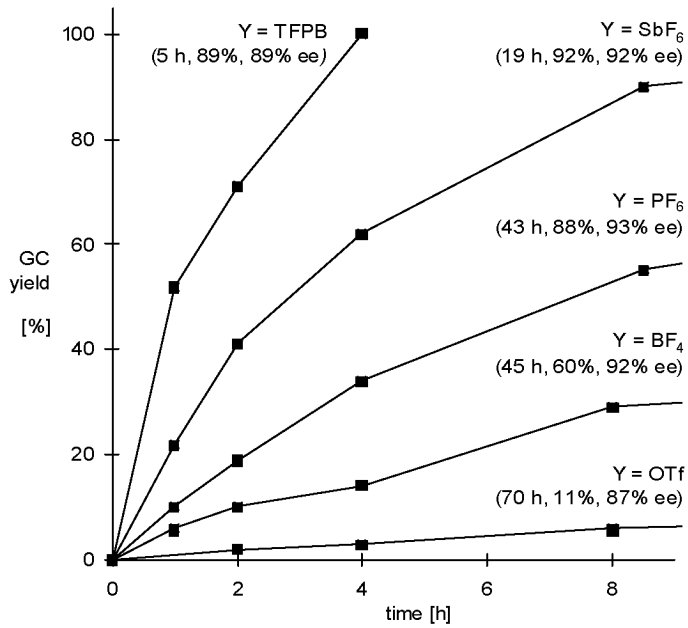

NMR measurements on model BIPHOP complexes. Attempts to use the methacrolein complex [Ru(η^5-C_5H_5)(BIPHOP-F)(OHC(CH_3)C=CH_2)][Y], **8**, directly in this study did not meet with success due to the presence of small amounts of the aquo-complex [Ru(η^5-C_5H_5)(BIPHOP-F)(H_2O)][Y], **9**. The same difficulty was encountered with the indenyl complexes where aquo-complex [Ru(η^5-C_9H_7)(BIPHOP-F)(H_2O)][Y], **10**, was present as an impurity.

The catalytic system was closely mimicked through the synthesis of the acrylonitrile complexes [Ru(η^5-C_5H_5)(NC-CH=CH_2)(BIPHOP-F)][Y], **11**, and [Ru(η^5-C_9H_7)(NC-CH=CH_2)(BIPHOP-F)][Y], **12**, (**Scheme 2.2**). The complexes **11** and **12** containing the same anions were readily obtained in quantitative yield from the reaction of the corresponding acetone complexes with excess acrylonitrile in CH_2Cl_2 at room temperature.

Scheme 2.2. Acrylonitrile complexes.

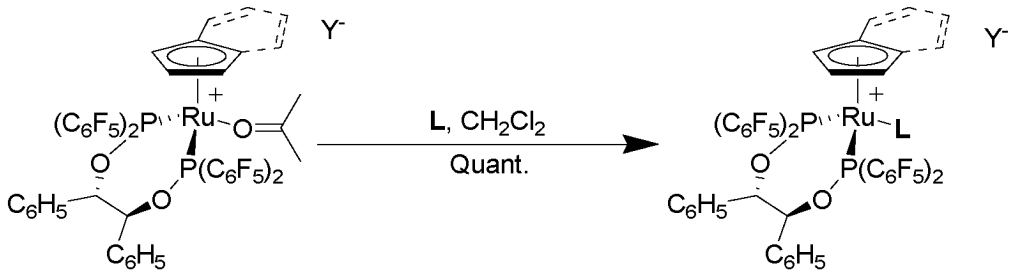

6,7

9a : η^5-C_5H_5 ; L : Water ; Y = BF_4
9b : η^5-C_5H_5 ; L : Water ; Y = SbF_6
9c : η^5-C_5H_5 ; L : Water ; Y = BArF
10a : η^5-C_9H_7 ; L : Water ; Y = BF_4
10b : η^5-C_9H_7 ; L : Water ; Y = SbF_6
10c : η^5-C_9H_7 ; L : Water ; Y = BArF

11a : η^5-C_5H_5 ; L : Acrylonitrile ; Y = BF_4
11b : η^5-C_5H_5 ; L : Acrylonitrile ; Y = BArF
12a : η^5-C_9H_7 ; L : Acrylonitrile ; Y = BF_4
12b : η^5-C_9H_7 ; L : Acrylonitrile ; Y = BArF
13a : η^5-C_5H_5 ; L : Acetonitrile ; Y = BF_4
13b : η^5-C_5H_5 ; L : Acetonitrile ; Y = BArF

The ^1H and ^{19}F PGSE results for **11** and **12** with Y = BF_4^- and $BArF^-$ in dichloromethane and acetone are given in **Table 2.4**.

Table 2.4 Diffusion Values,[b] Hydrodynamic Radii for **11a-b**, **12a-b** and **13**.

		CD_2Cl_2		$(CD_3)_2CO$	
	compound	D	r_h(Å)	D	r_h (Å)
cation [^{1}H]	**11a**, BF_4	7.84	6.8	9.72	7.5
anion [^{19}F]		9.67	5.5	27.36	2.6
cation [^{1}H]	**11b**, BArF	7.28	7.4	9.44	7.7
anion [^{1}H]		7.84	6.8	11.85	6.1
cation [^{1}H]	**12a**, BF_4	7.80	6.9	9.17	7.9
anion [^{19}F]		9.79	5.5	24.45	3.0
cation [^{1}H]	**12b**, BArF	7.20	7.4	9.16	7.9
anion [^{1}H]		7.90	6.8	11.44	6.3
cation [^{1}H]	**13a**, BF_4	7.95	6.7	9.82	7.4
anion [^{19}F]		8.96	6.0	24.19	3.0
cation [^{1}H]	**13b**, BArF	7.39	7.2	9.58	7.6
anion [^{1}H]		7.99	6.7	11.85	6.1

[b] Measured at 400 MHz, 2 mM; D values, 10^{-10} m^2 s^{-1}.

In dichloromethane solutions the experimental D-and derived r_h values for the BF_4^- anion, in both **11a** and **12a** (5.5Å) are clearly too large to arise from a simple solvate of BF_4^- and suggest surprisingly strong ion pairing. In solvents not promoting strong ion pairing, *e.g.,* acetone or methanol, the r_h value for the BF_4^- anion is normally *ca* 2.6 Å to 2.9 Å[1]. The 5.5 Å value was the largest r_h this research group has yet found for this anion in dichloromethane. However, the

cation r_h values, for **11a** and **12a**, *ca* 6.8-6.9 Å. are reasonable enough. To further explore the observed ion-pairing in dichloromethane, the ^{1}H-^{19}F HOESY spectra for **11a** and **12a** were measured. These show *selective* contacts (fragment A) to one of the methine CHO back-bone signals, the vinyl protons of the acrylonitrile, the η^5-Cp ligand and additional contacts to one phenyl group (see **Fig. 2.6**).

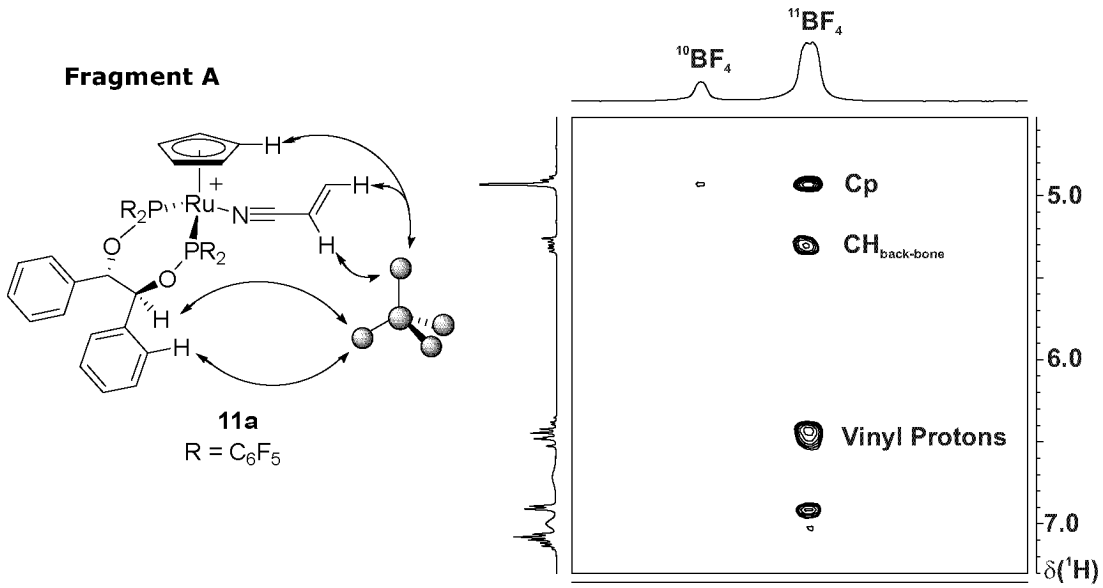

Fig. 2.6 The ^{1}H-^{19}F HOESY spectrum of complex [Ru(η^5-C_5H_5)(NC-CH=CH_2)(BIPHOP-F)][BF_4] **11a**. Note that only one of the CHO backbone resonances, at ca 5.3 ppm, shows a cross-peak and that there is selectivity to one of the phenyl rings. The second methine CHO signal appears to low frequency of the η^5-C_5H_5 resonance.

The BArF salts, **11b** and **12b**, in dichloromethane solution, both afford r_h values of 6.8 Å. These are close to what we find for the BINAP compound, **2d**, and other salts which has been reported[47]. A typical r_h value for $BArF^-$ salts in acetone or methanol is ca 6.1-6.3 Å; therefore a 6.8 Å value is consistent with some interaction, but would not be considered as a predominant ion pairing.

Solution studies on [Ru(η^5-C_5H_5)(CH_3CN)(BIPHOP-F)][BF_4] 13a.

The 5.5 Å r_h values observed in both **11a** and **12a** was sufficiently unexpected to further study the diffusion characteristics for the analogous acetonitrile complex [Ru(η^5-C_5H_5)(CH_3CN)(BIPHOP-F)][BF_4], **13a**, in dichloromethane (see **Table 2.4**). In this case, the relatively small experimental D-value, and resulting 6.0 Å r_h value for the BF_4^- anion is now so large that ion pairing has to be assumed. While not 100%, it is a major contributor to the total structure (see **Fig. 2.7**).

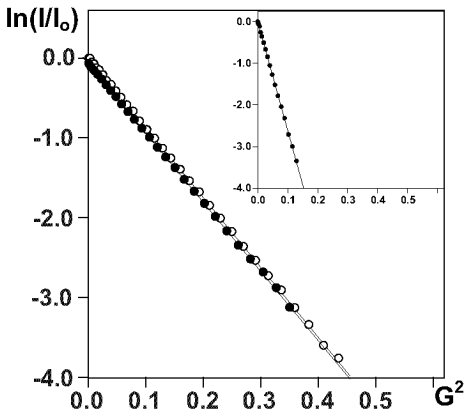

Fig. 2.7. Diffusion data for the complex [Ru(η^5-C_5H_5)(CH_3CN)(BIPHOP-F)][BF_4], **13a**, in dichloromethane . The white circles depict the translation of the cation while the black ones are those for the anion. The inset shows the diffusion for the anion in acetone-d_6

The size of the cation remains unchanged, as attaching BF_4^- does not significantly change its volume. Once again, the ^1H-^{19}F HOESY (see **Fig. 2.8**) confirms selective contacts. The r_h value from the BArF complex, **13b**, also suggests some ion-pairing; however, the absence of HOESY contacts from this anion, suggests that it lies near, but not too close to the cation.

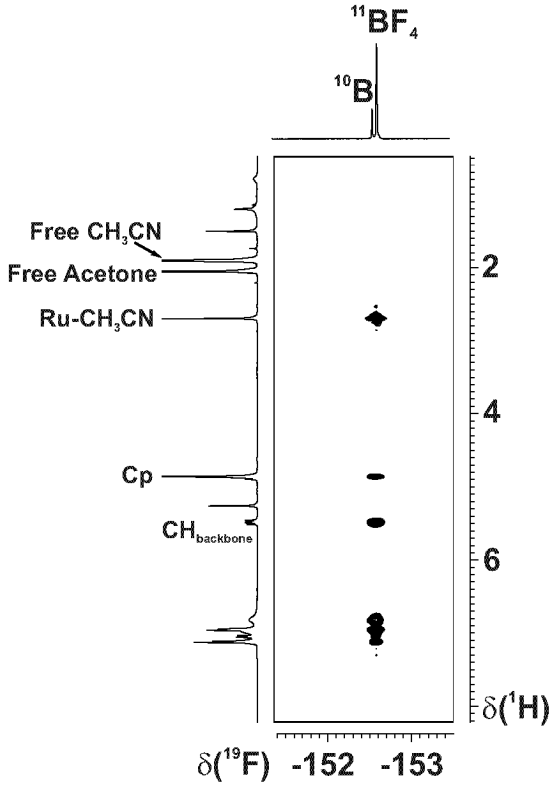

Fig. 2.8. The ^1H-^{19}F HOESY spectrum of complex [Ru(η^5-C_5H_5)(CH_3CN)(BIPHOP-F][BF_4] **13a**.

NMR Solution studies on the aquo-complexes [Ru(η^5-C_5H_5)(BIPHOP-F)(H_2O)][BF_4] 9a and [Ru(η^5-C_9H_7) (BIPHOP-F)(H_2O)][BF_4] 10a.

The aquo-complexes [Ru(η^5-C_5H_5)(BIPHOP-F)(H_2O)][BF_4], **9a** and [Ru(η^5-C_9H_7) (BIPHOP-F)(H_2O)][BF_4], **10a** are observed when the acetone analogues, e.g., [Ru(η^5-C_5H_5)(acetone)(BIPHOP-F)][BF_4] **6a**, were placed in wet acetone-d_6.

The complexed water shows a two proton resonance at *ca* δ = 3.5. Interestingly, the D-values/r_h (Å) in dichloromethane, for the BF_4^- anion (8.30/6.4 Å), water (7.86/6.8 Å) and Ru-cation (7.88/6.8 Å) are similar. This is understandable since HOESY spectroscopy shows a strong NOE between the BF_4^- and the water signal suggesting H-bonding as the source of this reduced BF_4^- translation. ^{1}H-^{1}H NOE studies show that the water signal is in slow exchange with free water and the exchange rate was estimated, based on magnetization transfer studies, to be ca 7s^{-1} in CD_2Cl_2 and 20-30 s^{-1} in CD_3COCD_3. This observation is not relevant for the Diels-Alder chemistry since the reaction solvent is dry.

Comments and conclusions. In the Diels-Alder catalytic chemistry in dichloromethane, no significant difference in the enantiomeric excesses as a function of anion is observed. However, the reaction rates are quite different. It has been established that the rate determining step for the CpRu catalyst, **6b**, is not the Diels-Alder reaction but the product/substrate exchange. This follows from the observation that the rate remains unchanged upon increasing five-fold the amount of diene[53]. Assuming that the BF_4^- anion ion-pairs strongly and is positioned close to the complexed dienophile, it may well interfere with the ligand exchange reaction sufficiently to slow the reaction. The $BArF^-$ anion is not so strongly ion paired and HOESY and X-ray[59] experiments reveal little or no contacts

between the CF_3 groups (or *ortho* aryl protons) and the cation, suggesting that this anion is not quite so close to the reactive center. Hence it is concluded that the $BArF^-$ anion is not accelerating but rather that the smaller BF_4^- anion inhibits this important step in the cycle with slower kinetics as the result.

Further, having seen the effect of the anion in different solvents on Ru-chemistry, it would interesting to extend the diffusion studies to other transition metal complexes like Rh, Pd, Pt… which will be discussed in the following chapters.

2.5 Rh (I)-MeO-Biphep complexes:

The interest in atropisomeric chelating phosphine compounds, e.g., Biphemp or MeO-Biphep, in connection with enantioselective homogeneous catalysis has continued unabated[44, 60, 61].

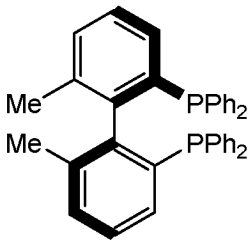

Biphemp

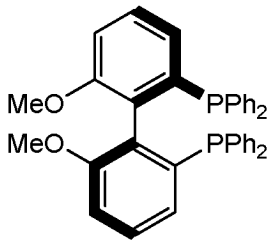

MeO-Biphep

Although these chiral auxiliaries can be used in a variety of C-C bond making reactions, much of the interest has centered on enantioselective hydrogenation[62, 63]. Within this area, catalyst precursors based on Rh(I) complexes of either 1,5-cyclooctadiene (1,5-COD) or norbornadiene have been routinely employed. Often one synthesizes a chiral salt of the type [Rh(1,5-COD)(PP)]X, **14**, where PP can represent one of the many existing atropisomeric chelating bidentate phosphine[63, 64]. This precursor reacts with molecular hydrogen to form active intermediates in the hydrogenation cycle.

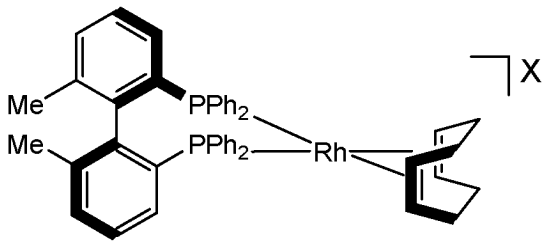

14, X=BF_4 (a), PF_6 (b), CF_3SO_3 (c)

In recent years the [2+2+1] cycloaddition of an alkyne, an alkene and CO (Pauson-Khand-type reaction), both in the intra- and intermolecular forms, has been performed catalytically using titanocenes and ruthenium, cobalt, rhodium and iridium systems[65, 66]. In particular rhodium(I) catalysts, when used in the presence of the atropisomeric diphosphine ligand Binap, give high optical yields. **Scheme 2.3** shows the [2+2+1] cycloaddition using Rh(I)-biphemp catalyst which shows an anion effect in catalysis.

Scheme 2.3. Pausan-Khand reaction by Rh(I) catalyst[67]

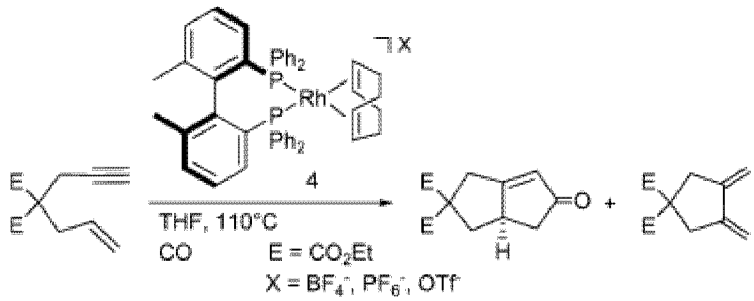

Each anion [X^-=BF_4, PF_6, OTf] shows a selectivity and difference in activity in these condensation reactions (**Figure 2.9**).

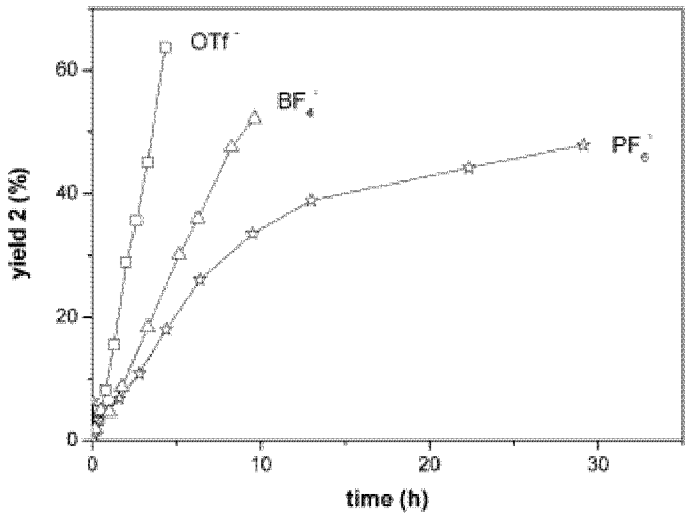

Figure 2.9. Anion effect in the cyclocarbonylation of the 1,6-enyne with [Rh(1,5-COD)(Biphemp)]X.

It is interesting that one rarely asks about the role of the anion, X, although, increasingly, one finds literature reports concerned with anion dependent homogeneously catalysed reactions. It is shown, below, that PGSE and HOESY studies reveal that all the anions do not behave the same way.

Results and Discussion:

Table 2.5. D and r_h values[a] for the complexes, **14**

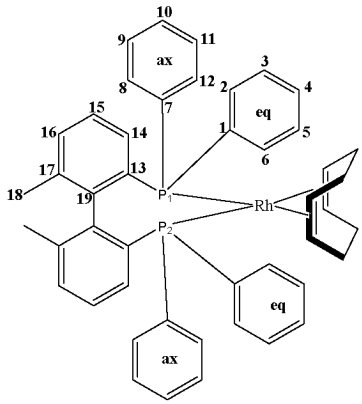

	Solvent		D[b]	r_h (Å)
14a BF_4^-	CD_2Cl_2	cation	8.68	6.2
		anion	13.38	4.0
	$CDCl_3$	cation	6.14	6.8
		anion	6.41	6.5
14b PF_6^-	CD_2Cl_2	cation	8.61	6.2
		anion	12.13	4.4
	$CDCl_3$	cation	6.23	6.7
		anion	5.97	6.9
14c $CF_3SO_3^-$	CD_2Cl_2	cation	8.79	6.1
		cation	12.04	4.4
	$CDCl_3$	cation	6.00	6.9
		anion	5.72	7.2

[a]2mM solutions in CD_2Cl_2. [b] ($\times 10^{-10}$ m^2 s^{-1}).

Table 2.5 shows D-values in dichloromethane and chloroform for **14** derived from PGSE measurements on 2mM solutions using ^1H (for the cation) and ^{19}F (for anion) as NMR probes. The following points are relevant: 1) As expected in dichloromethane, the cations are moving slower than the anions. 2) The strongly solvated anions, as 2 mM solutions in methanol,[1, 20, 47] afford r_h values of ca 2.7Å, 2.7Å and 3.1 Å, for BF_4^-, PF_6^- and CF_3 SO_3^-, respectively, i.e., much smaller values than those observed in **14**.

3) Consequently, the observed r_h values of > 4 Å, for all three salts, imply a significant amount of ion pairing. This ion pairing in solution is somewhat in contrast to the solid-state structure of **14a** in which the BF_4^- appears rather remote from the complex cation (see **Figure 2.9** for X-ray structure of cation). The relatively large r_h values for the cations in $CDCl_3$ arise due to the ion-pairing[1, 9, 20, 37, 47] (see **figure 2.10** and **Table 2.5**). The surprisingly large r_h values for the anions in **14b** and **14c** are believed to the additional aggregation due to the observed 2-3 equivalents of H_2O in the $CDCl_3$ samples.

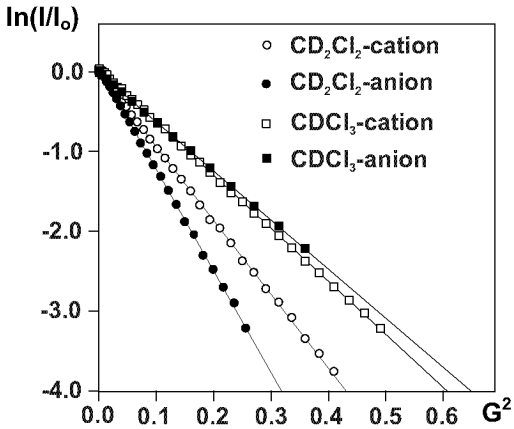

Figure 2.10 illustrates the diffusion of **14a** in two different solvents.

The presence of some ion pairing suggests possible close contacts which was investigated via ^1H,^{19}F HOESY measurements. This approach is slowly winning support as the method of choice for recognizing the structural implications of anion/cation interactions.[1, 5, 18, 68] **Figure 2.11** shows HOESY data for **14a**, from which an interesting selectivity is observed. It is found that the BF_4^- anion can be close to both of the two non-equivalent sets of *ortho* P-phenyl resonances (see inset in HOESY and the grey ball in X-ray which shows the approximate position of the anion).

There are also relatively strong contacts to *one* of the Biphemp backbone protons, H-14, and to only *one* of the two olefinic resonances plus a contact to a methylene group in the 1,5-COD. This latter resonance corresponds, presumably, to a CH_2 adjacent to the =CH showing the contact. There are no contacts to the Biphemp methyl group. Clearly the BF_4^- anion is choosing a selective pathway (presumably toward the slightly positive P-atoms) and does not drift around the periphery of the cation.

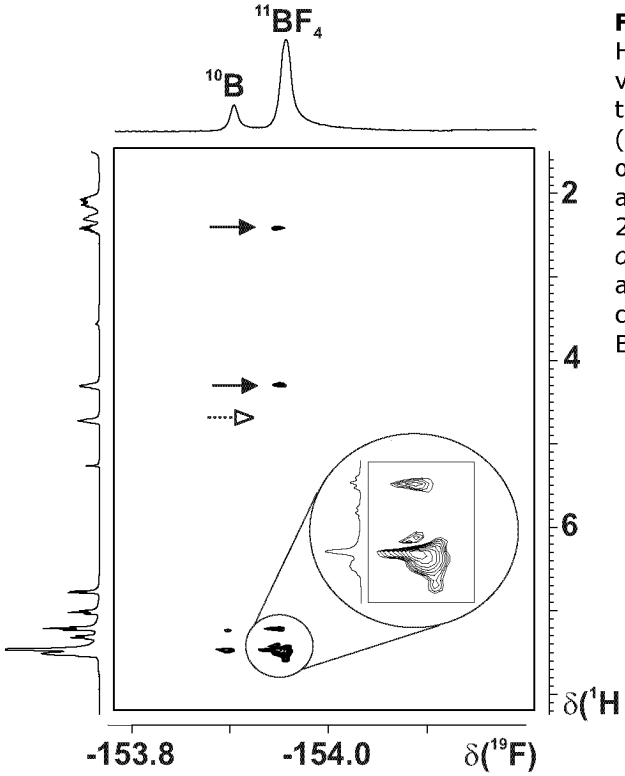

Figure.2.11 Section of the $^1H,^{19}F$ HOESY spectrum for **14a** showing various selective contacts to: a) One of the olefinic proton of the 1,5- COD (bold arrow, δ = 4.37) and not to the other (dashed arrow, δ = 4.72). b) One aliphatic proton of the 1,5- COD, δ = 2.58. c) Two non-equivalent sets of *ortho* P-phenyl resonances, δ = 7.21 and δ = 7.46 and d) a broad signal covering H-14, δ ca 7.5, from the Biphemp backbone. (CD_2Cl_2, 400MHz)

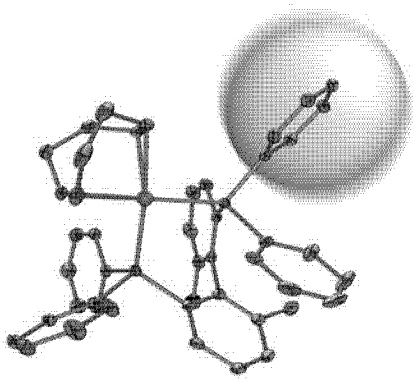

The analogous $^1H,^{19}F$ HOESY data for the PF_6^- salt **14b** again show contacts to the two non-equivalent sets of *ortho* P-phenyl resonances (pseudo-equatorial *stronger* than the pseudo-axial P-Phenyl ring) and one to H-14 from the Biphemp backbone(see **Figure 2.12**), but *no relatively strong contacts to the 1,5-COD ligand*.

For the triflate, **14c**, there are now generally *much weaker*

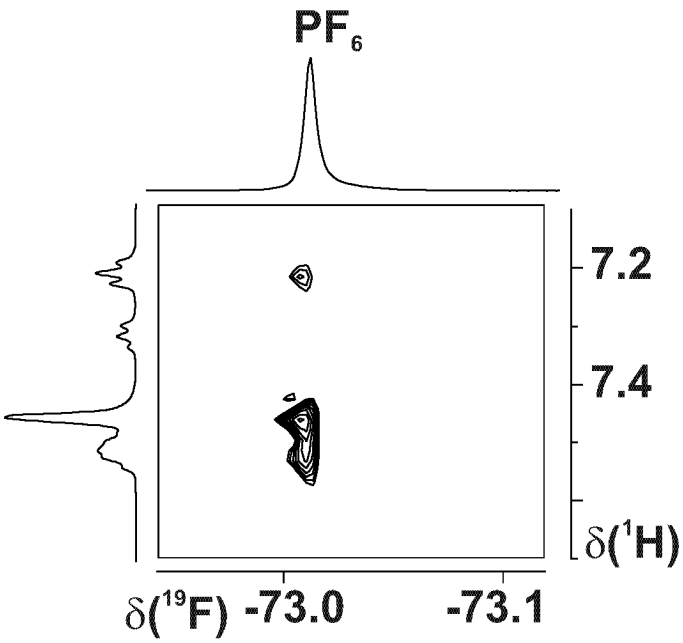

Figure 2.12 Section of the $^{19}F,^1H$- HOESY showing stronger contacts to the *ortho* protons of the pseudo-equatorial P-phenyl ring and to one proton, H-14, at ca 7.5 ppm, from the Biphemp backbone. There is a weaker contact to the *ortho* protons of the pseudo-axial P-phenyl ring and no contact to the olefinic protons. The 7.5 resonance is obscured by overlap with *meta* protons of the pseudo-equatorial P-phenyl ring

contacts. Specifically, the *ortho* P-phenyl resonances of the pseudo-equatorial ring are relatively strong, but there is a much weaker interaction with the pseudo-axial ring, and again nothing to the 1,5-COD.

The $^{1}H,^{19}F$ HOESY results point towards selective and related, but different motions for the three anions in **14**. The smaller BF_4^- anion can penetrate more effectively, and thus affords a larger number of slightly stronger NOE contacts. Although the PF_6^- anion is not much larger, it no longer comes as close to the coordinated 1,5-COD. The larger triflate finds an even more specific pathway, such that it avoids the coordinated 1,5-COD and seems to be more remote relative to the PPh_2 groups. Admittedly, the ^{19}F probe in the triflate anion is further removed (since the oxygen of the triflate carries the negative charge); nevertheless, the single strong observed NOE's are to the same positions as noted for **14a** and **14b**.

Conclusions: Selectivity in the approach of an anion to a transition metal cation has been noted in only a few cases, e.g., by Macchioni[17] and this laboratory[69]. Further, it is interesting that, although the bonding to the ligands is not influenced, each of the anions in **14** demonstrates its individuality.

2.6 Pd(II)-Oxazoline Complexes:

Since the pioneering work of Drent[70], the copolymerization of styrene or styrene analogues with carbon monoxide, catalyzed by palladium complexes, has been extensively investigated. Pd(II) complexes containing nitrogen bidentate or bioxazoline ligands with weakly coordinating anions have been used as active precatalysts. The reaction conditions involve high CO pressure, fairly high temperature and methanol as solvent.

Recently Consiglio and coworkers[71] showed the use of palladium complexes $[(N,N)Pd(H_2O)_2](X)_2$, where N,N = bis-oxazoline, as catalyst precursors, lead to polymers having all possible limiting steric structures (*isotactic*, *atactic*, *syndiotactic*), depending on copolymerisation reaction conditions. As these aquo complexes are quite unstable, more stable complexes [Pd((*R,S*)-Bz-BIOX)$(CH_3)(NCCH_3)$](X), **15** where X = CF_3SO_3(**a**), BF_4(**b**) and PF_6 (**c**)were prepared[72], and used as catalysts. The complexed acetonitrile complexes showed an anion effect in the copolymerization reactions, hence were subjected to diffusion and $^1H,^{19}F$-HOESY measurements.

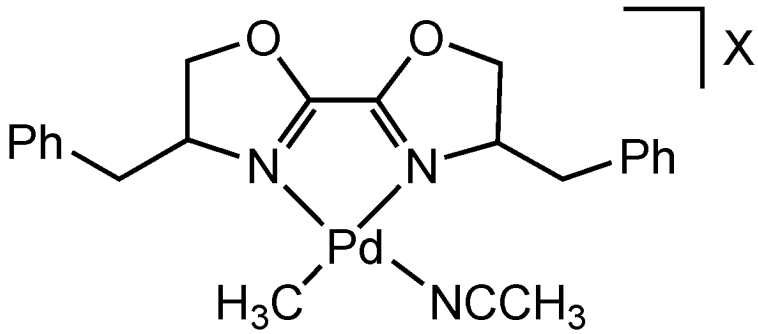

15 , X = CF_3SO_3(**a**), BF_4(**b**) and PF_6 (**c**)

Results and discussion

The complexes **15a-c** were characterized at room temperature in dichloromethane by ^{1}H, ^{13}C, ^{19}F, one dimensional spectra, plus ^{1}H-^{1}H COSY, ^{1}H-^{1}H NOESY , ^{13}C-^{1}H one-bond and long range correlation experiments. **Figure 2.13** depicts a section of the COSY in the benzylic proton region for complex **15c**. This figure allows us to distinguish between the weakly coupled AB spin system (δ= 2.77 and 3.04) and a strongly coupled AB spin system centered at δ= 2.93. ^{1}H-^{1}H NOESY measurements indicate that the weakly coupled benzylic protons were close to the complexed methyl group and those of strongly coupled spins close to the bound acetonitrile. These assignments were crucial for the discussion which follows.

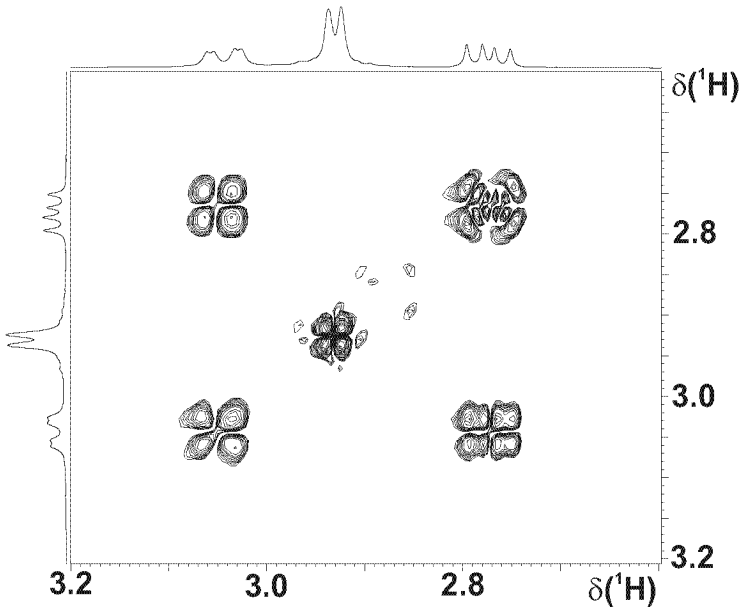

Figure. 2.13. Benzyl section of ^{1}H-^{1}H COSY for [Pd(BzBIOX)(CH_3)($NCCH_3$)](PF_6), (**15c**).

Pulsed-Gradient Spin-Echo (PGSE) diffusion measurements

The diffusion constants, D, from the PGSE measurements in dichloromethane/methanol (9:1) solutions on the salts [Pd((R,S)-Bz-BIOX)(CH_3)($NCCH_3$)](X),**15a-c**, are presented in **Table 2.6**.

Table 2.6. Diffusion coefficients measured for the complexes [Pd((R,S)-Bz-BIOX)(CH_3)($NCCH_3$)](X) (**15a-c**) in CD_2Cl_2: CD_3OD, 9:1.

X		Diff. coeff (D)	Radius[a] (r)
	cation	8.71	6.1
CF_3SO_3 **15a**	anion	11.01	4.9
	cation	8.80	6.1
BF_4 **15b**	anion	12.50	4.3
	cation	8.54	6.3
PF_6 **15c**	anion	11.60	4.6

[a] using viscosity of CH_2Cl_2 =0.410

While the D-values for the three cations do not differ much as a function of the anion, the r_h values for the anions suggest differing degrees of ion pairing. It is now known that dichloromethane solutions usually promote ion-pairing in salts of various transition metals[9, 20, 37]. For **15a-c** the highest degree of ion-pairing was found with triflate as the counterion, although the differences are not dramatic.

The effect of methanol as co-solvent was uncertain so that the D-values were measured for a model complex, **16**, which (1) was soluble in dichloromethane, methanol and dichloromethane/ methanol (9:1), (2) has the anion of interest and (3) has an oxazoline ring bound to palladium. These data (see **Table 2.7**) suggest that the ca 10% methanol has no effect, on the cation, and only a small effect on the triflate.

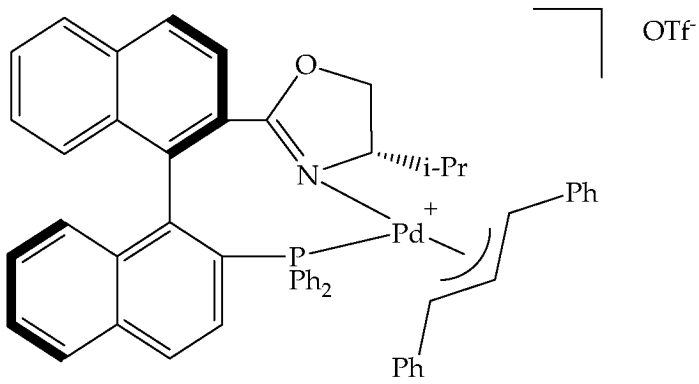

Model complex 16

Table 2.7. Diffusion Coefficients for the model complex **16**.

Complex Y		Diff. coeff (D)	Radius (r)
CD_2Cl_2	cation	8.02	6.7[a]
	anion	12.67	4.2[a]
CD_3OD	cation	5.92	7.0[b]
	anion	12.89	3.2[b]
CD_2Cl_2: CD_3OD (9:1)	cation	7.82	6.8[c] (6.7[d])
	anion	13.00	4.1[c] (4.0[d])

[a] viscosity of CH_2Cl_2 = 0.410, [b] viscosity of CH_3OH = 0.526,
[c] using viscosity of CH_2Cl_2, [d] viscosity of 90% CD_2Cl_2 + 10% CD_3OD = 0.422

$^{19}F,^{1}H$-HOESY NMR experiments

$^{19}F,^{1}H$-HOESY methods provide useful structural tools for salts with fluorine containing anions in that they help to localize the position of the counter-ion with respect to the cation. For the complex **15a** (X = CF_3SO_3) the $^{19}F,^{1}H$-HOESY spectrum shows a series of modest strength cross-peaks connecting the fluorine spins of the triflate to the protons of: a) palladium methyl b) the bound acetonitrile c) several oxazoline aliphatic protons and d) an aromatic resonance (**Figure 2.14**).

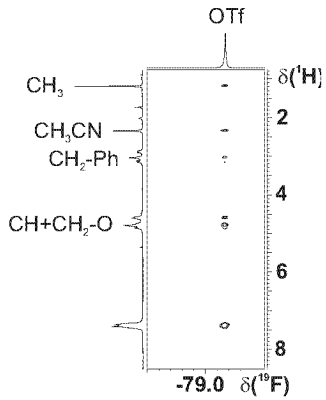

Fig. 2.14. ($^{1}H,^{19}F$)-HOESY spectra of complex [Pd((R,S)-Bz-BIOX)(CH_3)($NCCH_3$)] (CF_3SO_3) (**15a**)

The analogous spectrum for **15b** (and **15c**) is noteworthy in that the contact to the palladium methyl is *absent* and the cross-peak to the acetonitrile is stronger (see **Figures 2.14 and 2.15**). Based on detailed proton assignments for **15b,c**, it would appear that the BF_4^- and PF_6^- anions take up selective positions close to the acetonitrile ligand and closer to one half of the bidentate oxazoline ligand, i.e., the anion prefers to avoid the region of the negatively charged Pd-CH_3 group. This type of selective behavior for an anion is not unusual[73-75] [17].

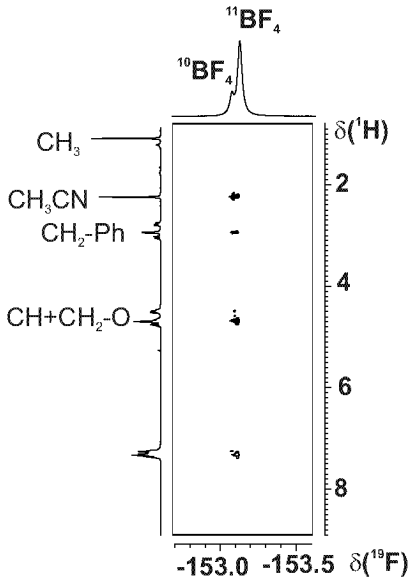

Fig. 2.15. (^{1}H,^{19}F)-HOESY spectra of complex [Pd((R,S)-Bz-BIOX)(CH_3)($NCCH_3$)](BF_4) (**15b**). Note the absence of a cross-peak involving the Pd-CH_3 group.

Comments and Conclusion: Based on all of the NMR data, it would seem that the triflate anion is, partially, occupying a pseudo fifth position on the side of the cation remote from the two benzyl-groups since it is in contact with both the Pd-CH_3 and Pd-$NCCH_3$ moieties. The ion-pairing is not 100%; however, assuming that a hydrodynamic radius, r_h of ca 3.0-3.2Å would be a reasonable estimate for a methanol solvated triflate[1], and that 100% ion-pairing would give an r_h value of ca 6.1Å, then the observed value of 4.9Å is suggestive of ca. 50-55% ion-pairing. Possibly, the difference in size between OTf^- and e.g. BF_4^-, combined with the differences in relative position and ion-pairing could lead to some difference in reactivity for the cation.

2.7 Concluding Remarks and future prospects:

NMR is not a very sensitive method; indeed, most methods are far more amenable to quantitative results. Nevertheless, its proven flexibility makes it indispensable. NMR will not replace X-ray crystallography, but its breath of applications makes it extremely attractive.

Conventional NMR methods depend on the interpretation of interactions explicitly included in the spin Hamiltonians, i.e., chemical shifts, scalar, dipolar and quadrupolar coupling constants. An empirically well-established parameter-to-structure relationship is generally essential for elucidating complex molecular structures. As the spin interactions tend to be rather local, it is often tedious to describe overall molecular properties such as size, shape, mass and charge. In this respect, the size and shape sensitive NMR techniques based on pulsed field gradient spin-echo methods add an invaluable tool to the coordination chemists' armory. With i) the widespread availability of self-shielded gradient equipment, ii) the proven reproducibility of results iii) the straightforward interpretation of "size", PGSE methods will find frequent application in solving problems in coordination chemistry and iv) the development of pulse sequences and gradient hardware has facilitated rapid, accurate, simple, selective and specific analysis of many systems.

The future of PGSE NMR is bright

(i) Commercially available spectrometers equipped with cryoprobes can be used to measure even smaller solute concentrations, which will be physiologically relevant to drug concentrations.

(ii) Characterization of the diffusion dynamic range for binding constant values will provide an insight into the technique's ability to distinguish between free and bound ligands, based on measured changes in diffusion coefficients when proteins are introduced.

(iii) With appropriate data processing schemes, becomes exceptionally valuable tool for mixture analysis, the separation of which is based on the molecular size.

(iv) Studying the role of the solvents in the electrolyte medium used in lithium batteries, based on the ability to recognize the ion-pairing.

It remains to be seen how far the PGSE NMR technique can find its application in other exciting fields of research.

2.8 Bibliography

[1] P. S. Pregosin, E. Martinez-Viviente and P. G. A. Kumar, *Dalton Trans.* **2003**, 4007-4014.

[2] D. E. Babushkin and H. Brintzinger, *J. Am.Chem. Soc.* **2002**, *124*, 12869-12873.

[3] E. J. Cabrita and S. Berger, *Magn. Reson. Chem.* **2001**, *39*, S142-S148.

[4] D. Zuccaccia, S. Sabatini, G. Bellachiom, G. Cardaci, E. Clot and A. Macchioni, *Inorg. Chem.* **2003**, *42*, 5465-5467.

[5] A. Burini, J. P. Fackler, R. Galassi, A. Macchioni, M. A. Omary, M. A. Rawashdeh-Omary, B. R. Pietroni, S. Sabatini and C. Zuccaccia, *J. Am. Chem. Soc.* **2002**, *124*, 4570-4571.

[6] C. Zuccaccia, G. Bellachioma, G. Cardaci and A. Macchioni, *Organometallics* **2000**, *19*, 4663-4665.

[7] N. E. Schlörer, E. J. Cabrita and S. Berger, *Angew. Chem.Int. Ed. Engl.* **2002**, *41*, 107-109.

[8] L. Avram and Y. Cohen, *J. Am.Chem. Soc.* **2002**, *124*, 15148-15149.

[9] M. Valentini, H. Ruegger and P. S. Pregosin, *Helv. Chim. Acta* **2001**, *84*, 2833-2853.

[10] W. S. Price, *Concepts Magn. Resonance* **1997**, *9*, 299-336.

[11] W. S. Price, *Concepts Magn. Resonance* **1998**, *10*, 197-237.

[12] P. Stilbs, *Prog. NMR Spectr.* **1987**, *19*, 1.

[13] P. Griffiths and P. Stilbs, *Current Opinion in Colloid & Interface Science* **2002**, *7*, 249-252.

[14] W. S. Price, P. Stilbs and O. Soderman, *J. Magn. Reson.* **2003**, *160*, 139-143.

[15] N. G. Stahl, C. Zuccaccia, T. R. Jensen and T. J. Marks, *J Am. Chem Soc.* **2003**, *125*, 5256-5257.

[16] R. K. Harris, K. A. Kinnear, G. A. Morris, M. J. Stchedroff and A. Samadi-Maybadi, *Chem. Commun.* **2001**, 2422-2423.

[17] A. Macchioni, *Eur. J.Inorg. Chem.* **2003**, 195-205.

[18] G. Bellachioma, g. Cardaci, A. Macchioni, G. Reichenbach and S. Terenzi, *Organometallics* **1996**, *15*, 4349-4351.

[19] D. Nama, Kumar, P. G. A., Pregosin, P. S., *Magn. Reson. Chem.* **2005**, *43*, 246-250.

[20] E. Martinez-Viviente, H. Ruegger, P. S. Pregosin and J. Lopez-Serrano, *Organometallics* **2002**, *21*, 5841-5846.

[21] I. Fernandez, E. Martinez-Viviente and P. S. Pregosin, *Inorg. Chem.* **2004**, *43*, 4555-4557.

[22] A. Pichota, P. S. Pregosin, M. Valentini, M. Wörle and D. Seebach, *Angew. Chem.Int. Ed. English* **2000**, *112*, 153-156.

[23] C. Zuccaccia, N. G. Stahl, A. Macchioni, M.-C. Chen, R. J. A. and T. J. Marks, *J. Am. Chem. Soc.* **2004**, *126*, 1448-1464.

[24] K. Fagnou and M. Lautens, *Angew. Chem. Int. Ed. Engl.* **2002**, *41*, 27-47.

[25] Y.-X. Chen, M. V. Metz, L. Li, C. L. Stern and T. J. Marks, *J. Am. Chem. Soc.* **1998**, *120*, 6287-6305.

[26] A. Macchioni, G. Bellachioma, G. Cardaci, M. Travaglia, C. Zuccaccia, B. Milani, G. Corso, E. Zangrando, G. Mestroni, C. Carfagna and M. Formica, *Organometallics* **1999**, *18*, 3061-3069.

[27] E. P. Kündig, C. M. Saudan and G. Bernardinelli, *Angew. Chem.* **1999**, *111*, 1298-1301.

[28] E. P. Kündig, C. M. Saudan and F. Viton, *Adv. Synth. Catal.* **2001**, *343*, 51-56.

[29] D. A. Evans, J. A. Murray, P. von Matt, R. D. Norcross and S. J. Miller, *Angew. Chem.* **1995**, *107*, 864-867.

[30] U. Burckhardt, M. Baumann and A. Togni, *Tet. Asymm.* **1997**, *8*, 155-159.

[31] C. Bianchini, C. Mealli, M. Peruzzini and F. Zanobini, *J. Am. Chem. Soc.* **1992**, *114*, 5905.

[32] B. Binotti, A. Macchioni, C. Zuccaccia and D. Zuccaccia, *Comments on Inorganic Chemistry* **2002**, *23*, 417-450.

[33] K. Gruet, E. Clot, O. Eisenstein, D. H. Lee, B. Patel, A. Macchioni and R. H. Crabtree, *New J. Chem.* **2003**, *27*, 80-87.

[34] A. Macchioni, A. Magistrato, I. Orabona, F. Ruffo, U. Rothlisberger and C. Zuccaccia, *New J. Chem.* **2003**, *27*, 455-458.

[35] B. Binotti, C. Carfagna, E. Foresti, A. Macchioni, P. Sabatino, C. Zuccaccia and D. Zuccaccia, *J. Organomet. Chem.,* **2004**, *689*, 647-661.

[36] M. Aresta, A. Dibenedetto, I. Papai, G. Schubert, A. Macchioni and D. Zuccaccia, *Chem.-Eur. J.* **2004**, *10*, 3708-3716.

[37] E. Martinez-Viviente and P. S. Pregosin, *Inorg. Chem.* **2003**, *42*, 2209-2214.

[38] E. Martinez-Viviente, P. S. Pregosin, L. Vial, C. Herse and J. Lacour, *Chem. Eur. J.* **2004**, *10*, 2912-2918.

[39] R. Noyori and S. Hashiguchi, *Acc. Chem. Res.* **1997**, *30*, 97-102.

[40] R. Noyori and H. Takaya, *Acc. Chem. Res.* **1990**, *23*, 345.

[41] T. Geldbach, P. S. Pregosin, A. Albinati and F. Rominger, *Organometallics* **2001**, *20*, 1932-1938.

[42] T. J. Geldbach, D. Drago and P. S. Pregosin, *J. Chem. Soc. Chem. Commun.* **2000**, 1629.

[43] T. J. Geldbach, D. Drago and P. S. Pregosin, *J. Organomet. Chem.* **2002**, *643*, 214-222.

[44] T. J. Geldbach and P. S. Pregosin, *Helv. Chim. Acta* **2002**, *85*, 3937-3948.

[45] A. G. Orpen, L. Brammer, F. H. Allen, O. Kennard, D. G. Watson and R. Taylor, *J. Chem. Soc. Dalton* **1989**, S1-S83.

[46] G. Bellachioma, B. Binotti, G. Cardaci, C. Carfagna, A. Macchioni, S. Sabatini and C. Zuccaccia, *Inorg. Chim. Acta* **2002**, *330*, 44-51.

[47] P. G. A. Kumar, P. S. Pregosin, J. M. Goicoechea and M. K. Whittlesey, *Organometallics* **2003**, *22*, 2956-2960.

[48] U. Kölle, *Coord. Chem. Rev.* **1994**, *135-136*, 623.

[49] M. Mahon, M. K. Whittlesey and P. T. Wood, *Organometallics* **1999**, *18*, 4068-4074.

[50] M. D. Hargreaves, M. F. Mahon and M. K. Whittlesey, *Inorg. Chem.* **2002**, *41*, 3137-3145.

[51] J. M. Goicoechea, M. D. Hargreaves, M. F. Mahon and M. K. Whittlesey, *unpublished results*.

[52] H. Kagan and O. Riant, *Chem. Rev.* **1992**, *92*, 1007-1019.

[53] E. P. Kundig, C. M. Saudan and G. H. Bernardinelli, *Angew. Chem.* **1999**, *111*, 1298-1301.

[54] A. J. Davenport, D. L. Davies, J. Fawcett, S. A. Garratt and D. R. Russell, *J. Chem. Soc. Dalton Trans.*. **2000**, 4432-4441.

[55] D. Carmona, F. J. Lahoz, S. Elipe and L. A. Oro, *Organometallics* **2002**, *21*, 5100-5114.

[56] N. M. Brunkan and M. R. Gagne, *Organometallics* **2002**, *21*, 1576-1582.

[57] E. P. Kundig, C. M. Saudan and F. Viton, *Advanced Synthesis & Catalysis* **2001**, *343*, 51-56.

[58] E. P. Kundig, M. C. Saudan, V. Alezra, F. Viton and G. Bernardinelli, *Angew. Chem. Int. Ed.* **2001**, *40*, 4481.

[59] P. G. A. Kumar, P. S. Pregosin, M. Vallet, G. Bernardinelli, R. F. Jazzar, F. Viton and E. P. Kuendig, *Organometallics* **2004**, *23*, 5410-5418.

[60] C. J. den Reijer, P. Dotta, P. S. Pregosin and A. Albinati, *Canad. J.Chem.* **2001**, *79*, 693-704.

[61] N. Feiken, P. S. Pregosin and G. Trabesinger, *Organometallics* **1997**, *16*, 3735-3736.

[62] R. Noyori, *Advanced Synthesis & Catalysis* **2003**, *345*, 1-1.

[63] E. de Wolf, A. L. Spek, B. W. M. Kuipers, A. P. Philipse, J. D. Meeldijk, P. H. H. Bomans, P. M. Frederik, B. J. Deelman and G. van Koten, *Tetrahedron* **2002**, *58*, 3911-3922.

[64] M. T. Reetz, L. J. Goossen, A. Meiswinkel, J. Paetzold and J. F. Jensen, *Org. Lett.* **2003**, *5*, 3099-3101.

[65] S. E. Gibson and A. Stevenazzi, *Angew. Chem.-Int. Edit.* **2003**, *42*, 1800-1810.

[66] J. Blanco-Urgoiti, L. Anorbe, L. Perez-Serrano, G. Dominguez and J. Perez-Castells, *Chem. Soc. Rev.* **2004**, *33*, 32-42.

[67] T. M. Schmid and G. Consiglio, *Chem. Comm.* **2004**, 2318-2319.

[68] C. Zuccaccia, A. Macchioni, I. Orabona and F. Ruffo, *Organometallics* **1999**, *18*, 4367-4372.

[69] D. Drago, P. S. Pregosin and A. Pfaltz, *Chem. Comm.* **2002**, 286-287.

[70] E. Drent and P. H. M. Budzelaar, *Chem. Revs.* **1996**, *96*, 663-681.

[71] A. Gsponer, B. Milani and G. Consiglio, *Helv. Chim. Acta* **2002**, *85*, 4074-4078.

[72] D. Sirbu, G. Consiglio, B. Milani, P. G. A. Kumar, P. S. Pregosin, S. Gischig, *J.Organomet.Chem* **2005**, *Accepted*.

[73] A. Macchioni, C. Zuccaccia, E. Clot, K. Gruet and R. H. Crabtree, *Organometallics* **2001**, *20*, 2367-2373.

[74] G. Bellachioma, G. Cardaci, A. Macchioni and C. Zuccaccia, *J. Organomet. Chem.* **2000**, *594*, 119-126.

[75] B. Binotti, A. Macchioni, C. Zuccaccia and D. Zuccaccia, *Comments Inorganic Chem.* **2002**, *23*, 417-450.

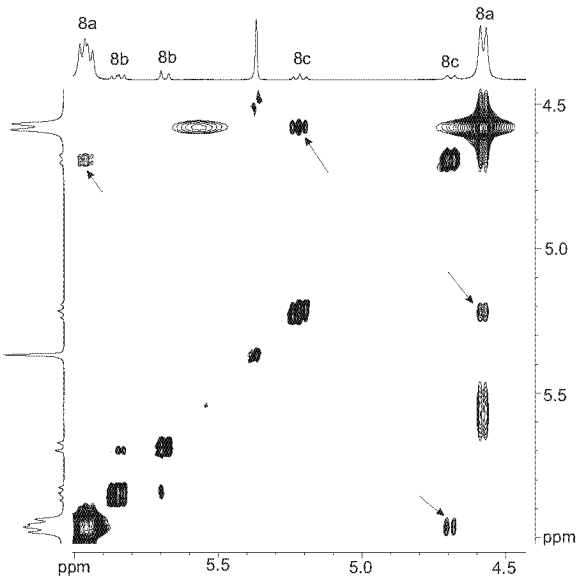

Chapter 3

Multidimensional NMR Solution Studies on Chiral Phosphine Complexes

3.1 Introduction:

Nucleophilic attack on transition metal-complexed olefin, diene and dieneyl systems is among the most useful of organometallic processes for the synthesis of complex organic molecules. Not only does complexation reverse the normal reactivity of these functional groups, changing them from nucleophiles to electrophiles, but the process also results in the formation of new bonds between the nucleophile and the olefinic carbon and new metal-carbon bonds that can be elaborated[1,2].

3.1.1 π-Olefin complexes

Olefin complexes of many metals are wide spread in literature but Palladium is the most versatile and widely used in organic transformations[3]. Palladium(II)-olefin complexes gained such an importance as they are both easily generated and highly reactive. Palladium chloride is the most common catalyst precursor which is commercially available. However the oligomer is easily disrupted by treatment with alkali metal chlorides, such as LiCl or NaCl, providing the considerably more soluble, hygroscopic monomeric palladate, M_2PdCl_4. Numerous Pd(II) complexes of the type L_2PdCl_2 are easily formed from $PdCl_2$ and the appropriate ligand L. The most useful Pd(II) complexes are $PdCl_2(PPh_3)_2$, $Pd(OAc)_2$ and $PdCl_2(RCN)_2$.

Palladium(II) complexes are extremely important in organopalladium chemistry. They are typically electrophilic, soluble in most common organic solvents, and stable to air. Thus, they are easily stored and handled. The most common organic substrates for Pd(II) are electron-rich species, such as olefins, alkynes and arenes.

The intramolecular cyclization of palladium π-olefin and π-alkyne complexes is a powerful method in organic synthesis. This process involves the fast and reversible complexation of the olefin or alkyne by a Pd(II) salt. The resulting π-olefin or π-alkyne complexes are stable but reactive in the presence of a nucleophile. Nucleophilic attack on the π-olefin species usually occurs anti to the metal at the more substituted vinylic carbon to give a σ-alkylpalladium(II) complex, which may undergo a wide variety of processes. Depending on the reaction conditions, these subsequent processes may involve palladium β-hydride elimination, reduction, nucleophilic substitution of the metal, transmetalation, or various insertion processes as outlined in **Scheme 3.1**.

Scheme 3.1[3]

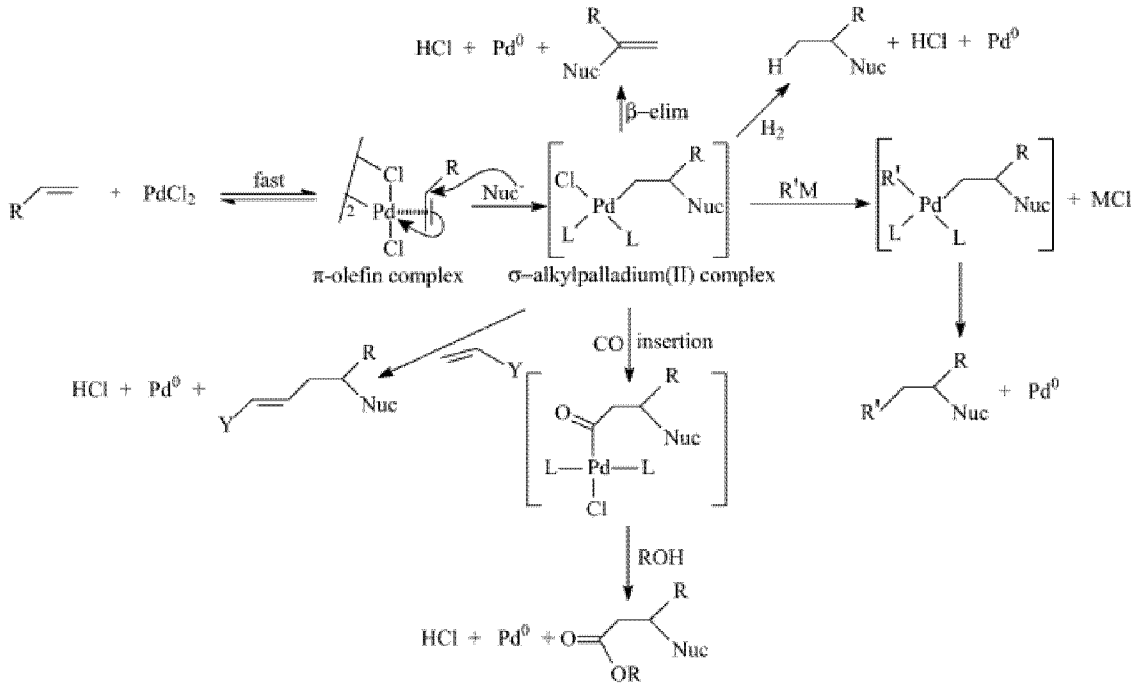

Pd(0) is usually produced in the final step, which means that a reoxidant is required to transform Pd(0) to Pd(II) to affect a process catalytic in palladium. Reoxidants commonly used are $O_2/CuCl_2$, benzoquinone, O_2/DMSO, $FeCl_3$, and $K_2S_2O_8$.

3.1.2 π-allyl complexes:

Development of asymmetric metal-catalyzed reaction has played a significant role in allowing synthetic access to biologically important molecules. Among the transition metal catalysts used for the catalytic asymmetric reactions, palladium is recognized to be the most versatile metal, which catalyses a wide variety of asymmetric reactions including cross-coupling, hydrosilylation of olefins, Heck-type reaction, Wacker-type oxidation and allylic substitution reactions[4]. Soon after invention of the Wacker process[5] (1956), which was the starting point of modern palladium chemistry, the first (π-allyl)Pd complex was reported (1959) by Smid and Hafner. C-C bond forming substitution reactions with (π-allyl)Pd complexes were discovered in 1965 by Tsuji, then vigorously developed by Trost and coworkers since 1973[1].

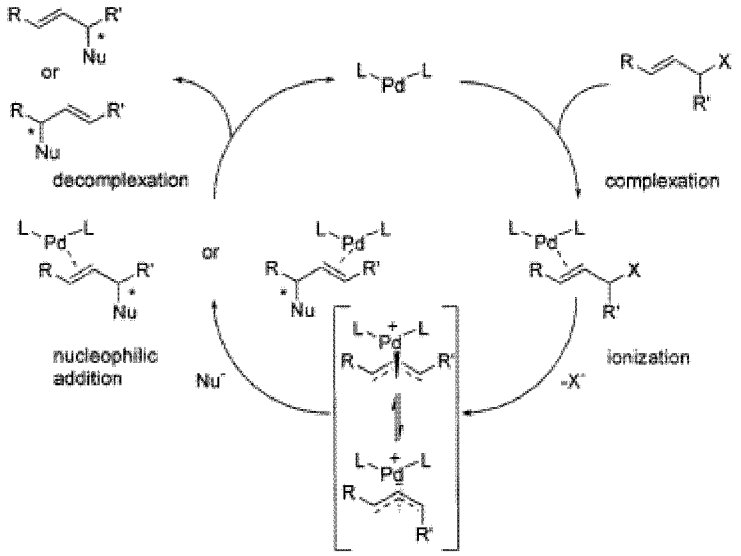

Scheme 3.2[1]. Catalytic cycle in Palladium catalyzed Asymmetric Allylic Alkylation reactions

Scheme 3.2 shows the usual catalytic cycle involved in Palladium-catalysed allylic alkylations. The first attempt, using a stoichiometric allylic substitution, was reported by Trost and Dietsche in 1973. Most allylic substitution reactions furnish a potentially chiral

product. It was logical to try to achieve enantioselectivity with the help of a chiral ligand L^*.

One of the most exciting and challenging subjects in the research of catalytic asymmetric synthesis is the development of a chiral ligand which will influence the reaction efficiency in terms of catalytic activity and enantioselectivity. Most of the chiral phosphine ligands prepared and used for catalytic asymmetric reactions hitherto are the bisphosphines which are, in general, anticipated to be effective in constructing a chiral environment by chelate coordination to the metal[6]. On the other hand, only a limited number of monodentate chiral phosphine ligands have been reported. However, there exist transition metal-catalyzed reactions where bisphosphine-metal complexes cannot be used because of their low catalytic activity and/or low selectivity toward a desired reaction pathway, and, therefore, chiral monodentate phosphine ligands are required for the catalytic asymmetric synthesis to be viable. Hayashi has reported the sythesis of MOP-palladium catalysts which were used in asymmetric hydrosilylation of olefins and hydroboration of enynes which involved (π-allyl) palladium intermediates[7].

Interest in how the MOP donor binds a transition metal is related to the question of chirality transfer. It would be useful to know if the MOP class favors chelation via the backbone, rather than a monodentate mode. In the latter situation, a relatively rigid chiral pocket might arise via restricted rotation around M-P and /or P-C bonds.

3.2 Bonding modes in Monodentate Phosphine Complexes

3.2.1 Background:

The biaryl-based homobidentate ligands are commonly found in the literature, among which BINOL is one of the best known representatives of axially chiral molecules (**Scheme 3.3**).

Scheme 3.3

Homobidentate 1,1'-Binaphthyls (C_2-Symmetrical)

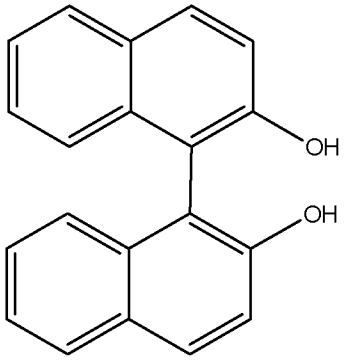

BINOL[8]

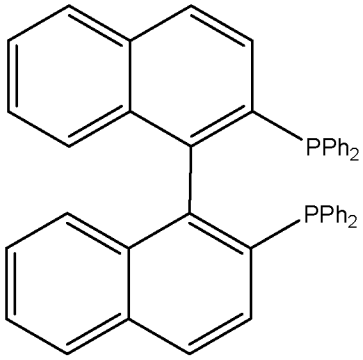

BINAP[8]

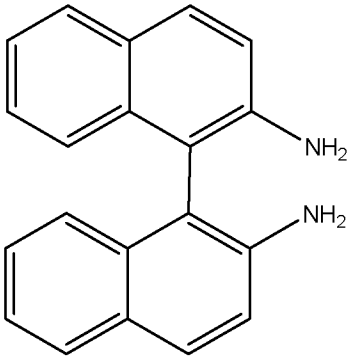

BINAM[8]

Heterobidentate 1,1'-Binaphthyls (non-C_2-Symmetrical)

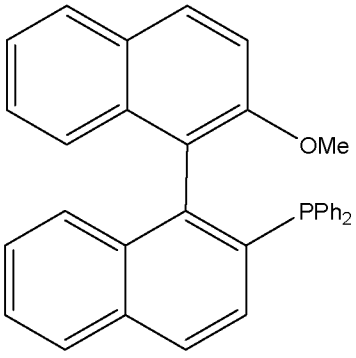

MOP[9]

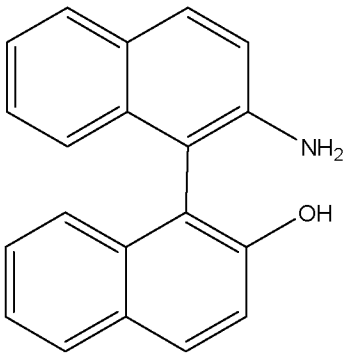

NOBIN[10]

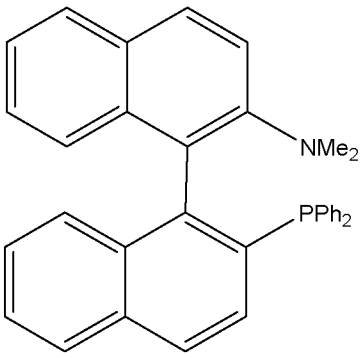

MAP[10]

Noyori[8], Hayashi[9], Kocovsky,[10] among several others, in a series of fine papers, have pointed out that the above auxiliaries can be used in

a variety of enantioselective homogeneous catalysis. Although much interest has centered on Ru(II)- or Rh(I)-catalysed enantioselective hydrogenation, palladium-catalysed carbon-carbon (and carbon-nitrogen and carbon-oxygen, etc.) bond making reactions are increasingly becoming popular[11-13]. Frequently, chiral catalysts employ tertiary phosphine derivatives as auxiliaries. Indeed, bidentate chiral phosphines have become so popular that these are increasingly commercially available, e.g., Duphos and Binap. However, the recent literature shows that much effort is being invested in the applications of monodentate chiral auxiliaries, e.g., MOP, **1-4**.

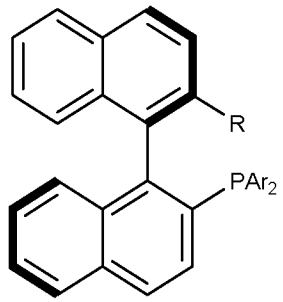

Ar = Ph(**a**), 3,5-di-*t*-butylphenyl(**b**), 3,5-dimethylphenyl(**c**)

1, R = H

2, R = OMe

3, R = CN

4, R = OH

The phosphine ligands, **b** and **c**, are MOP analogues with a substitution at 3 and 5 positions in the aromatic ring.

The MOP ligands are good auxiliaries for the Pd-catalysed regioselective and enantioselective hydrosilylation reaction[14], **Scheme 3.4**, with the branch product being favored. Although the structural coordination chemistry associated with chiral bidentate phosphine auxiliaries has been well studied, there is relatively little literature on the structural transition metal chemistry associated with **1-4**. Further, that which is known with respect to the interactions of MOP/MAP with Pd(II), affords a rather mixed picture. **Scheme 3.5** shows a few of the complexes†, by Hayashi[9], Ding[15], Kocovsky[16], Faller[17] etc., revealing that a number of binding modes are possible.

† Some of these complexes have appeared after the research to be discussed here.

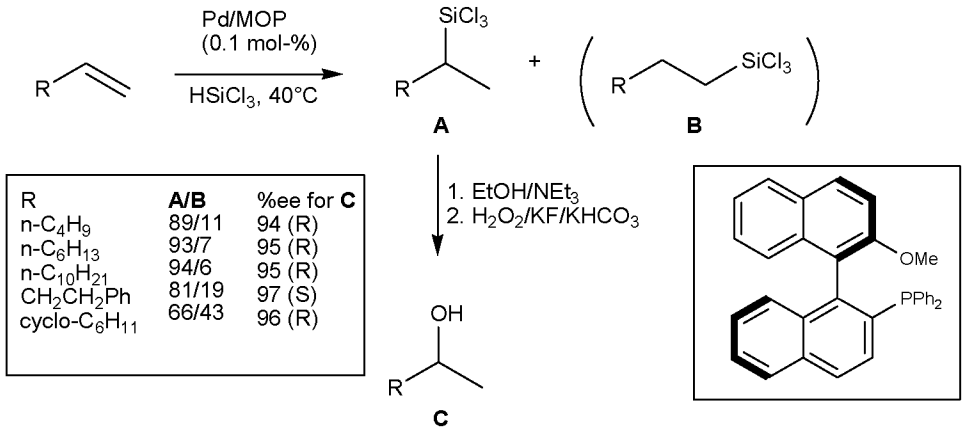

R	A/B	%ee for C
n-C_4H_9	89/11	94 (R)
n-C_6H_{13}	93/7	95 (R)
n-$C_{10}H_{21}$	94/6	95 (R)
CH_2CH_2Ph	81/19	97 (S)
cyclo-C_6H_{11}	66/43	96 (R)

Scheme 3.4. Result of the enantioselective Hydrosilylation from terminal Alkene with a MOP-Ligand[14].

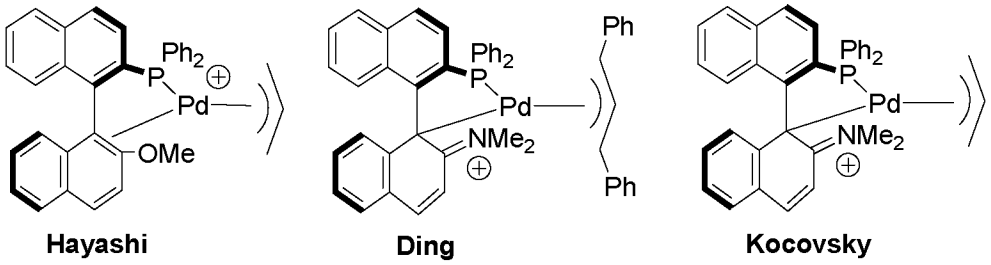

Hayashi **Ding** **Kocovsky**

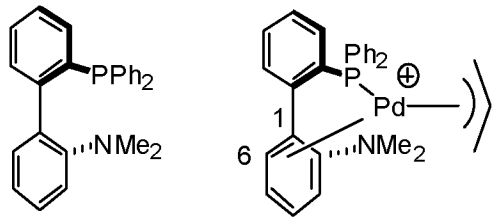

Faller

Scheme 3.5. MOP (or MAP) complexes showing novel interactions

It would seem that it is not easy to predict how the MOP-type ligands will bind to Pd(II) since both σ-and π-bonds can be formed using different parts of the aryl backbones. In any case, MOP and related-type ligands seem to be capable of acting as multidentate ligands. The following sections deal with the different binding modes adopted by Pd-MOP upon subtle variations of the other coordinated ligand.

The complexes reported in the following sections are prepared by Dr. P. Dotta[18] (MOP) and D. Huber (Phosphoramidite) for which author is indebted; only the NMR part is carried out by the author.

3.2.2 Pd(II)-acetyl acetonate MOP complexes:

The new Pd-MOP acetyl acetonate complexes [Pd(acac)(**2a** or **2b**)]BF_4, **5a,b**, were prepare[18] starting from [Pd(acac)$(CH_3CN)_2$]BF_4 whereas [Pd(acac)(**4-H**)], **6**, was obtained directly from $Pd(acac)_2$ by adding **4** (**Scheme 3.6**). In the preparation of **6** one acac ligand functions as a base. The ligand **2b** was used in a catalytic study and serve only as an additional example[18].

Scheme 3.6

$$Pd(acac)_2 + HBF_4 \xrightarrow[-\text{ Hacac}]{CH_3CN} [Pd(acac)(CH_3CN)_2]BF_4 \quad (1)$$

$$[Pd(acac)(CH_3CN)_2]BF_4 \xrightarrow[-\text{ 2 } CH_3CN]{\mathbf{2}} [Pd(acac)(\mathbf{2})]BF_4 \quad \mathbf{5} \quad (2)$$

$$Pd(acac)_2 \xrightarrow[-\text{ Hacac}]{\mathbf{4}} [Pd(acac)(\mathbf{4\text{-}H})]BF_4 \quad \mathbf{6} \quad (3)$$

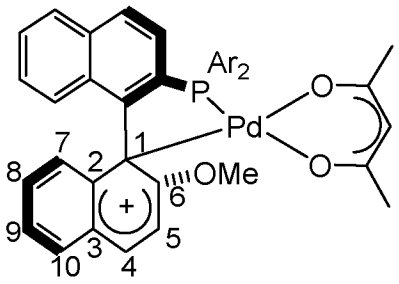

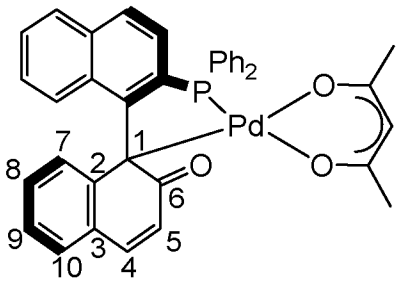

5a Ar = Phenyl
5b Ar = 3,5-di-*t*-Bu-phenyl

6

The structures for cationic **5a** and neutral **6** were proved by X-ray diffraction methods[19] and solution NMR studies.

In order to determine to what extent the naphthyl backbone interacts with the metal, ^{13}C NMR studies were undertaken. This nucleus was chosen because the coupling constants ($^{n}J(M,^{13}C)$ or $^{n}J(^{1}H,^{13}C)$) and the ^{13}C chemical shifts serve as a tool in determining the structure of the complex[20-22]. Selected ^{13}C NMR data for the ligands and their complexes, **5** and **6**, are shown in **Table 3.1**.

Table 3.1. δ ^{13}C (in ppm) for the Complexes and Ligands.

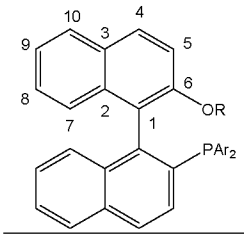

R= Me, Ar= Phenyl **2a**
R= Me, Ar= 3,5-di-*t*-Bu-Phenyl **2b**
R= H, Ar= Phenyl **4**

Position	2a	5a	2b	5b	4	6
1	122.1	**86.7**	122.2	**86.9**	118.3	**70.5**
2	134.4	140.2	134.2	139.8	133.7	146.1
3	129.1	129.5	128.9	129.3	128.8	128.8
4	130.2	147.1	130.0	146.9	130.2	142.8
5	113.0	113.3	113.5	113.4	117.7	127.6
6	155.5	166.3	155.1	166.4	151.4	**193.7**
7	125.4	125.9	a)	126.3	125.0	126.5
8	126.8	131.4	a)	a)	126.8	127.9
9	123.7	127.4	a)	a)	123.4	123.9
10	128.3	130.4	127.8	130.3	128.2	128.7

a) not assigned

The ^{31}P spectra reveal that, in solution, only a single isomer was observed for both **5** and **6**. As there is little to distinguish **5a** from **5b**, only the former will be discussed. **Figures. 3.1** and **3.2** show the $^{13}C,^{1}H$ long-range correlations which provide the key assignments for the fully substituted carbon resonances. The proton AX spin system, from the signals for H4 and H5, is readily assigned via COSY spectroscopy. Further, the second AX pattern (in the phosphine naphthyl moiety) is readily detected via a $^{31}P,^{1}H$ correlation and thus is

easily differentiated from H4 and H5. One can also use the ^{3}J(C6, H(MeO)) interaction to confirm the assignment of C6.

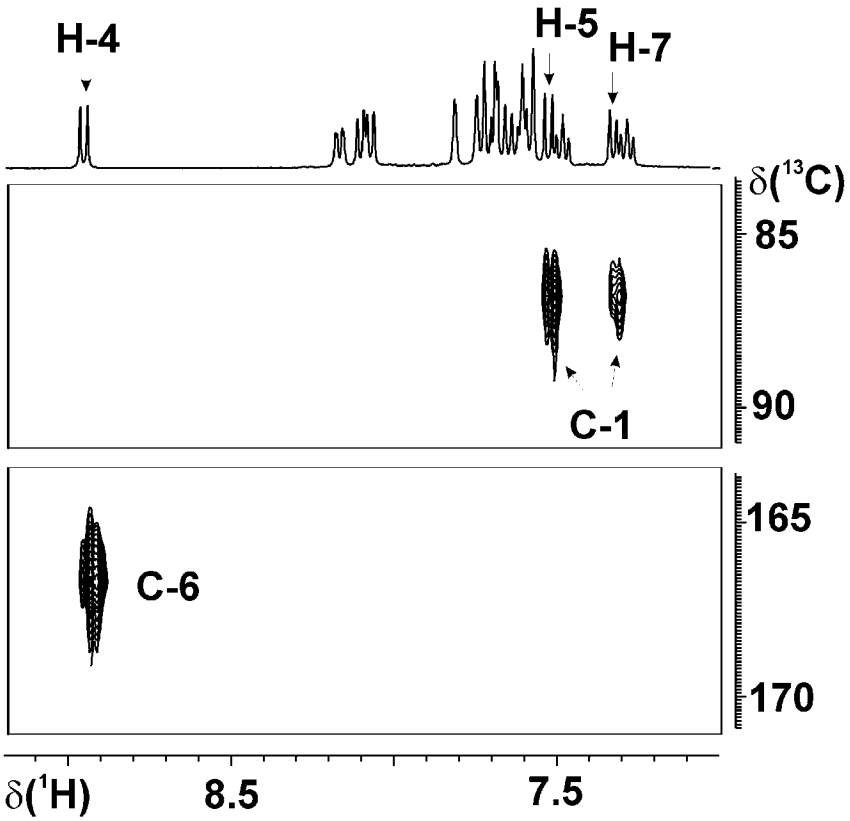

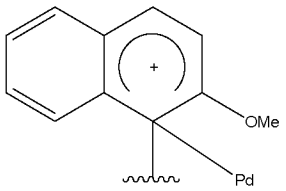

Figure 3.1. ^{13}C long range correlation for **5b**. The chemical shift of the MeO-C ipso-carbon, C6, resonance is clear, at δ = 166.4, via the correlation to H4, whereas H5 and H7 correlate to the pseudo -sp^3-carbon, C(1) (500 MHz, CD_2Cl_2).

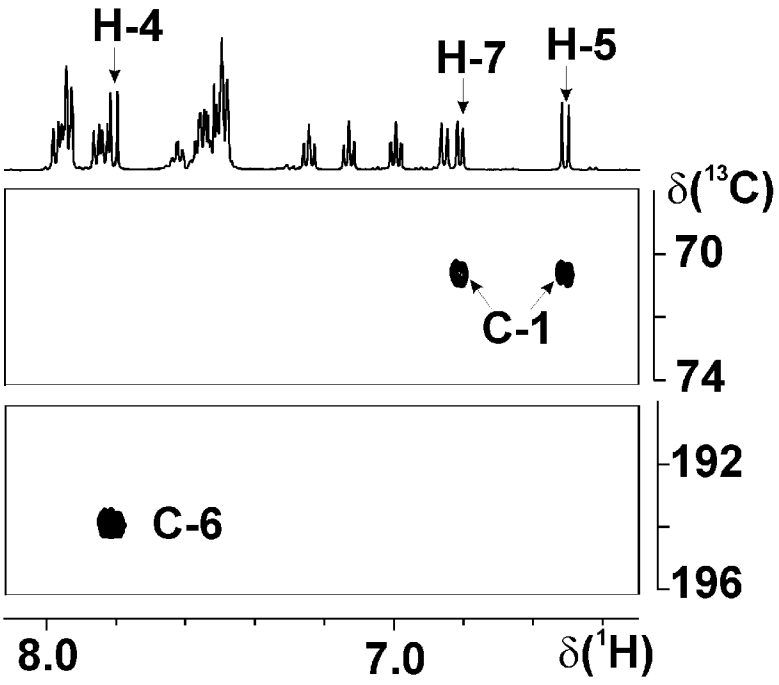

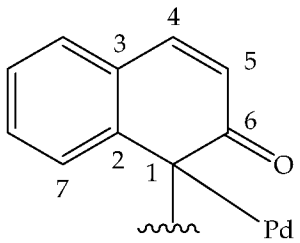

Figure 3.2. ^{13}C long range correlation for **6**. The chemical shift of the ketone C=O is clearly revealed by the correlation to H4, where as H5 and H7 correlate to the pseudo -sp^3-carbon, C(1) (500 MHz, CD_2Cl_2).

The ketone carbon[23] in **6** , at δ = 193.7, is readily observed (see **Fig. 3.2**) and found at a much higher frequency than one would expect for a phenolic sp^2 carbon. Moreover, the organic ^{13}C NMR literature[24] suggests that this is exactly the correct δ value for the carbonyl of an α,β-unsaturated ketone.

For both **5a** and **6** the ipso carbons, C1, involved in the Pd-bonding, appear at low frequency, δ = 86.7, 70.5, respectively, in the aliphatic region of the spectrum, thereby supporting their formulation as pseudo sp^3 carbons. As expected, based on the relatively short Pd-C bond length in **6**[19], this C1 resonance appears at the lowest frequency.

Salt **5a** contains a primarily organic cation, in that, formally,

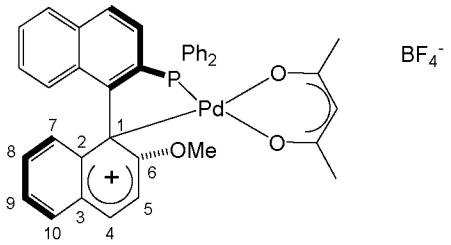

5a

the local co-ordination sphere about the Pd-atom is neutral. The ^{13}C signal of the β carbon of an α,β-unsaturated organic ketone or ester should be found at ca 140-150 ppm[24], so that the observed chemical shift value of C4, 142.8 ppm, in **6** is as expected. However, the observed chemical shift of 147.1 ppm for C4 in **5a**, suggests that this carbon carries some of the cation positive charge (see **Scheme 3.7** and **Table 3.1**). **Scheme 3.7** gives the ^{13}C coordination chemical shifts for **5a** and **6**. These data reveal relatively large $\Delta\delta$ values for the resonances of C4 and C6 in **5a**, 16.9 and 10.8 ppm, respectively.

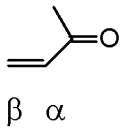

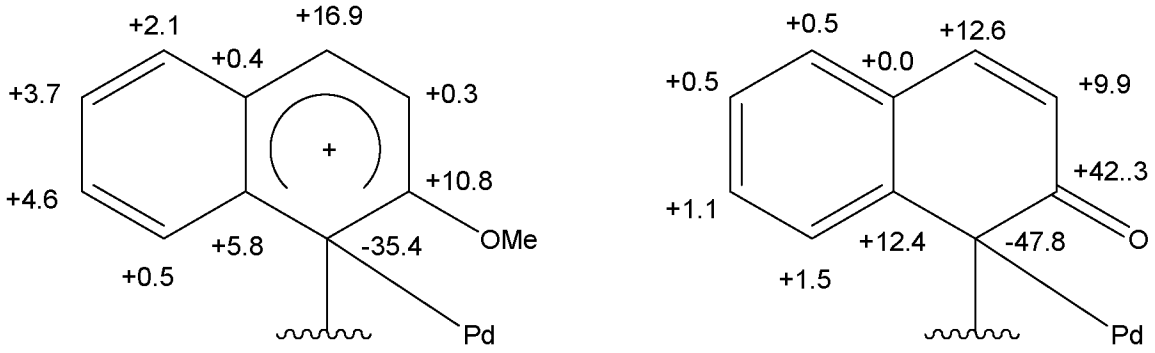

Scheme 3.7 $\Delta(\delta\ ^{13}C)$ values (in ppm) for complexes **5a** (left) and **6** (right), $\Delta(\delta\ ^{13}C)$= $\delta\ ^{13}C$ (coordinated Ligand)- $\delta\ ^{13}C$ (free Ligand)

Continuing for **5a**, the methoxy-bearing carbon, C6 at 166.3 ppm (rather than at 155.5ppm as found in the ligand itself), appears at relatively high frequency suggesting that this carbon position, along with C4, also shares in the positive charge of the cation.

We note that the ^{31}P chemical shifts for **5a** and **6**, δ = 48.5, 46.5, respectively**,** appear at considerably higher frequency than for trans-$PdCl_2$(**2**)$_2$, δ = 29.7.

Dinuclear Pd(I) Compound, 7.

During the preparation of the acetylacetonate compound, **5**, a modest quantity of a new dinuclear Pd(I) species was obtained as a side-product and its structure determined via X-ray diffraction[25]. Once the structure was known, the new dinuclear complex, **7**, could be prepared[25] in good yield by direct reaction of the known Pd(I) dimer, $[Pd_2(CH_3CN)_6](BF_4)_2$, with two equivalents of MeO-MOP as shown in the **equation 3.1**:

$$[Pd_2(CH_3CN)_6](BF_4)_2 \xrightarrow{2\text{MeO-MOP}} \mathbf{7} \qquad (\mathbf{3.1})$$

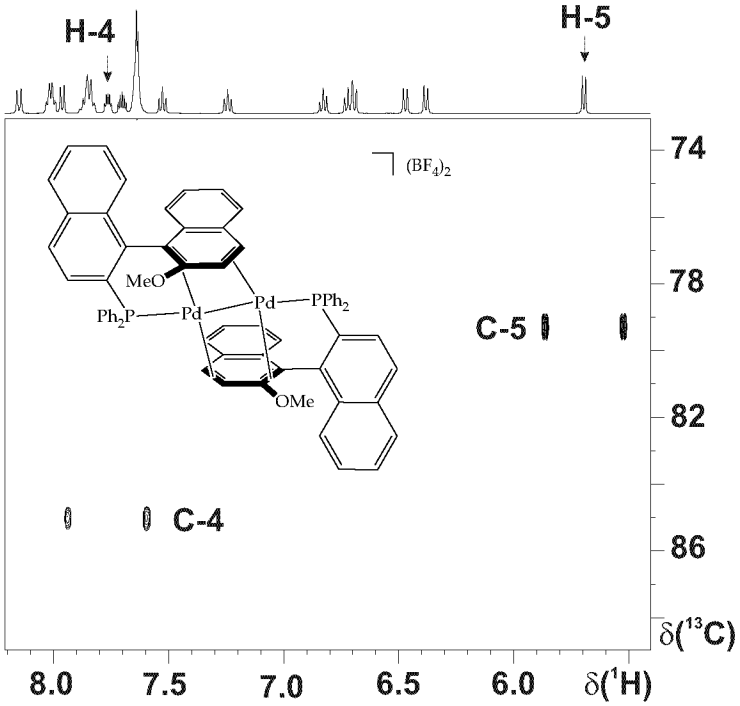

Figure 3.3 Section of the ^{13}C HMQC spectrum for **7**, showing the cross-peaks for the two coordinated =CH resonances, at relatively low frequency.

Table 3.2. ^{13}C chemical shifts (in ppm) for **2a** und **7** (500 MHz, CD_2Cl_2, RT)

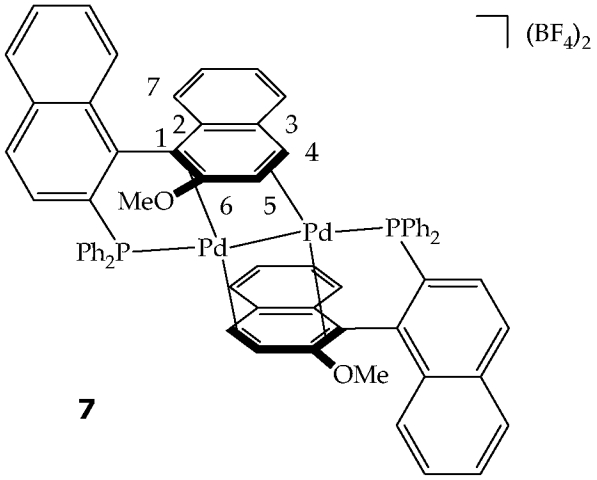

7

Position	Ligand 2a	complex 7	Δδ
1	122.0	**99.7**	-22.3
2	134.4	131.6	-2.8
3	129.1	123.4	-5.7
4	130.2	**85.0**	-45.2
5	113.0	**79.4**	-33.6
6	155.5	**136.7**	-18.8
OMe	55.7	57.6	+1.9

In this complex, the naphthyl backbone of **2a** acts as a bridging diene ligand. The solution structure for **7** was determined, primarily, via ^{13}C NMR studies. The ^{13}C data for **7** (see **Fig. 3.3** and **Table 3.2** for data and numbering) show that the two fully substituted carbons, 1 (99.7 ppm) and 6 (136.7 ppm), and the two =CH carbons 4 (85.0 ppm) and 5 (79.4 ppm) show typical strongly low frequency shifted signals, due to the π-complexation. Consequently, the solution structures were assigned to be as shown above in the table.

There are several structural reports of di (or poly) olefins bridging Pd(I) dimers[26], so that there is precedence for the basic structure for **7**; nevertheless it is noteworthy that the MOP ligand complexes in this fashion.

Comments and conclusions: It seems clear that, in solution, the MOP class will find one of the possible chelating modes with which to complex to Pd(II) when given the opportunity. The presence of either of the electron-donating substituents, Me_2N or MeO, can lead to molecular structures, in both solid and solution states, that favor a σ-bond between C1 and the Pd atom. If the MOP oxygen atom carries an H-atom, this is readily lost to afford the keto-anion. The keto-anion structure is easily recognized via its characteristic ^{13}C carbonyl chemical shift. Since the parent MOP ligand, **1** (H-MOP), may not readily form structures such as **5** or **6**, it seems likely that individual ligands within the MOP class may well behave differently under catalytic conditions.

3.2.2 Pd(II)-benzyl amine MOP complexes :

To further explore the new bonding modes in the MOP type complexes, ^{13}C NMR studies were planned for the cyclometalated complexes of Pd(II) with MOP auxiliaries were prepared[25] as shown in **Scheme 3.8**. The decision for a cyclometalated Pd complex was based on the fact that many catalytic cycles involving palladium (e.g., hydrosilylation or cross-coupling) contain a reactive species with a metal-carbon σ-bond.

Scheme 3.8

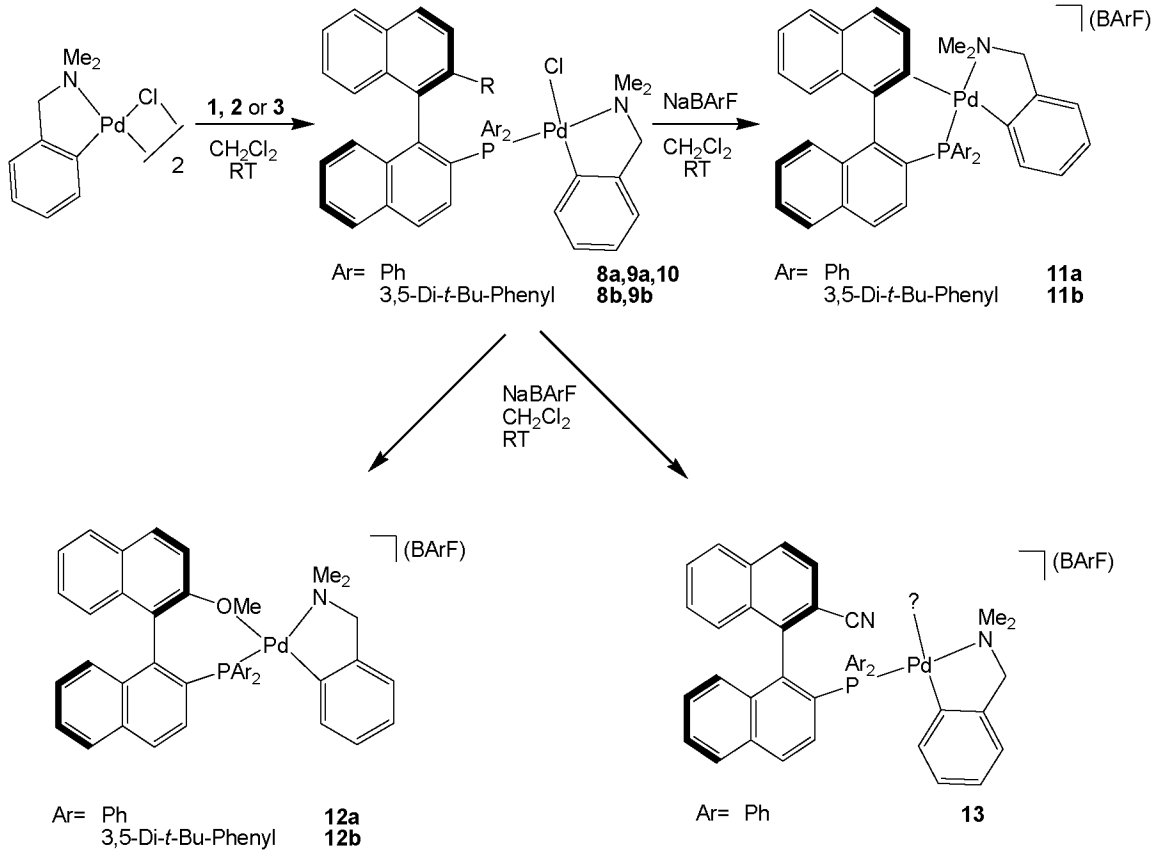

The chloro-bridged cyclopalladate-dimer was treated with 2 equivalents of MOP (H-MOP, **1**, MeO-MOP, **2** and CN-MOP, **3**) in dichloromethane to afford the complexes **8**, **9** and **10** respectively, with the aryl groups being both phenyl and 3,5-di-*t*-butyl phenyl.

Note that the NMe_2 groups are close to the MOP backbone and *trans* to the P as in the above structures, which will be explained further below.

Table 3.3. ^{13}C-NMR-Data for complexes **8** und **11**, (500 MHz, CD_2Cl_2)

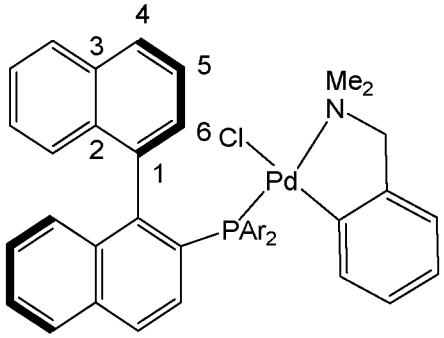

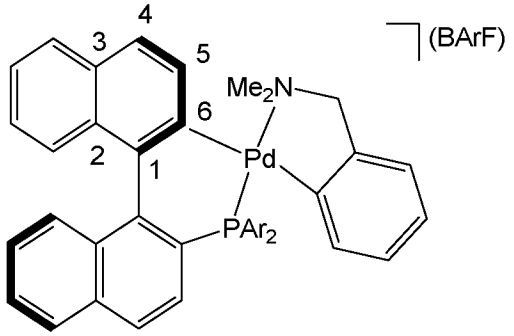

Ar= Ph **8a** Ar= Ph **11a**
3,5-Di-*t*-Bu-Phenyl **8b** 3,5-Di-*t*-Bu-Phenyl **11b**

Position	8a	11a	8b	11b
1	133.4	**149.2**	136.2	**150.3**
2	133.0	132.0	133.4	132.1
3	133.3	134.5	133.0	134.6
4	129.2	131.3	129.3	131.1
5	125.0	127.5	125.1	127.7
6	131.0	**106.6**	131.7	**105.4**

Scheme 3.9. ^{13}C coordination shifts (in ppm) in the complexes **11a** (left) und **11b** (right) relative to the Chloride complexes **8a** and **8b**. $\Delta\delta = \delta(\mathbf{11}) - \delta(\mathbf{8})$

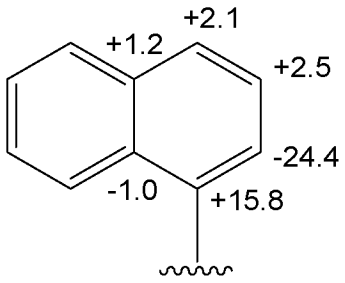

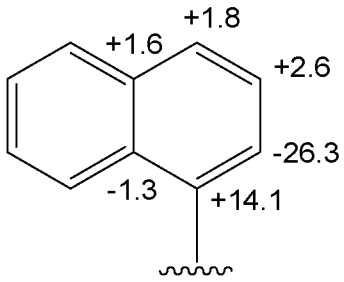

Table 3.3 shows the pertinent naphthyl backbone ^{13}C data for H-MOP complexes **8** and **11**. The backbone carbon C-1 has now shifted to *higher* frequency by 15.8 and 14.1 ppm, for **11a** and **11b**, respectively, See **Scheme 3.9**, while C-6 (which is closer to the Pd-atom) has shifted markedly to *lower* frequency (-24.4 and –26.3 ppm,

for **11a** and **11b**, respectively). These NMR data are considered to be consistent with some weak σ-bonding character between C-6 and the Pd-atom, in analogy to what has been observed in **5**. The much smaller coordination chemical shift for C-6 in **11a** and **11b** (ca –25 ppm), relative to **5** (ca –50 ppm) arises due to the presence of a good sigma-donor (the cyclopalladated carbon) rather than the acetyl acetonate oxygen donor, in **5**, i.e., differences in *trans* influence effects. It is suggested that some positive charge reside at C-1 and thus the high frequency shift, although some of the charge is surely delocalized over the naphthyl fragment. The possibility of an η^1-π bond cannot be excluded, i.e., an interaction from the π-orbital of a single naphthyl carbon, as this has been proposed recently[27]; however, an η^1-bond does not usually result in a strong high frequency shift for the adjacent carbon. Further, the $^1J(^{13}C,^1H)$ values for the hydrogen at C-6 are 163 Hz and 155 Hz, for **8a** and **11a**, respectively. These data are consistent with a one bond proton-carbon interaction, hence the possibility of an agostic interaction is ruled out. In any case, whether the new interaction represents an extremely weak σ-bond or some form of π-polarization, this represents yet another new bonding possibility for Pd-MOP.

Scheme 3.8 also shows structures for the cyclopalladated MeO-MOP complexes, **12a** and **12b**. The chloride from complex **9a** and **9b** was extracted using NaBArF in dichloromethane affording the new derivatives, **12a** and **12b**, in which the methoxy oxygen atoms of **2a** and **2b** are now complexed to the Pd(II). As mentioned earlier about the placement of NMe_2 groups close to the MOP backbone, the NOESY

results support that the MeO-and Me_2N-groups are close to one another (see **Fig. 3.4**).

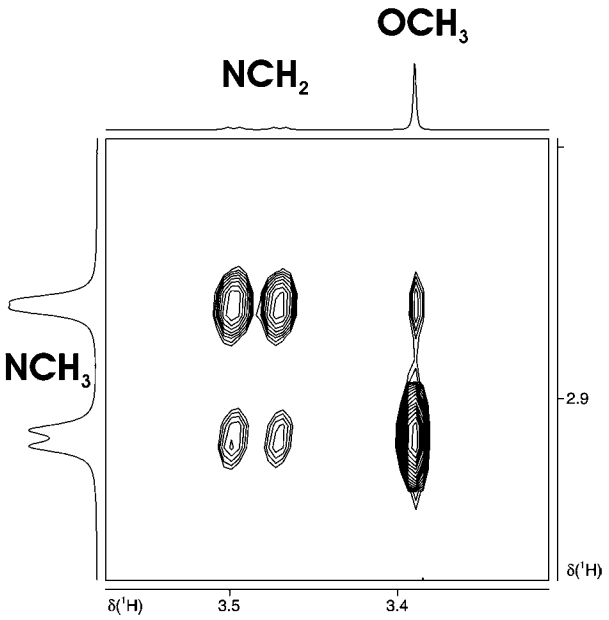

Figure 3.4. Section of the 2D-NOESY-Spectrum for **12a**, showing cross-peaks due to the NOEs from the proximate MeO (and NCH_2) groups to the nonequivalent NMe_2 groups (on the *y*-axis). One of the N-methyl groups is coupled to the MOP 31P atom. (500 MHz, CD_2Cl_2)

Table 3.4. ^{13}C chemical shifts (in ppm) for **9** und **12** (500 MHz, CD_2Cl_2)

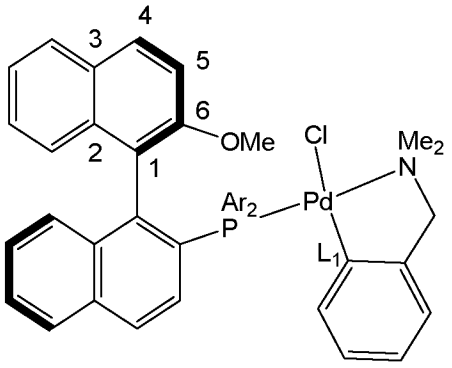

Ar= Ph **9a**
3,5-Di-*t*-Bu-Phenyl **9b**

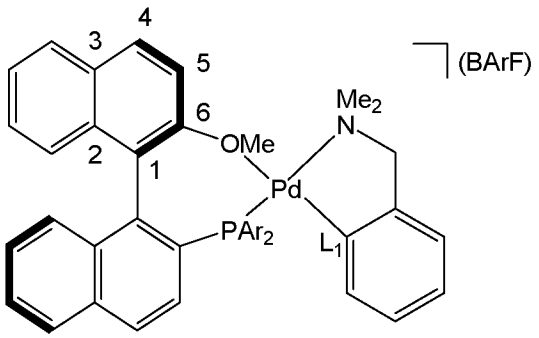

Ar= Ph **12a**
3,5-Di-*t*-Bu-Phenyl **12b**

Position	9a	12a	9b	12b
1	119.9	125.2	121.6	125.4
2	134.6	132.7	134.5	133.2
3	129.1	132.2	128.9	131.9
4	130.6	132.8	130.4	133.0
5	112.2	119.5	113.8	119.5
6	154.7	155.5	155.6	155.2
OCH_3	55.3	**65.8**	56.3	**65.8**
L1	151.8	**140.9**	151.6	**141.6**

Selected ^{13}C NMR results from the naphthyl backbone for these new compounds are given in **Table 3.4**. Note that, for **12a** and **12b**, there is a 9.5-10.5 ppm high frequency shift of the methoxy carbon, relative to **9a** and **9b**, respectively, due to the oxygen coordination. The cyclopalladated carbon resonance, L1, is shifted ca 10-11 ppm to low frequency in agreement with the expectation of a weaker ligand than chloride in *trans* position. The aromatic carbons C1-C6 change minimally relative to the chloride analogue. In conclusion, the MeO-MOP ligand shows yet another bonding mode by chelation via the Oxygen of the OMe–group to the metal.

Scheme 3.8 (Page 88) also shows an analogous reaction sequence for **3**, the cyano-MOP derivative. The product, **13**, gives a singlet in the ^{31}P NMR spectrum, plus a microanalysis and a mass spectrum consistent with the formulation: [Pd($C_6H_4CH_2NMe_2$)(**3**)](BArF). The IR spectrum shows a modest 10 cm^{-1} change in the CN frequency on going from **10** to**13**. A complexed water signal cannot be found in either the IR or ^{1}H NMR of **13**. Addition of Bu_4NCl leads to formation of **10** (reverse reaction) cleanly. The ^{13}C data for **13** are given in **Table 3.5**, and show that the naphthyl backbone does *not* interact with the metal, i.e., there is no evidence for π- or σ-complexation. Although the exact structure of **13** is not certain (it still might be a dynamic aquo complex, or the nitrile might be involved, weakly, with the Pd(II)), compound **13** does *not show the naphthyl backbone interaction* related to that found for **11a** or **11b**. The complex **13** cannot be believed to be a three-coordinate Pd(II) complex.

Table 3.5. ^{13}C-NMR-Data (in ppm) for the complexes **10** und **13** (500 MHz, CD_2Cl_2)

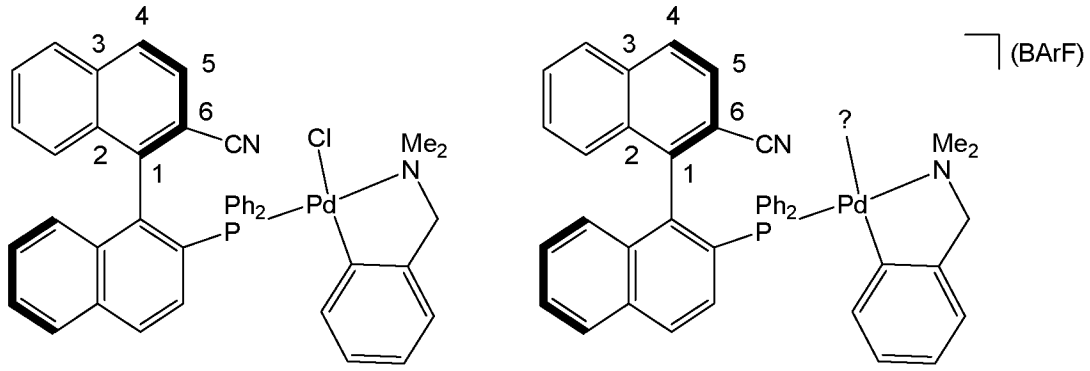

10 **13**

Position	10	13
1	142.9	146.2
2	133.0	132.0
3	134.9	136.0
4	129.3	131.6
5	127.1	125.2
6	112.4	107.3

In connection with the characterization of the new BArF cations **11**, **12** and **13**, it was noted that the electron spray ionisation mass spectra (from methanol) shows a major signal for **13**+MeOH, i.e., the solvated NC-MOP analogue, whereas, the H-MOP and MeO-MOP cations, **11** and **12**, gave strong peaks for the molecular ion, *without solvent*, presumably because the fourth coordination position is blocked as described above.

3,5- meta dialkyl effect in MOP and related catalysis

In several studies, Pregosin[28-30] *et al* and several others have shown that introduction of 3,5-di-alkylphenyl groups onto the P-donor of the auxiliary (instead of the routine phenyl substituent) enhances the ee's in Heck and allylic alkylation chemistry. The monodentate auxiliary MOP, introduced by Hayashi[9], has been successfully applied to enantioselective hydrosilylation reactions (shown below)

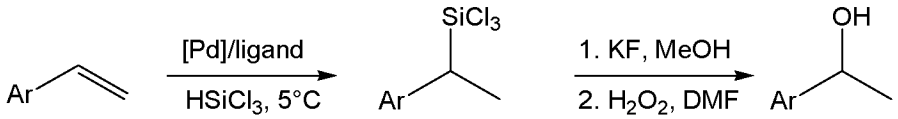

It has been reported that the above reaction with the meta-substituted phenyl MOP-auxiliaries proceeds slower and gives a better ee (phenyl (74%) < 3,5-di-methylphenyl (86%) <3,5-di-t-butylphenyl (98%)[31].

To better understand the results from the catalytic experiments using MOP, NMR structural studies on the model complexes **8a-c** were undertaken.

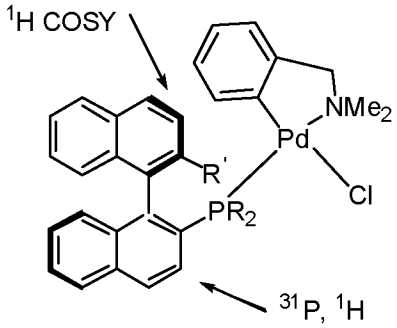

8

a, = R = Ph, R′ = H

b, = R = 3,5-di-*t*-butylphenyl, R′ = H

c, = R = 3,5-dimethylphenyl, R′ = H

The ^{31}P, ^{1}H and ^{13}C assignments for the two different P-(3,5-dialkylphenyl) rings in **8b,c** were made by first assigning both of the two-spin systems (indicated by arrows in **8**) using proton-proton and phosphorus-proton correlations, followed by NOE's to assign the remaining protons. Once the protons are assigned, the two P-aryl rings can be distinguished via NOE's. **Fig. 3.5** shows a slice through the NOESY spectrum for the 3,5-methylphenyl complex, **8c**. The pseudo-axial ring in the molecule is proximate to the binaphthyl backbone, see fragment **A**, and reveals eight different NOE's arising from the methyl groups, six from the backbone plus two strong interactions involving the immediately adjacent *ortho* and *para* protons. The pseudo-equatorial ring shows only four NOE's from the methyl groups, two

very weak interactions to the backbone and, again, the two strong interactions involving the proximate *ortho* and *para* protons.

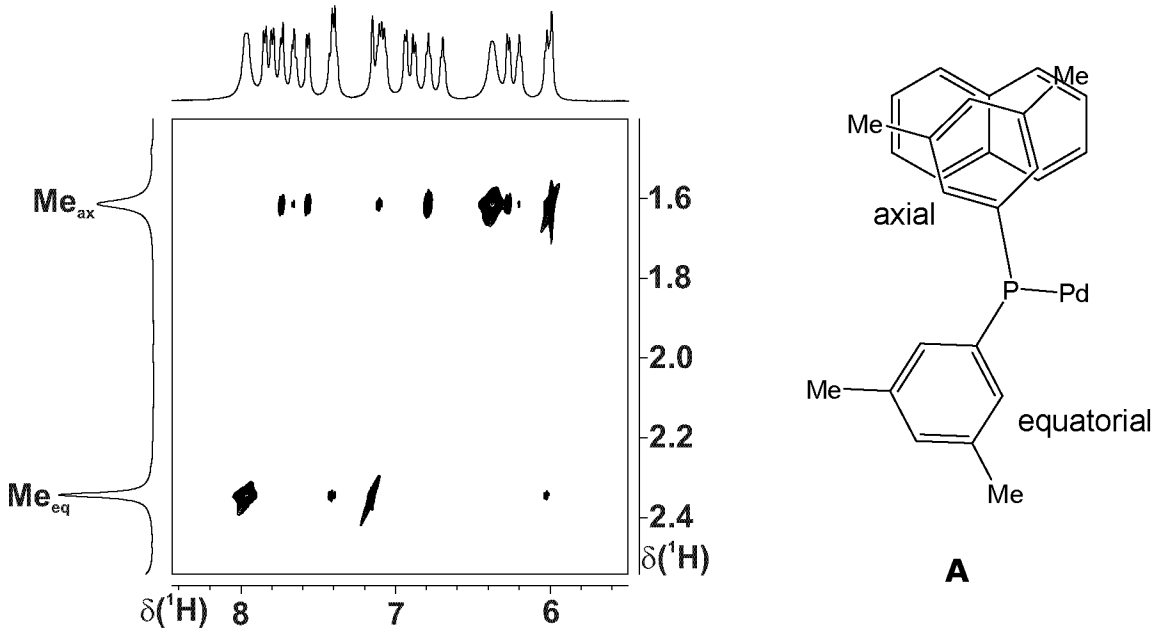

Figure 3.5. A slice through the ^{1}H, ^{1}H NOESY spectrum of the 3,5-dimethylphenyl MOP analogue, **8c**. The pseudo-axial aryl ring, associated with the low frequency methyl signal, reveals many more contacts to the aromatic backbone than does the pseudo-equatorial analogue. Indeed, for the methyl group at higher frequency, the two most intense contacts stem from the adjacent *ortho* and *para* protons of the 3,5-dimethylphenyl moiety and not from the inter-ring NOE's (CD_2Cl_2).

The cis chloride ligand in **8** is not very bulky; however, the aryl moiety associated with the cyclometallated ring lies ca *in* the coordination plane and is thus sterically significant with respect to the proximate MOP ligand. **Fig. 3.6** shows sections of the appropriate variable temperature ^{1}H spectra for the *meta* di-substituted complexes **8b** (left side) and **8c** (right side). At ambient temperature, the 18-proton *t*-butyl signal of the pseudo-axial ring in **8b** is quite broad, and at 273K, broad but resolved. At 233K all four 12-proton signals are resolved. The spectra for the dimethyl analogue, **8c**, reveal the first set of resolved methyl signals at 233K, i.e., the barrier to rotation is

lower. The aryl protons of **8a** begin to show well-resolved *ortho* proton resonances from the P-aryl moieties below 200K. These data point to selective restricted rotation induced by the presence of the 3,5-dialkyl groups.

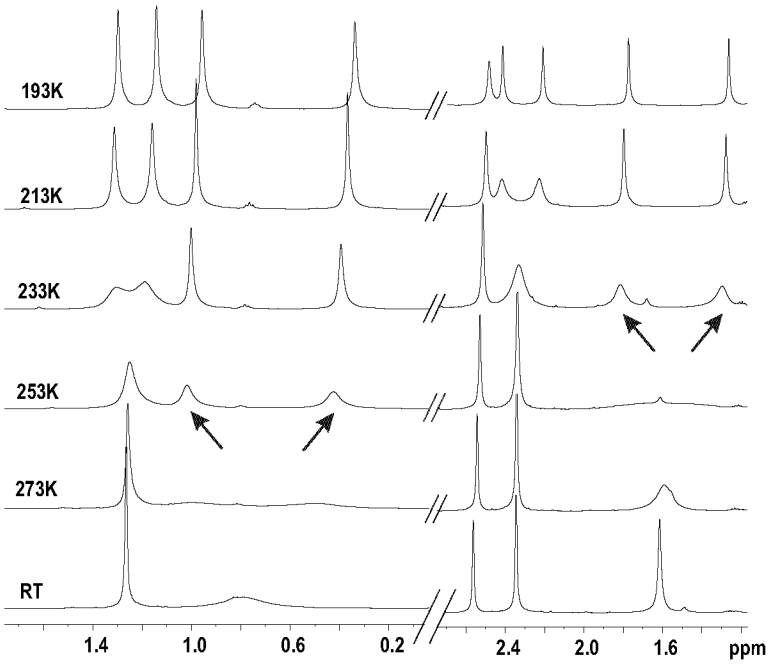

Figure 3.6: ^{1}H NMR spectra measured as a function of temperature for the complexes **8b** and **8c** in the methyl region. For the 3,5-di-*t*-butylphenyl complex (left) the restricted rotation is clearly visible at 253K, whereas for the 3,5-dimethylphenyl compound (right) the restricted rotation is recognized at 233K, for **8c**, the ca 2.55 ppm resonance stems from a *N*-methyl group (CD_2Cl_2).

In conclusion, it was seen that the 3,5-meta dialkyl effect is not only limited to bis-phosphine or oxazoline ligands, but also found in MOP-auxiliaries. The effect, arising due to restricted rotation of the chiral pocket, on the enantioselectivity might be quite subtle but useful[31].

3.2.4 Pd(II) and Pt(II)- allyl MOP complexes

3.2.4.1 Pd(II)-allyl with two MOP ligands coordinated:

It is now clear that a single MOP can be involved as chelating ligand. However, since the MOP (**1-4**) ligand is relatively large, there is some uncertainty as to the number of MOP molecules capable of coordinating to a transition metal. Specifically, for **2**, with an estimated cone angle of 200°[7, 9], it has been stated[32] that for "MeO-MOP…the π-allyl palladium cannot accommodate two molecules of phosphine ligand because of the steric bulkiness…". To test if it was possible to accommodate two MOP ligands on the same metal, zero valent Pd-complexes **14** (characterized by X-ray[33]) and **15** (characterized by NMR) were prepared (**Scheme 3.10**).

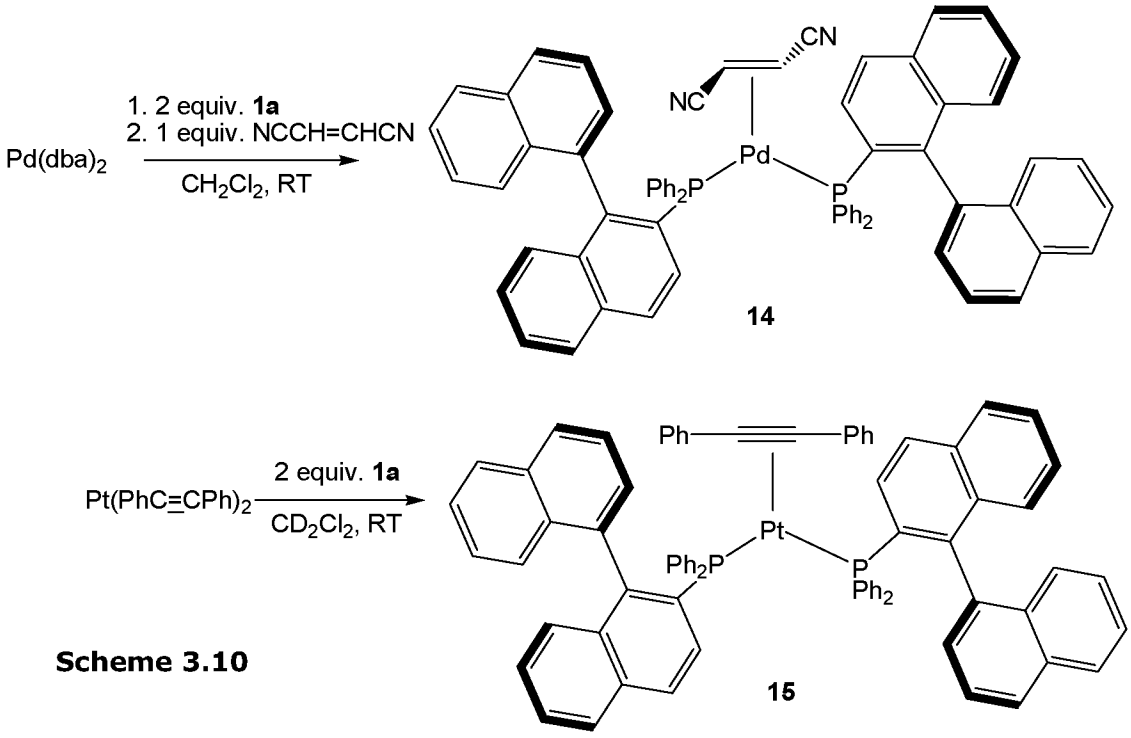

Scheme 3.10

Complex **15** was not isolated; however, at 233K in dichloromethane its ^{195}Pt NMR spectra revealed the triplet multiplicity expected for a bis

phosphine complex ($^{1}J(^{195}Pt,^{31}P)$ = 3590 Hz, δ ^{195}Pt = -4968), thereby confirming the presence of two complexed MOP ligands within the coordination sphere.

As a structural model for the Pd(II) oxidation state, one equiv. of the di-nuclear allyl-complex $[Pd(\mu\text{-}Cl)(\eta^3\text{-}C_3H_5)]_2$ was allowed to react with 2 equiv. of $AgBF_4$ and 4 equiv. of MeO-MOP, **2a** . The isolated yellow-orange product (53%), whose ^{31}P NMR spectrum is shown in **Fig. 3.7**, contains three components, in the ratio 1.0:0.8:1.4 and a small amount of phosphine oxide. The three MOP containing species are suggested to be **16-18** (**Scheme 3.11**).

Compound **16** represents the expected bis phosphine product. Its ^{31}P NMR reveals an AB spin system, plus five ^{1}H and three ^{13}C NMR resonances for the allyl-ligand. The axial and equatorial nature of the two PPh_2 groups renders the two ^{31}P signals (just barely) non-equivalent with respect to the allyl group.

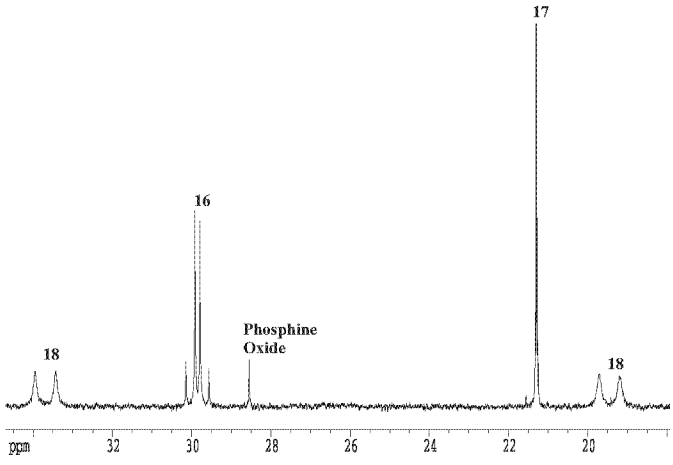

Fig. 3.7. ^{31}P NMR spectrum of **16-18** at ambient temperature. Complex **16** shows an AB spectrum, complex **17** a singlet and **18** and AX spin system. The ^{31}P line widths in **18** indicate an exchange process and 2-D exchange spectroscopy at 253K confirms that the two MeO-MOP ligands exchange places.

Scheme 3.11

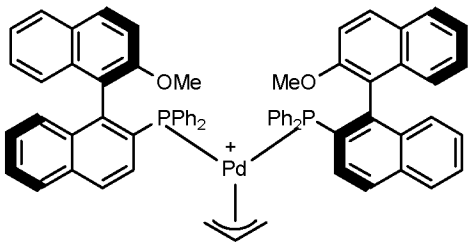

16

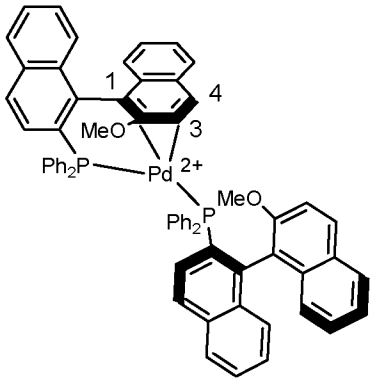

18

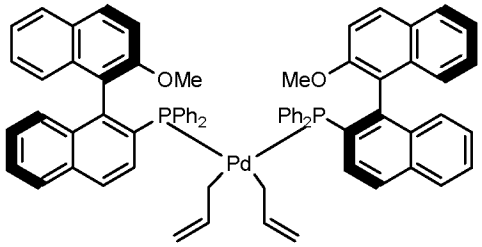

17

The η^1 allyl form in **17** is recognized by its characteristic proton and carbon NMR resonances i.e., diastereotopic aliphatic CH_2 protons and an ABX spin system at relatively high frequency, typical for a vinyl group, see **Fig. 3.8**.

The bis allyl complex, **17**, represents the first example of a stable bis η^1 allyl chiral compound. Generally, η^1 allyl compounds are rarely observed. For complexes of chiral ligands, there is only one other example, **19**, in which this isomeric form is stable[34].

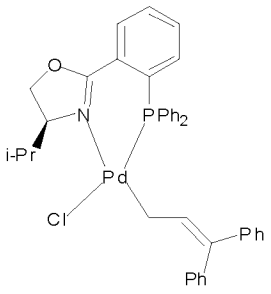

19

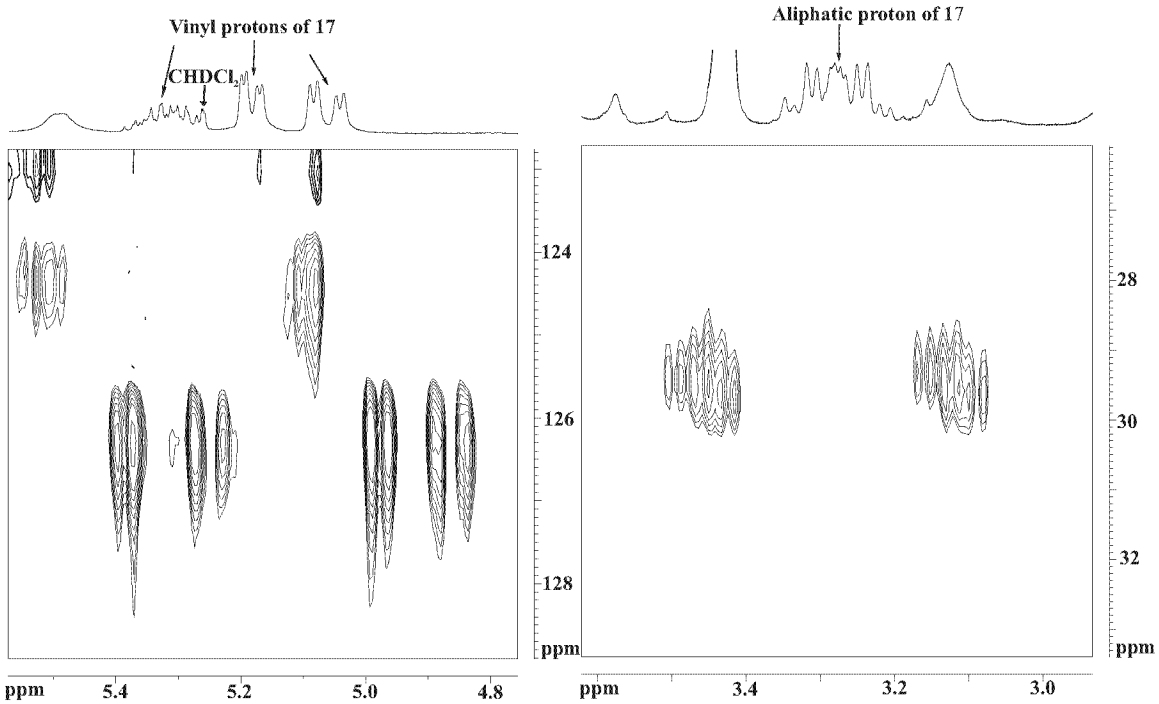

Fig. 3.8. The proton resonances of the vinyl group of **17**. The 1-D spectra show the normal ^{1}H chemical shifts for a routine vinyl group at δ ca 5.0-5.4. The cross-peaks arise from two sections a 2-D C,H one-bond correlation and show the expected vinyl ^{13}C chemical shifts, δ ca 124-126, and not those expected for a Pd-allyl ligand.

The presence of the two MOP ligands in **17** is confirmed by PGSE diffusion measurements[35, 36]. The smaller diffusion constants, D, for **17**, in dichloromethane (D = 8.71 and 8.63 x $10^{-10}m^2s^{-1}$ from ^{1}H and ^{31}P measurements, respectively), reflect the observed difference in volume between a single free MOP ligand (D = 10.59 and 10.89 x $10^{-10}m^2s^{-1}$ from ^{1}H and ^{31}P data, respectively) and a complex containing two such large molecules. The ratio of D-values ($D_{ligand}/D_{complex}$), ca 1.24, is exactly what is expected for ca double the volume. Clearly, there is facile transfer of an allyl ligand from one metal centre to another, perhaps due to the ease of η^3 to η^1 Isomerisation.

The two MOP ligands in **17** can also be confirmed by the sp^3 carbon of the vinyl fragment which shows a coupling to the two phosphorus of the MOP ligand coordinated.

Diene complex **18** shows two very different ^{31}P resonances, δ = 19.4 and δ = 33.7, $^{2}J_{PP}$ = 83 Hz, with the former signal associated with the chelate ring. This difference arises due to a novel Pd-MOP interaction, i.e., one MOP ligand serves as a six electron donor. The η^4 olefin bonding in **18** was identified via a set of $^{13}C,^{1}H$ correlations with the key CH-carbon signals for the complexed olefin assigned (at 253K) to δ $^{13}C1$ = 103.6, δ $^{13}C2$ = 127.7, δ $^{13}C3$ = 80.4 and δ $^{13}C4$ = 86.3. The corresponding CH-protons for C3 and C4 appear at δ 5.49 and 7.35. Use of **1a**, the unsubstituted MOP analog, affords the three analogous products. Consequently this chemistry is not restricted to MOP derivatives possessing an electron donating substituent.

Although there is now some literature for MOP naphthyl bonding[10, 16], the "normal" π (or σ)-complexation occurs via the fully substituted carbon atoms 1 and 2 and not, carbons 3 and 4. Consequently, the olefin bonding in **18** is unique for Pd. Interestingly, the same reaction using **3** (R = CN) instead of either **1** or **2** gave only complexes analogous to **16** and **17**, some phosphine oxide, but no olefin complex analogous to **18**. We believe that the cyano group in **3** decreases the donor capability of the diene, thus suppressing chelate formation in **18**. Consequently, the structural chemistry of the MOP class is not trivial and postulated reaction mechanisms involving this group of compounds may need to strongly differentiate between **3** and **1** or **2**.

Conclusions The above results clearly show that both Pd(0) and Pd(II) are capable of coordinating two MOP ligands in pseudo cis position. Interestingly, and perhaps because these MOP ligands are quite large, η^3 to η^1 Isomerisation is not only facile, but the η^1 form is relatively

stable. Further, the choice of MOP ligand is not trivial in that both MOP compounds **1** and **2** show: a) stronger propensity towards intra-molecular olefin complexation (from the naphthyl backbone) than does its cyano-analogue, **3** and b) a novel diene chelate bonding interaction from its backbone.

3.2.4.2 Pd(II)-allyl with One MOP-ligand coordinated:

Our initial results with *bis*-MOP allyl complexes prompted us to extend these to complexes with a single MOP ligand. Hayashi[32] and Kocovsky[37] have already proposed the structure of several Pd(II)-MOP allyl complexes. As there was still some question about the bonding mode i.e., η^1 or η^2 interactions with the carbons of the MOP backbone, additional solution studies related to both Pd(II) and Pt(II) allyl were carried out. The complexes were obtained by the usual bridge splitting of the $[Pd(\mu\text{-}Cl)(\eta^3\text{-}C_3H_5)]_2$ dimer using two equivalents of the MOP ligands (**1**,**2** and **3**) in dichoromethane at room temperature (**Scheme 3.12**). On the abstraction of the chloride, a free coordination site is created which can be occupied by many potential ligands. All the complexes synthesized have two isomers owing to the orientation of the allyl group i.e.,

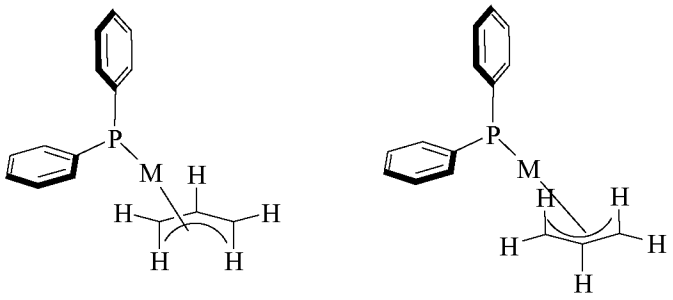

Scheme 3.12.

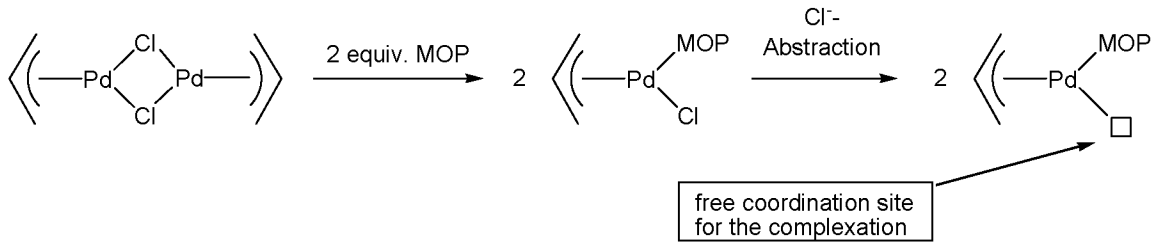

Scheme 3.13 outlines the syntheses of the mono-MOP complexes PdCl(η^3-C_3H_5)(**2b**), **20** and PdCl(η^3-C_3H_5)(**1b**), **21** (characterized by X-ray[38]) which have 3,5-di-*t*-butylphenyl substituents instead of the normal phenyl groups on the phosphine. Abstraction of the chloride using NaBArF in dichloromethane leads to [Pd(η^3-C_3H_5)(**2b**)]BArF, **22** and [Pd(η^3-C_3H_5)(**1b**)]BArF, **23**.

Scheme 3.13. Synthesis of the Pd-Allyl-complexes using ligands **1b** and **2b**.

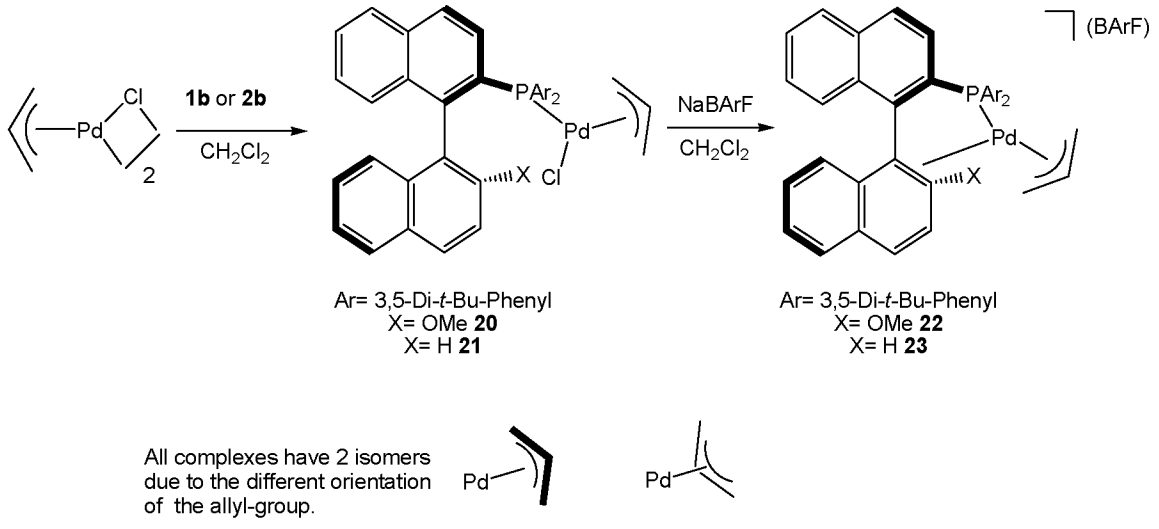

Selected ^{13}C NMR data for the complexes **20-23** are shown in **table 3.6**. **Figures 3.9** show the ^{13}C,^{1}H-long range correlations which provide the key assignments for the fully substituted carbons in **22**. The protons H-5 and H-7 show a long range correlation to C-1 at ca. 103ppm and the carbon C-6 shows a normal chemical shift of ca

155ppm i.e., no change from **20** to **22**. This is in agreement with the earlier reports[37] from Kocovsky. This type of interaction can be attributed to η^1-type which Hayashi[32] has reported.

Scheme 3.14 shows the ^{13}C coordination chemical shift for complex **22**. These data reveal relatively large Δδ values for the resonances of C1 in **22** (ca. 17ppm for both isomers).

Table 3.6. ^{13}C chemical shifts (in ppm) for **20**-**23** (500 MHz, CD_2Cl_2)

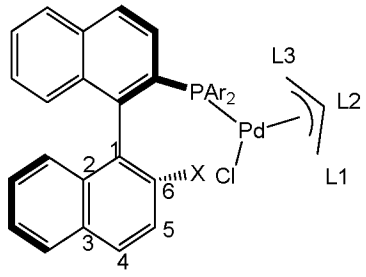

Ar= 3,5-Di-*t*-Bu-Phenyl
X= OMe **20**
X= H **21**

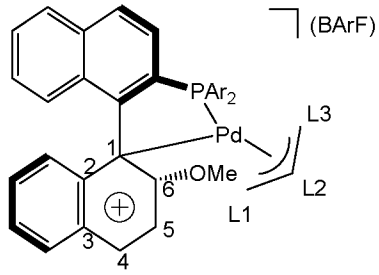

Ar= 3,5-Di-*t*-Bu-Phenyl
X= OMe **22**

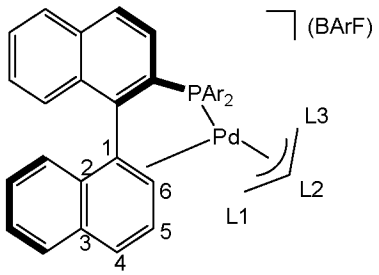

Ar= 3,5-Di-*t*-Bu-Phenyl
X= H **23**

Position	**20**[a)] Major/minor	**22**[b)] Major/minor	**21**[c)] Major/minor	**23**[d)] Major/minor
1	120.4/120.0	**103.2/103.1**	136.8	**129.2/130.7**
2	135.7/134.8	133.1/132.2	133.7	134.1/134.1
3	128.4/128.5	129.4/129.1	133.3	133.9/133.6
4	129.3/129.9	135.0/135.0	128.1	129.4/129.5
5	114.9/114.6	116.1/115.5	126.5	131.1/131.1
6	156.2/156.1	155.3/156.4	131.1	**107.4/106.4**
OCH_3	56.6/56.3	57.9/58.8	-	-
L1	80.3/79.3	100.8/100.3	79.0/79.2	99.3/100.3
L2	117.1/117.6	121.8/121.5	116.0/117.0	122.7/120.5
L3	66.2/60.4	56.5/56.8	61.3/58.5	61.5/58.9

Two isomers found at [a)] 273 K [b)] 223 K [c)] 253 K, assigned for major isomer

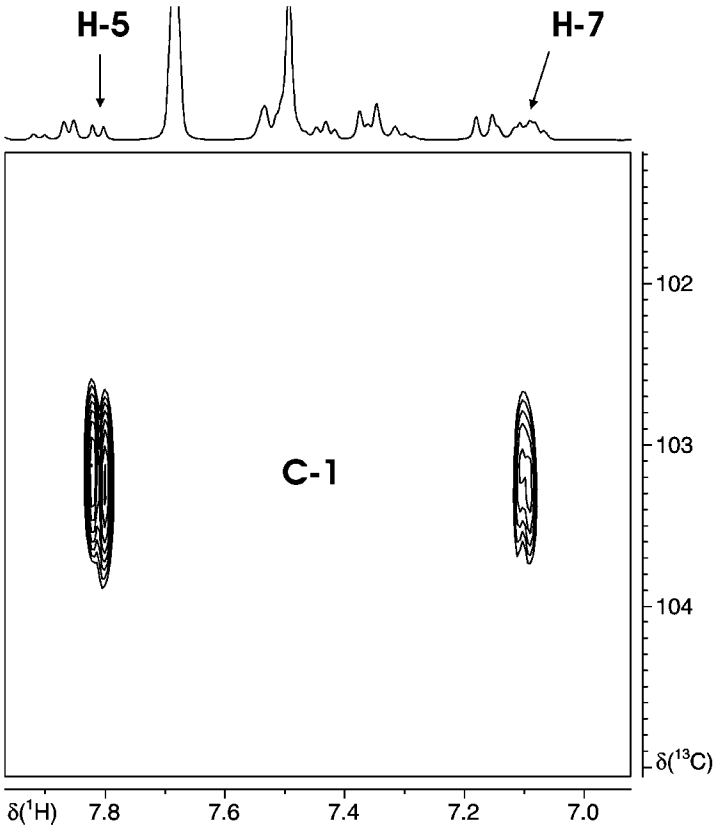

Figure 3.9. $^{13}C,^{1}H$-HMBC-correlation spectrum for **22** showing contacts from protons H(5) and H(7) to C(1) (500 MHz, CD_2Cl_2, 223 K).

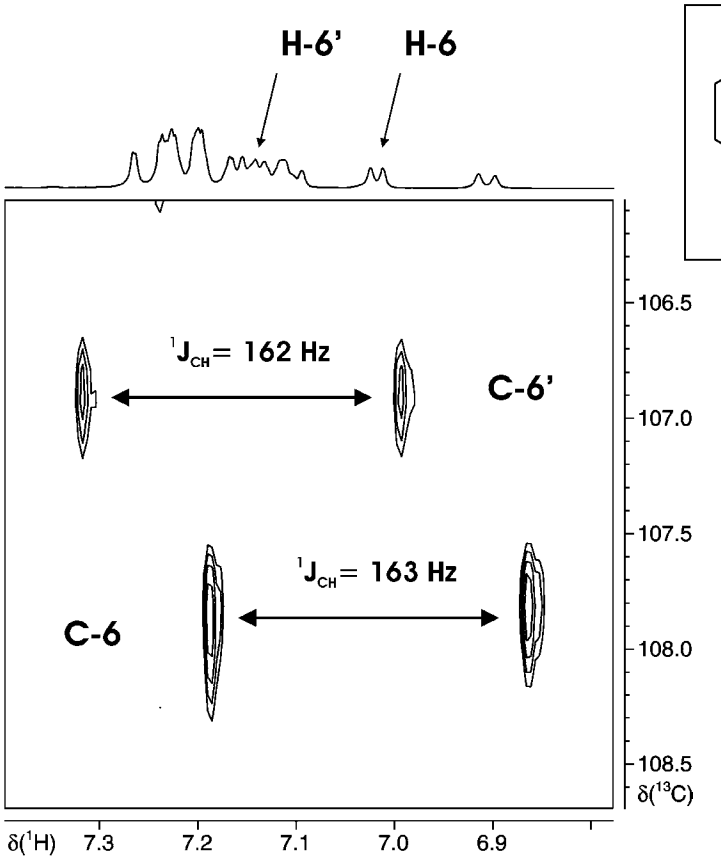

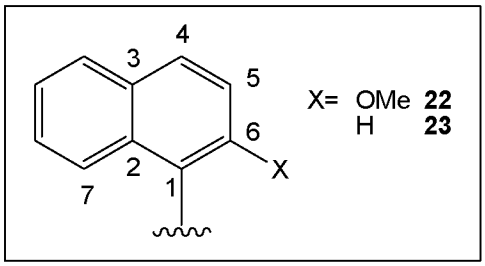

Figure 3.10. $^{13}C,^{1}H$-HMQC correlation spectrum for **23**, showing one bond proton interaction to C(6) and C(6') (arising from two different allyl orientation) with respect to the Chloride-complex **21.** Also shown is the $^{1}J_{CH}$-coupling constant ca. 163 Hz (500 MHz, CD_2Cl_2, 273 K).

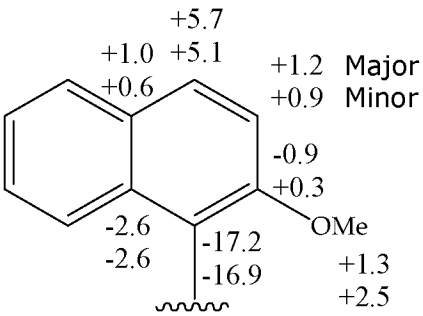

Scheme 3.14. Δ(δ ^{13}C) coordination chemical shifts (in ppm) for **22** (two allyl isomers) relative to the chloride complex **20**. Δδ= δ(**22**)- δ(**20**)

Table 3.6 also shows the ^{13}C chemical shifts for the H-MOP complexes PdCl(η^3-C_3H_5)(**1b**), **21** and [Pd(η^3-C_3H_5)(**1b**)]BArF, **23**. The protons were readily assigned via COSY spectroscopy and carbons via the ^{13}C-^{1}H one-bond correlation (**Figure 3.10**). **Scheme 3.15** shows the Δ(δ ^{13}C) coordination chemical shifts which indicate a polarized π-bond shifted towards the carbon C-6.

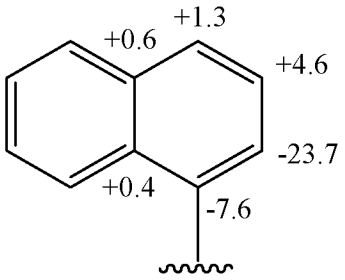

Scheme 3.15. Δ(δ ^{13}C) coordination chemical shifts (in ppm) for **23** relative to the chloride complex **21**. Δδ= δ(**23**)- δ(**21**)

Both the carbons C-1 and C-6 has shifted to low frequency (7.6 and 23.7ppm respectively), which can be considered to be consistent with some weak π-bonding character shifted towards C-6 and the Pd atom.

In conclusion, it was proven that in the case of MeO-MOP auxiliary, the metal bound to the carbon in a η^1-mode whereas with H-MOP, it prefers a η^2-fashion. Further studies on Pt-MOP complexes (discussed in next section) will enlighten on the truth of this conclusion.

3.2.4.3 *Dynamic studies on [PdCl(η^3-C_3H_5)(2a)] complex*

It is well known that the allyl group can take up two different orientations, endo (**A**) and exo(**B**) (both syn/syn), in complexes of this type.

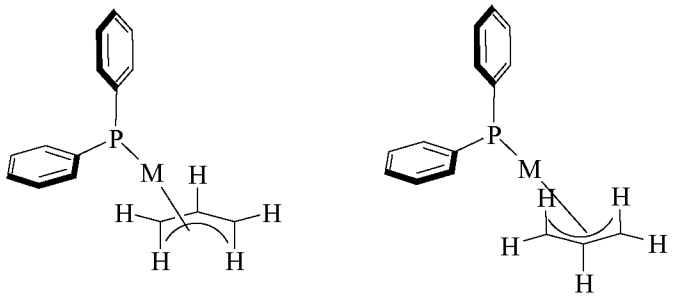

A **B**

The ^{1}H spectrum for the neutral chloro complex **20** (without t-butyl groups, as these obscure several important allyl resonances) revealed a series of broad signals for the allyl protons which indicate a dynamic process. On cooling to 273K, the proton spectrum is sharp enough to reveal proton-proton and proton-phosphorus interactions. The phase-sensitive ^{1}H-NOESY (mixing time = 50ms, 273K) shows some exchange peaks arising from the different allyl isomers (**figure 3.11**).

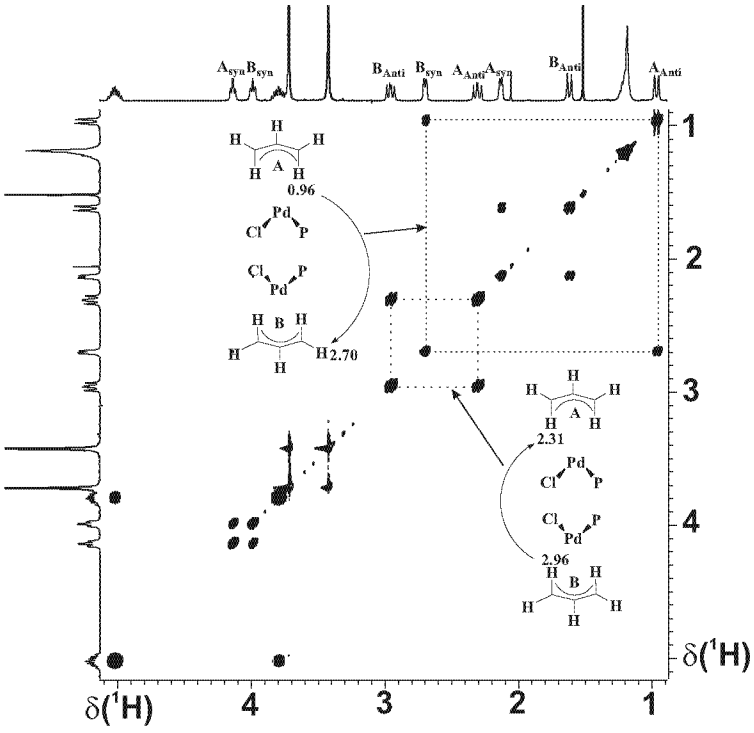

Figure 3.11. Exchange spectra of [PdCl(η^3-C_3H_5)(**2a**)] at 273K with a mixing time of 50ms.

The ^{1}H-^{1}H NOESY measurements were carried out using several different mixing times (50ms, 100ms, 200ms and 600ms), thereby allowing an estimate of the exchange rate = $2.16s^{-1}$(10) (T_1 relaxation times were around 500ms). The cross-peaks connecting the two-allyl resonances (and those stemming from the central allyl protons, $CH_2C\mathit{H}CH_2$) clearly indicate the exchange. Further, one finds selective syn/anti exchange for the allyl methylene proton pairs *trans* to the chloride ligand. The syn and anti allyl methylene protons *trans* to phosphorus do *not* exchange positions on going from one isomer to the other. It is well known that the $\eta^3 \rightarrow \eta^1$ isomerization mechanism can be under either electronic or steric control and examples of both have been reported. Apparently, in **20**, the former dominates, in that the allyl opens trans to P-donor to afford a Pd-C σ-bond trans to Cl. Rotation around the sp^3-sp^2 C-C bond, exchanges the syn and anti protons trans to chloride ligand, and after η^3-η^1 isomerization, the process is complete(see **scheme 3.16**). It seems that the C-C bond rotation in the allyl fragment is faster (top) rather than the M-C bond rotation (bottom).

Interestingly, if one increases the mixing time to 600ms, i.e., one waits longer, then new cross-peaks are observed in the exchange spectrum at 273K (see **Fig. 3.12**). These new exchange peaks can be assigned to an exchange process involving syn protons which were in pseudo-*trans* position to the P-donor, but which are now occupying syn positions pseudo-*trans* to the chloride (i.e. no syn/anti exchange, but positional exchange). We believe that this slower process arises from isomerization of the "T" shaped three coordinate complex, as indicated in **Scheme 3.16**, bottom. Taken together, these results represent a rare example of the distinction between these two mechanisms

(rotation around the C-C bond vs T-isomerization) via use of the 2-D mixing time.

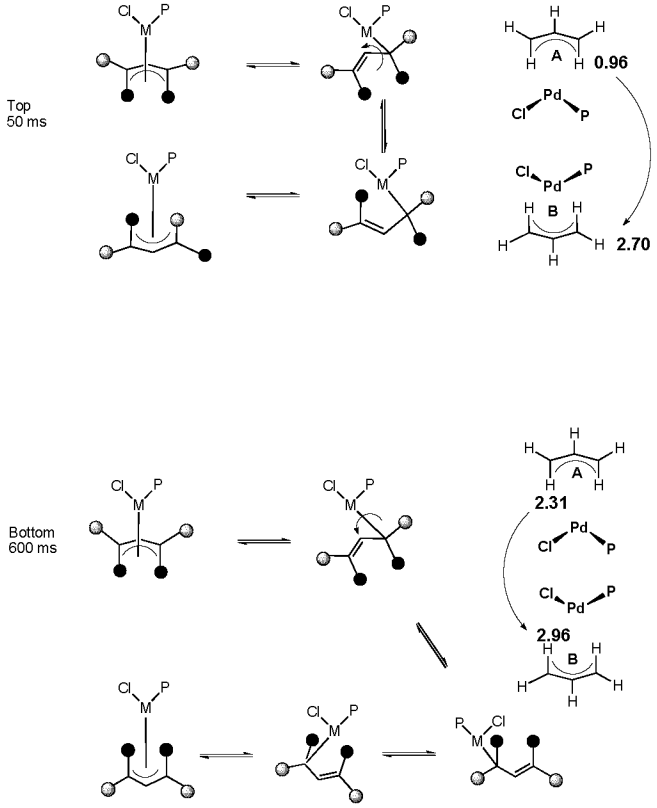

Scheme 3.16 Mechanism showing the isomerization mechanisms for the allyl fragment in the [PdCl(η^3-C_3H_5)(**2a**)] complex

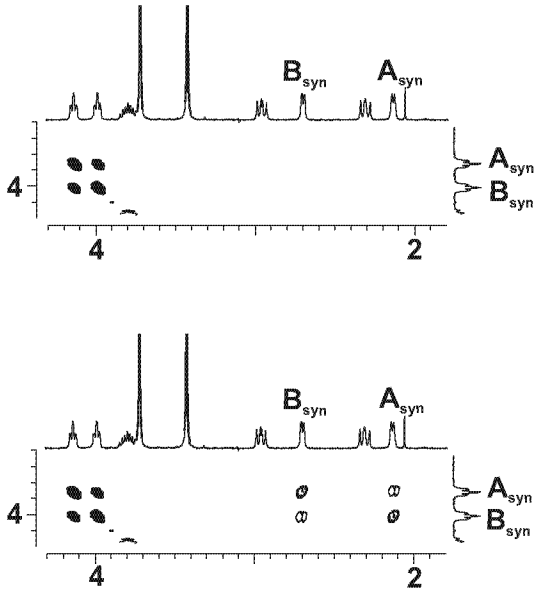

Figure 3.12. A comparison of sections of the two exchange spectra for the different mixing times (top = 50ms, bottom = 600ms). Note the appearance of the new cros-peaks in the slice with a new 600ms mixing time (bottom).

3.2.4.4 Pt(II)-allyl complexes with 1a and 2a:

In order to test the bonding mode which was seen in the Pd(II)-allyl complexes, the Pt(II) analogues, **24** and **25**, were prepared (**Scheme 3.17**). The change of metal will provide extra information via the ^{195}Pt-^{13}C coupling since the bonding mode (η^1 or η^2) should markedly affect these values. The Pt(II)-complexes prepared had a substituted allyl ($CH_2C(CH_3)CH_2$) instead of the normal η^3-C_3H_5. **Table 3.7** lists the pertinent naphthyl ^{13}C chemical shifts for complexes **24** and **25**.

Scheme 3.17

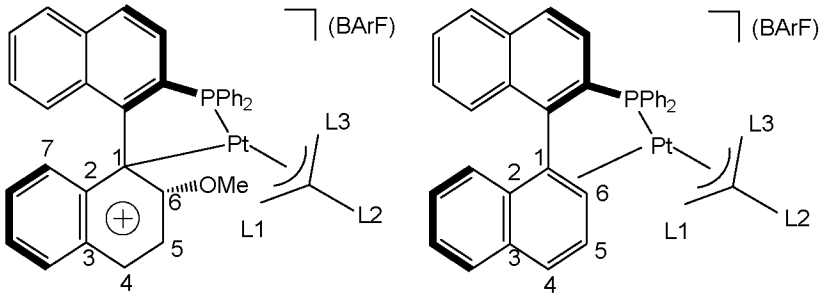

24 **25**

Figure 3.13 shows the ^{13}C-^{1}H long-range correlation of H-5 and H-7 to the ipso carbon C-1 in [Pt(η^3-allyl)(**2a**)]BArF, **24**. The ^{195}Pt-^{13}C coupling constants are $^{1}J(^{195}Pt,^{13}C_1)$ = 109.2Hz and $^{1}J(^{195}Pt,^{13}C_6)$ = 15.3Hz which indicates that the carbon C-1 is weakly σ-bonded to the metal in an η^1-fashion. Typical σ-bonded ligands e.g., a Pt-CH_3 interaction, afford $^{1}J(^{195}Pt,^{13}C)$ = 300-700Hz, so that the 15.3Hz value seems more suggestive of a two-bond than a one-bond interaction[22].

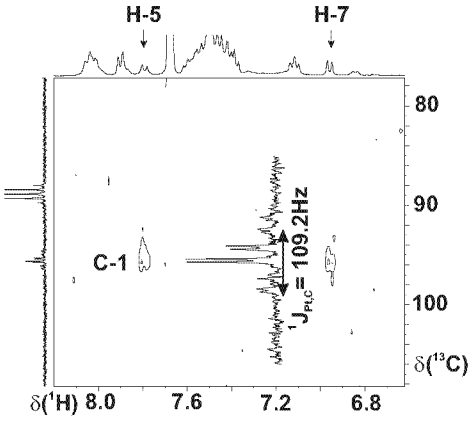

Figure 3.13. ^{13}C-^{1}H long range correlation for the [Pt(η^3-allyl)(**2a**)]BArF, **24**. Note that the carbon C-1 is shown for both endo and exo-allyl isomers with ^{195}Pt satellites.

Table 3.7 ^{13}C chemical shifts (in ppm) for **24** and **25** (400 MHz, CD_2Cl_2)

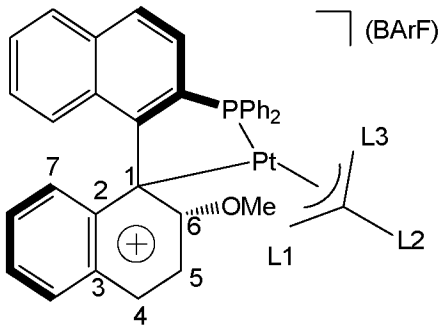

24

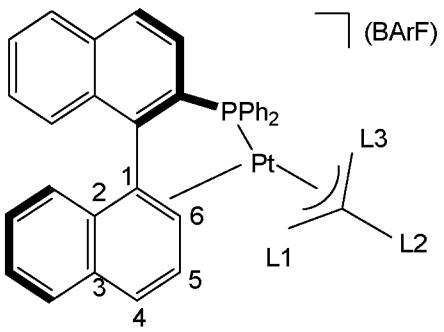

25

Position	**24** Major/minor	**25** Major/minor
1	**96.1/95.8**	**116.1/118.7**
2	137.4/137.3	132.6/132.0
3	128.0/127.2	132.8/132.2
4	136.0/137.0	129.9/129.7
5	117.7/116.3	131.9/132.5
6	152.2/156.0	**95.0/96.1**
OCH_3	57.2/57.3	-
L1	89.0/89.5	89.4/92.4
L2	23.9/22.7	24.2/23.0
L3	46.8/45.5	54.5/49.4

24: $^1J_{Pt,C}$= 109.2 (C1), $^1J_{Pt,C}$= 15.3 (C6)
25: $^1J_{Pt,C}$= 89.0 (C1), $^1J_{Pt,C}$= 56.1 (C6)

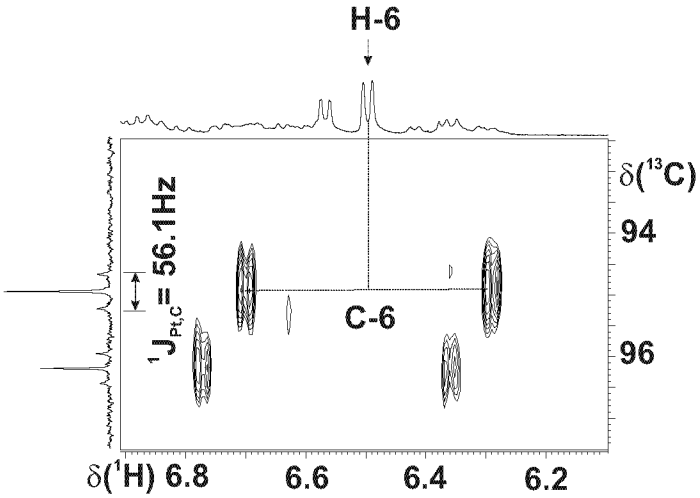

Figure 3.14. One bond CH-correlation for H-6 in the complex [Pt(η^3-allyl)(**1a**)]BArF, **25**. The ^{195}Pt satellites with $^1J(^{195}Pt,^{13}C_6)$ = 56.1Hz, for both exo and endo isomers are also shown.

The ^{13}C-^{1}H one-bond correlation for the carbon C-6 (**Figure 3.14**) and ^{13}C-^{1}H long-range correlation from H-5 to C-1 (**Figure 3.15**) in [Pt(η^3-allyl)(**1a**)]BArF, **25** were measured. The ^{195}Pt-^{13}C coupling constants are relatively small, but of similar size i.e., $^{1}J(^{195}Pt,^{13}C_1)$ = 89.0Hz and $^{1}J(^{195}Pt,^{13}C_6)$ = 56.1Hz, which indicates that the metal is weakly bound to the phosphine moiety in an η^2-fashion (Strong π-bonding in Pt(II)-(η^2-olefin) complexes, e.g., K[PtCl3(C2H4)] are of the order of 150Hz[22]).

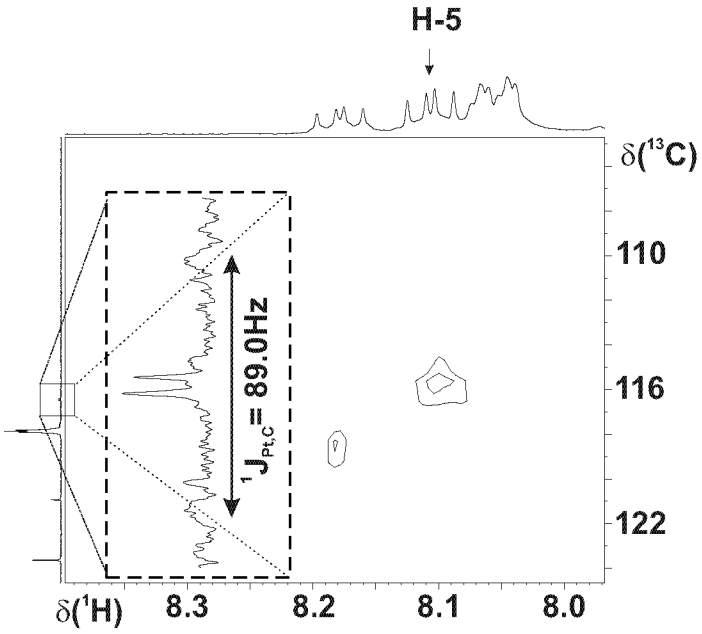

Figure 3.15. ^{13}C-^{1}H long range correlation from H-5 to C-1 in the complex [Pt(η^3-allyl)(**1a**)]BArF, **25**. The ^{195}Pt satellites with $^{1}J(^{195}Pt,^{13}C_1)$ = 89.0Hz, for both exo and endo isomers are also shown.

In conclusion, it was proven that in the case of MeO-MOP auxiliary, the platinum binds to the carbon in a η^1-mode whereas with H-MOP, it prefers a η^2-fashion. This is in accordance with the earlier studies on the analogues of palladium allyl complexes.

3.2.4.5 Pd(II)-allyl complex with ligand 3b:

The complex PdCl(η^3-allyl)(**3b**), **26** was prepared via the usual bridge splitting reaction using 2 equivalents of CN-MOP ligand, **3b**(**Scheme 3.18**). Abstraction of the chloride from **26** gives the complex [Pd(η^3-allyl)(**3b**)]BArF, **27**, generated in-situ. **Scheme 3.19** shows the broad ^{31}P solution spectrum at room temperature which was obtained by adding 1 equivalent of NaBArF. Upon cooling to 213K, numerous signals were obtained which on addition of excess of acetonitrile generates only 2 signals (i.e., exo and endo acetonitrile complex). These signals can be attributed to the coordination of the acetonitrile to the metal via the nitrogen atom. Although the exact structure of **27** is not certain, it *does not show the naphthyl backbone interaction* as in **22** and **23**.

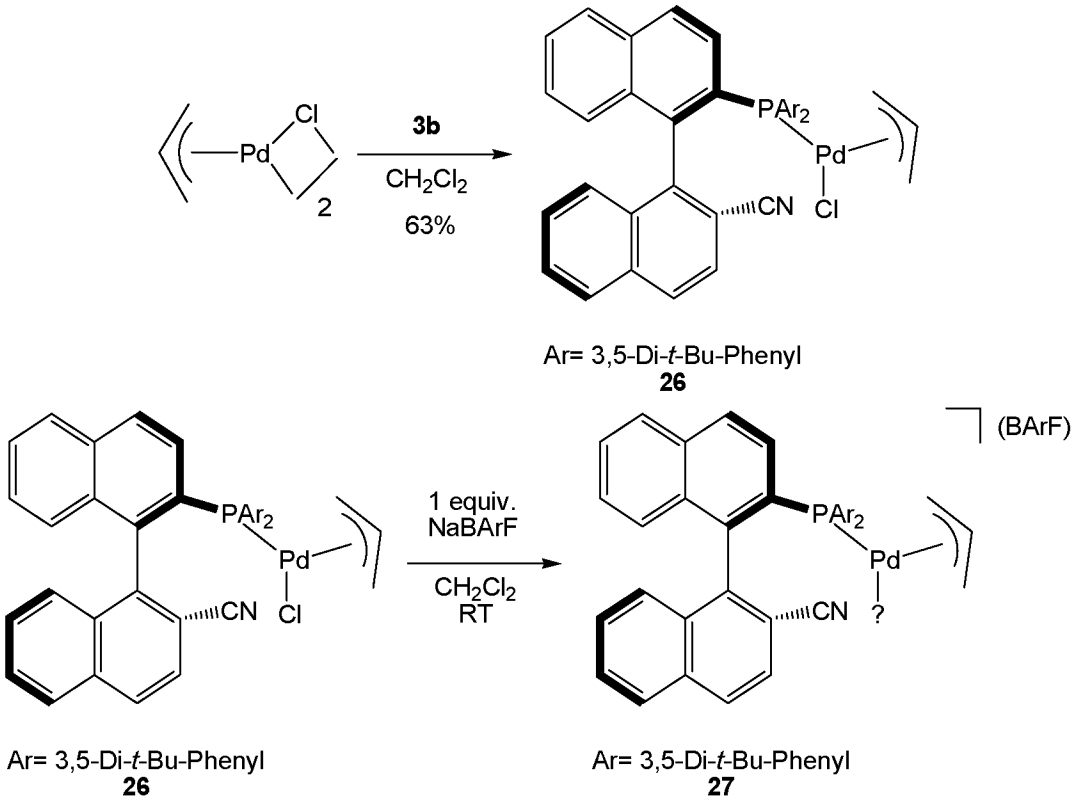

Scheme 3.18. In-situ preparation of the cationic complex **27**

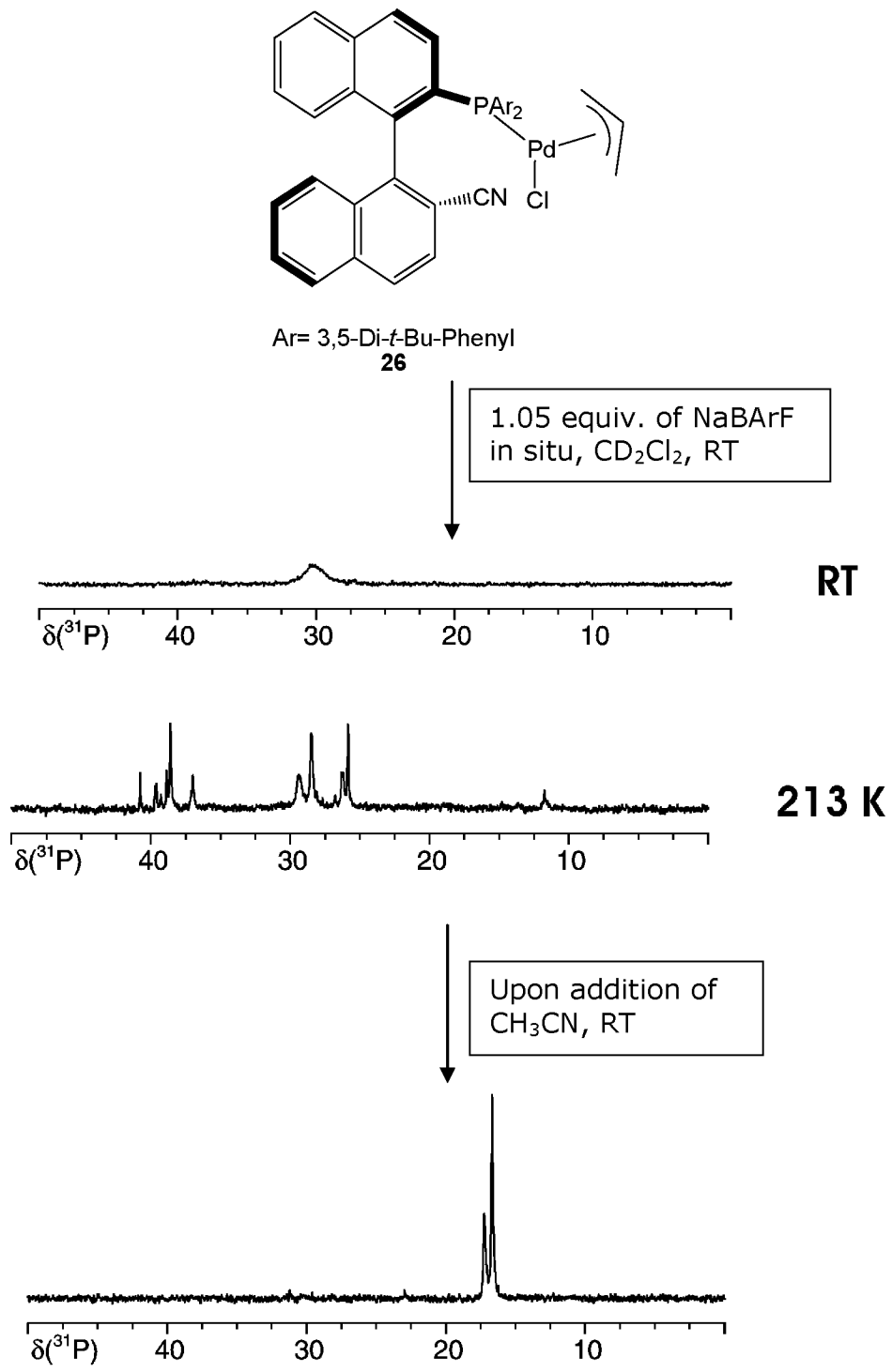

Scheme 3.19. ^{31}P-NMR-Spectrum for the complex **27** generated *in-situ* by abstraction of the chloride from **26** at room temperature and at 213 K and then upon adding Acetonitrile at room temperature (400 MHz, CD_2Cl_2).

3.2.5 Ru(II)-Phosphoramidite complexes

Chiral bidentate ligands have dominated the field of asymmetric catalysis in past decades and a number of privileged ligands including Binol, Taddol, bisoxazolines and a variety of bisphosphines have found widespread application[39]. The pioneering work on rhodium catalyzed asymmetric hydrogenation producing optically active amino acids, as reported by Knowles[40], was however based on monodentate phosphine ligands. A limited number of monodentate chiral ligands have found application in asymmetric catalysis. Recently a number of new highly selective phosphorus based monodentate chiral ligands such as phosphines, phosphonites, phosphites and phosphoramidites have been introduced[41, 42]. Binol- and Taddol-based phosphoramidites are among the most successful members of this new class of chiral ligands (**Scheme 3.20**).

Scheme 3.20. Monodentate phosphoramidite ligands

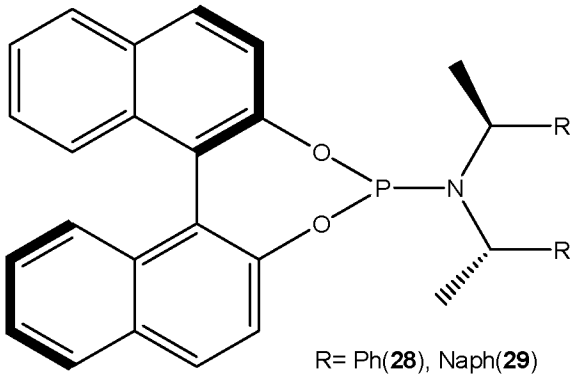

R= Ph(**28**), Naph(**29**)

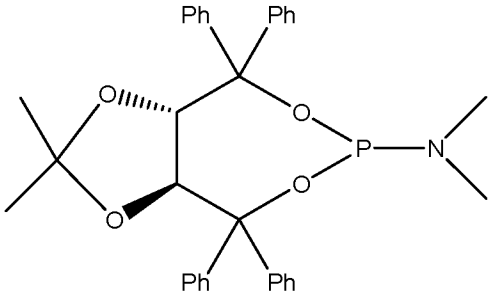

Taddol

Results and discussion:

Mezzetti and coworkers[43] have shown that [$RuCl_2$(*p*-cymene)(**28**)],**30** and [$RuCl_2$(*p*-cymene)(**29**)],**31**, catalyzes the cyclopropanation of styrene and α-Me-styrene with ethyl diazoester after chloride abstraction with $TlPF_6$ or $(Et_3O)PF_6$. With α-

methylstyrene, good enantioselectivities were observed (up to 86 and 87 % ee for the *cis* and *trans* cyclopropane derivative, respectively) (**Scheme 3.21**).

Scheme 3.21

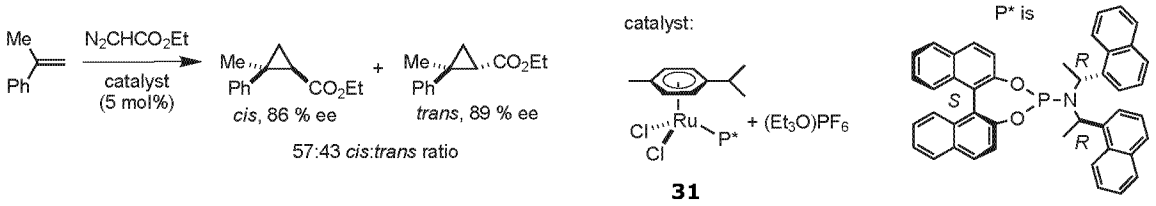

Given our interest in how related monodentate ligands bind, solutions of **30** and **31** in which chloride has been abstracted to give a 16e$^-$ species (**32** and **33** respectively), were provided by coworkers of Dr.Mezzetti. The formulation of **32** (Ph) and **33** (Np) as [RuCl(*p*-cymene)(P*)]PF_6 implies a 16-electron count, which is not supported by the light yellow colour of the complexes. A binuclear formulation was excluded based on molecular volume data obtained by PGSE measurements (see below). A combination of multinuclear multidimensional NMR measurements indicated that **32** and **33** are six-coordinate complexes in which the coordination sphere of the 16-electron fragment [RuCl(η^6-*p*-cymene)(P*)]$^+$ is saturated by means of an η^2-interaction between the ruthenium(II) atom and the phenyl (**32**) or one double bond of the naphthyl ring (**33**) of one of the CH(Me)Ar substituents, see **Scheme 3.22**.

It was evident from the observed line widths for several proton resonances in the aromatic region that both **32** and **33** exhibited dynamic character on the NMR time scale. Upon cooling the samples to –20 °C, these signals sharpened sufficiently. Both one-bond and

long-range carbon-proton correlations for **32** (see **Figure 3.16**) and **33** were measured.

Scheme 3.22

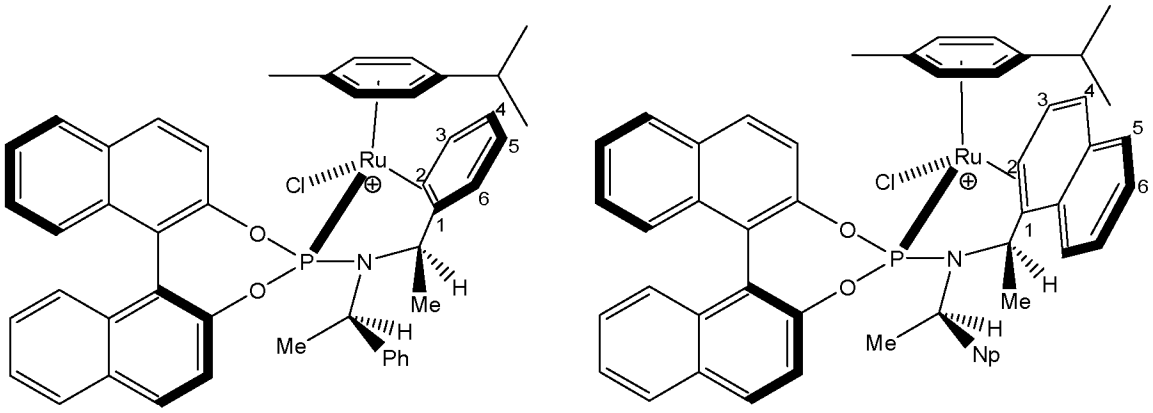

32 **33**

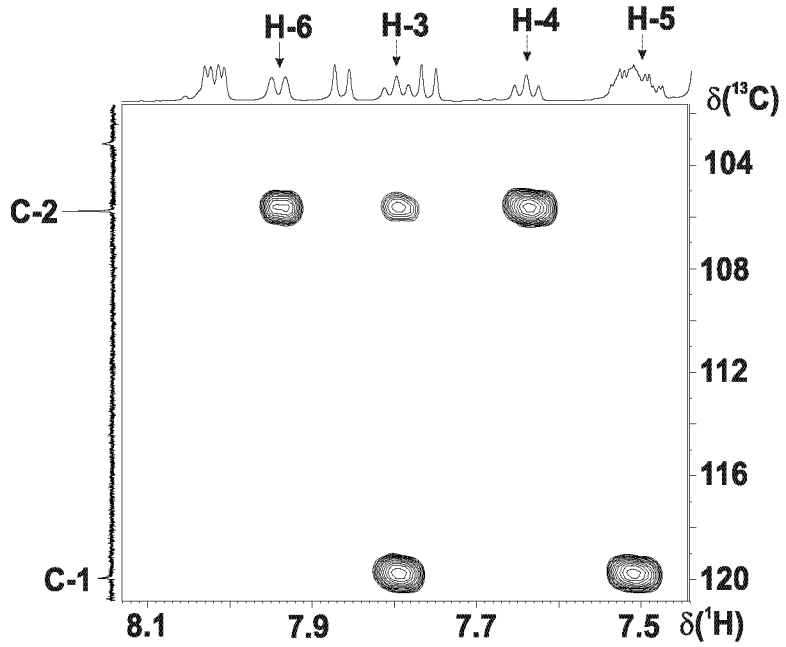

Figure 3.16. CH long range correlation showing strong contacts from H-4 and H-6 and a weak contact from H-3 to C-2. Further, strong contacts from H-3 and H-5 to C-1 in complex **32**.

Protons H(3) and H(5) correlate to C(1), δ= 120.0 (for **32**) and δ= 100.9(for **33**), via three-bond interactions as do protons H(4) and H(6) to C(2), δ= 105.7 (for **32**) and δ= 96.8 (for **33**) (**Table 3.8**).

Table 3.8. Selected ^{13}C Chemical Shift Values for **30**, **32**, **33** and 3**4**.

	30	**32**	**33**	**34**
C(1)	144.4	120.0	100.9	106.3
C(2)	128.2	105.7	96.8	82.0
C(3)	127.6	136.4	131.8	90.7
C(4)	126.3	131.3	132.6	99.0
C(5)	ca 127.6	130.6	[a]	105.5
C(6)	ca 128.2	134.6	[a]	81.5

[a] the ^{13}C Chemical Shift values are in the region 128-132ppm.

In **32**, the coordination chemical shift, $\Delta\delta$, for C(1) is 24.4 ppm, whereas that for C(2) is 22.5 ppm. These $\Delta\delta$ values are indicative of a modest-to-weak π-olefin type complex[22]. The second, non-complexed phenyl ring has carbon chemical shifts in the normal aromatic region and shows two equivalent *ortho* (and *meta)* protons, i.e., there is no restricted rotation at this temperature. This confirms that one of the diastereotopic phenyl rings is bonded to the ruthenium in an η^2-fashion. The analogous $\Delta\delta$ values for **33** are larger, 44.5 ppm and 31.4 ppm, for C(1) and C(2), respectively. The differences in $\Delta\delta$ are likely to be related to the fact that, in **33**, one does not lose the aromaticity through complexation. The relevant ^{13}C chemical shift values derived from the NMR measurements are shown in **Table 3.8**.

The ^{13}C chemical shift values for the η^6 -*p*-cymene ligand are rather normal, but suggest an asymmetric bonding to ruthenium. The averaged CH-arene ^{13}C chemical shifts in **32** and **33** are δ 91.0 and 94.8, respectively (**Fragment 1**). These values are somewhat smaller than those measured for, e.g., the model [Ru(Binap(**A**)/ MeO-Biphep(**B**))(Cl)(*p*-cymene)]Cl, indicating a substantial π-backbonding to the *p*-cymene of **32** and **33**. The ^{31}P resonances for **32** and **33** are found at δ 153.0 and δ 166.5, respectively.

Fragment 1

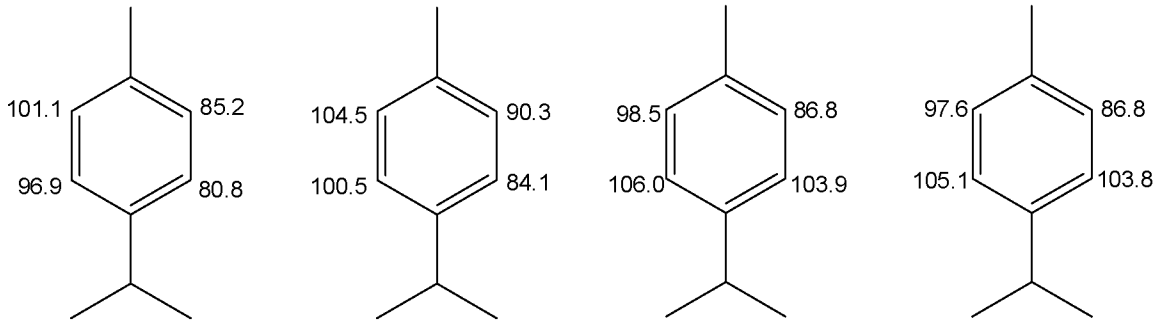

32	***33***	***A**-Binap*	***B**-MeO-Biphep*
avg= 91.0	94.8	98.5	98.3

PGSE (Pulse Gradient Spin Echo) diffusion measurements for **32** and **33** confirm that these salts are mononuclear. The diffusion coefficients (**Table 3.9**) decrease only slightly on going from the neutral dichloro complexes **30** and **31** to **32** and **33**.

Table 3.9. Diffusion coefficients ($X10^{-10}m^2sec^{-1}$) and hydrodynamic radii(Å)of **28-34**.

		$D(M^+)$	r_h
Ph- ligand (**28**)		10.06	5.3
$[RuCl_2(p\text{-cymene})(\mathbf{28})]$ (**30**)		8.66	6.2
$[RuCl(p\text{-cymene})(\eta^2\text{-}\mathbf{28})]PF_6$ (**32**)	cation	8.12	6.6
	anion	9.83	5.4
$[RuCl(\eta^6\text{-}\mathbf{28})](PF_6)_2$ (**34**)	cation	6.55	8.2
	anion	8.45	6.3
Napth-ligand (**29**)		9.44	5.7
$[RuCl_2(p\text{-cymene})(\mathbf{29})]$ (**31**)		8.21	6.5
$[RuCl(p\text{-cymene})(\eta^2\text{-}\mathbf{29})]PF_6$ (**33**)	cation	8.18	6.6
	anion	11.80	4.5

Interestingly, the hydrodynamic radius, r_h for the anion PF_6, 5.4Å is so large, that a considerable amount (>50%) of ion pairing is

present. The hydrodynamic radius of PF_6 in methanol is 2.6-2.7Å[44]. For 100% ion pairing the r_h values for the cation and anion would be identical, i.e., 6.6Å in **32**. The ion pairing in the naphthyl analog is not as marked.

Loss of *p*-Cymene. On standing in CD_2Cl_2 solution, **32** convert into a new complex **34** featuring a singlet at δ 149.0. The process takes place also in the solid state, albeit on a longer time scale[45]. Mass spectroscopy and elemental analysis suggest the empirical formula [RuCl(**28**)] for **34**. The same combination of NMR multinuclear and PGSE methods used for **32** and **33** indicates that **34** is the binuclear species $[RuCl(\mathbf{1a},P,\eta^6\text{-}C)]_2$, in which a phenyl ring of the N–CH(Me)Ph moiety binds ruthenium in an η^6-fashion (**Figure 3.17**).

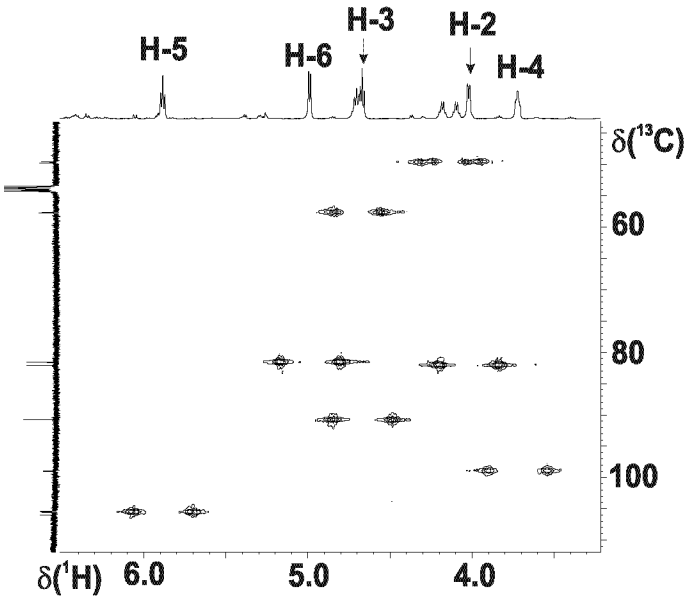

Figure 3.17. One bond CH correlation showing the five aromatic protons of the bound phenyl-ring plus the two N(CH)Me protons in complex **34**.

^1H and ^{13}C NMR data confirmed the absence of the η^6-*p*-cymene and that only one phenyl ring is freely rotating. The $^{31}P,^1H$ HMQC correlation allowed us to assign the different N–CH(Me)Ph methine

protons and carbons and, thus, to connect these to the corresponding bound and free phenyl rings. As expected a set of six ^{13}C signals from one of the N–CH(Me)Ph phenyl rings is displaced to lower frequency (see **Table 3.8**), thus confirming an η^6-complexation to ruthenium. Distinct patterns are observed for the two N–CH(Me)Ph methine protons. That belonging to the η^6-complexed moiety appears as a doublet of quartets (δ = 4.14, $^3J_{P,H}$ = 42.4Hz), whereas that of the dangling N–CH(Me)Ph group is observed as a multiplet (δ = 4.70, $^3J_{P,H}$ = 13.7Hz). These very different $^3J_{P,H}$ values reflect the different conformations of the N–CH(Me)Ph groups. These data are in good agreement with predictions based on the Karplus equation[46]. These coupling constant data, combined with inspection of molecular models, suggest that only a certain binding mode (as in **fragment 2**) is possible without any serious interactions to the naphthyl groups.

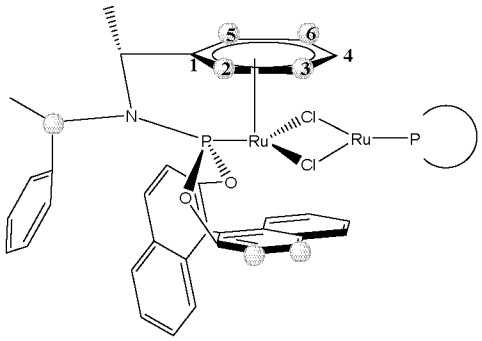

Fragment 2.

The PGSE measurements in CD_2Cl_2 show a much larger r_h value for the cation in **34**, consistent with its dinuclear structure (**Table 3.9**). Again we note very substantial ion pairing of the PF_6, in that the r_h- value 6.3Å is relatively large. The hydrodynamic radius of PF_6 in methanol is 2.6-2.7Å[44]. For 100% ion pairing the r_h values for the cation and anion would be identical, i.e., 8.2Å in **34**.

In order to localize the anion in **34**, ^{19}F-^{1}H HOESY measurements were carried out. **Figure 3.18** shows part of the spectrum and reveals specific, *strong* contacts to several aromatic resonances of the Binol and some few weaker contacts to the complexed arene ring. There is also a *strong* cross-peak arising from one CH methine, that which is not associated with the complexed arene. Analysis of these data suggests that the anion approaches the Ru in a specific fashion i.e., it sneaks through the crowded region of the backbone thereby avoiding the bridging chloride ligand.

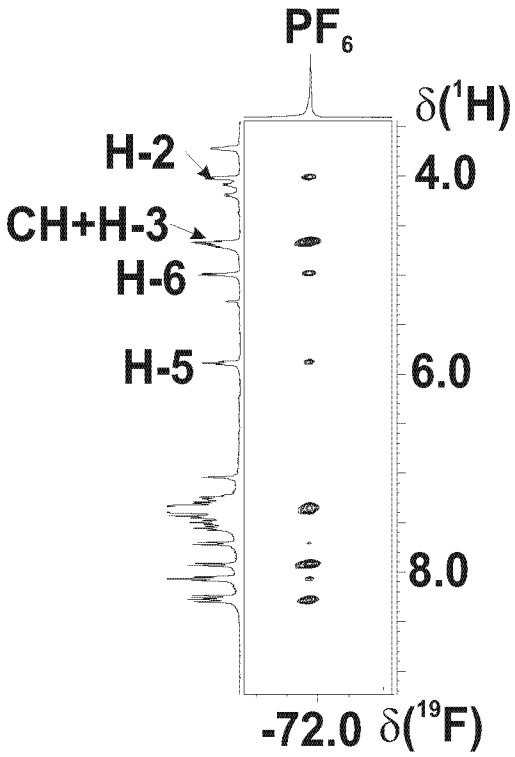

Figure 3.18. ^{19}F-^{1}H HOESY for complex **34** in which the anion, PF_6, showing preferential contacts to the bound Phenyl-ring in addition to other aromatic protons.

Conclusion: It seems evident from the above discussions of this chapter that the monodentate ligands (MOP or Phosphoramidite) do like to have a chelation when given a chance. Usually the possible site of chelation is from the backbone which is close to the metal centre.

3.3 P,N ligands:

Chiral P,N type ligands were found to induce excellent enantioselectivities in Pd-catalysed allylic alkylations with 1,3-diphenylallyl acetate and other symmetrically substituted allyl substrates. Further evaluation of these readily accessible ligands has led to several other useful applications in asymmetric catalysis[47]. Transition metal complexes containing these chiral P,N-auxiliaries and specifically those by Helmchen[48], Pfaltz[49] or Togni[50] and co-workers, are now routinely used as catalysts in enantioselective homogeneous catalysis.

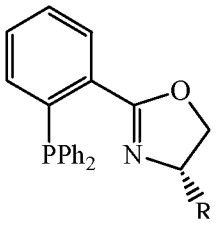

Pfaltz, Helmchen[28,29]

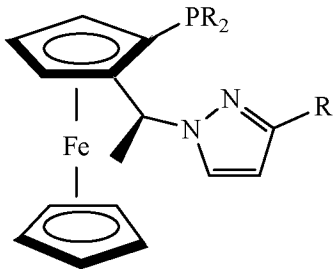

Togni[30]

3.3.1 Background

Pregosin and coworkers have recently shown[29, 51] that, in the chiral back-bone of **35**-**37**, the orientation of the oxazoline ring, is perpendicular to the Cl-Pd-Cl plane. For the enantioselective allylic alkylation (equation **3.3.1**) of a 1,3-diphenyl allyl compound, this structural change (which shifts the position of the i-Pr group relative to substrate) induces a change in the observed product enantiomer. Further by introducing *meta* alkyl groups on the P-phenyl substituents, e.g., **36**

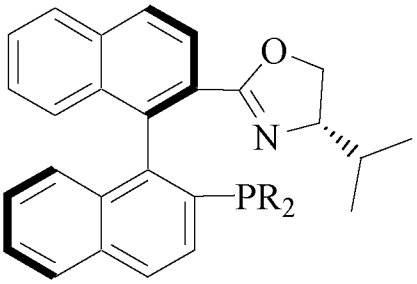

35 R = Ph,
36 R = 3,5-di-methylphenyl
37 R = 3,5-di-*t*-butylphenyl

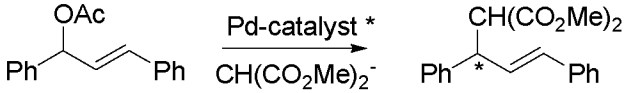

Equation **3.3.1**. Allylic Alkylation

and **37**, it was observed[29, 51, 52] that the enantiomeric excess, ee, in a Heck arylation increases when the *meta* substituents increase in size. Although the methyl groups of **36** result in a significant improvement in the ee relative to **35**, the best ee results from using **37**. This is yet another manifestation of what Pregosin *et al* have named the "*meta*-dialkyl effect" on enantioselectivity.[29, 53, 54] This effect arises, partially, from restricted rotation around P-C bonds with the resulting chiral pocket becoming slightly more rigid. The additional rigidity of the chiral pocket increases the correlation with substrate, thus affording a slightly more selective catalyst. There are a number of catalytic reactions for which "*meta*-dialkyl effects" have been shown to be useful[52].

The complexes [Pd(η^3-PhCHCHCHPh)(**35**)]OTf, **38**, [Pd(η^3-PhCHCHCHPh)(**36**)]OTf, **39** and [Pd(η^3-PhCHCHCHPh)(**37**)]OTf, **40** were prepared and tested in the catalysis[29, 31, 51]. It has been observed earlier[29] that the ee in the Pd-catalysed allylic alkylation of eq. **3.3.1** increases from ca 91%, with **35** as auxiliary, to ca 97% with **36** (See **table 3.10**). Surprisingly, the ee sinks to ca 66% with **37** and an explanation for this observation was sought based on detailed NMR studies.

Table 3.10:

Entries	Catalyst[a)]	time (h)	Yield[b)] (%)	ee[c)] (%) (Conf.)
1	[PdCl(η^3-PhCHCHCHPh)]$_2$ /**3**	4	90	91 (R)
2[d)]	[PdCl(η^3-PhCHCHCHPh)]$_2$ /**4**	2	99	97 (R)
3	[PdCl(η^3-PhCHCHCHPh)]$_2$ /**5**	4	84	66 (R)

[a)] 1 mol-% [PdCl(η^3-PhCHCHCHPh)]$_2$ and 2.5 mol-% Ligand, respectively. 2 mol-% Pd(dba)$_2$ and 2.5 mol-% Ligand [b)] based on isolated product [c)] Assigned using HPLC with a Chiracel OD-H column [d)] literature[55]

3.3.2 3,5 meta-dialkyl effect

The previously prepared[55] model cationic 1,3-diphenylallyl complexes, [Pd(η^3-PhCHCHCHPh)(**35**)]CF_3SO_3, **38** and [Pd(η^3-PhCHCHCHPh)(**36**)]CF_3SO_3, **39**, exist in CD_2Cl_2 solution as a mixture of only two isomers, the syn/syn endo and syn/syn exo isomers, with the former the most abundant. These compounds are not exchanging on the NMR time scale based on 2-D exchange spectra. The descriptors exo and endo refer to the position of the central allyl proton relative to the i-Pr group (it is to be noted that the i-Pr group is not "below" the co-ordination plane as the dotted line in e.g., **40a**, might indicate, due to the ring twist noted above).

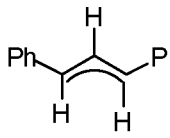

syn/syn isomer

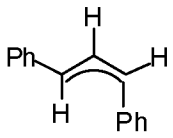

syn/anti isomer

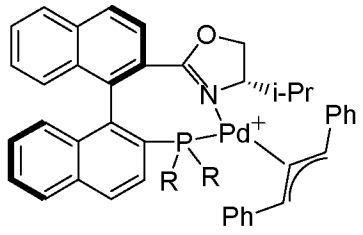

40a, syn/syn endo diastereomer

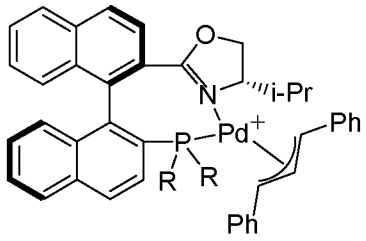

40c, syn/syn exo diastereomer

R = 3,5-di-*t*-butylphenyl, both cations as triflate salts

In contrast to **38** and **39**, which show only two, the ^{31}P NMR spectrum of **40** revealed *four* species, **a-d**, in the ratio ca 12.3 : 0.88 : 1 : 0.13, respectively. A summary of the NMR data for **40a** is given in **Table 3.11**.

Table.3.11 Chemical shifts (ppm) and coupling constants (Hz) for **40a**

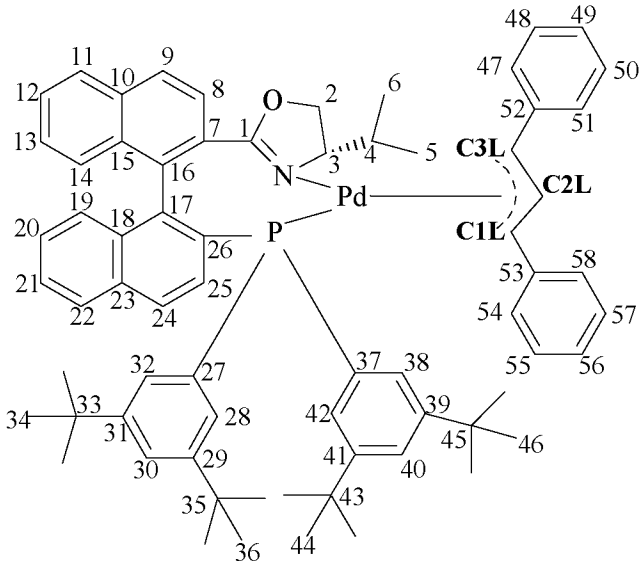

No.	^{1}H	^{13}C	Coupling constants
1.	----	171.1	----
2a.	3.50t[a]	73.0	$^{2}J_{HH}=^{3}J_{HH}$= ca 9[b]
2b.	3.79t[a]	73.0	$^{2}J_{HH}=^{3}J_{HH}$= ca 9[b]
3.	3.39 m	73.7	
4.	0.62 m	30.8	
5.	0.29 d	16.6	$^{3}J_{HH}$=6.1
6.	1.07 d	21.8	$^{3}J_{HH}$=6.6
7.	----	133.6	
8.	7.95	122.5	$^{3}J_{HH}$=8.3
9.	8.41 d	131.2	$^{3}J_{HH}$=8.3
10.	----	132.9	
11.	8.02 d	128.8	$^{3}J_{HH}$=8.0
12.	7.46t[a]	128.2	$^{3}J_{HH}$=2x ca 8[b]
13.	6.83t[a]	129.5	$^{3}J_{HH}$=2x ca 8[b]
14.	6.12 d	126.2	$^{3}J_{HH}$=8.4
19.	6.70	126.3	
20.	7.23t[a]	127.8	$^{3}J_{HH}$=2x ca 8[b]
21.	7.53t[a]	128.2	$^{3}J_{HH}$=2x ca 8[b]
22.	7.57	125.7	
24.	7.95	129.9	
25.	6.96t[a]	127.2	$^{3}J_{HH}=^{3}J_{PH}$= ca 8.5[b]
26.	----	133.9	
27.	----	128.5	
28,32.	6.90	127.9	
29,31.	----	151.8	
30.	7.59	130.3	
33,35.	----	35.4	
34,36	1.31	31.6	

37.	----	133.0	
38,42.	6.87 d	129.6	$^{3}J_{PH}$=12.5
39,41.	----	151.2	
40.	7.31	127.5	
43,45.	----	35.0	
44,46.	1.18	31.4	
C1L.	4.58 d	65.5	$^{3}J_{HH}$=10.0
C2L	6.35	109.0	
C3L.	5.96 dd	105.2	$^{3}J_{PH}$=13.8, $^{3}J_{HH}$=8.8 $^{2}J_{PC}$= ca 20
47,51.	7.90 d	128.4	$^{3}J_{HH}$= 6.8[c]
48,50.	6.35	131.0	
49.	6.67	127.6	
52.	----	131.0	
53.	----	136.7	
54,58.	6.70	127.5	$^{3}J_{HH}$=8.5[c]
55,57.	6.61	128.4	
56.	6.83	127.8	$^{3}J_{HH}$=2x ca 8 [b,c]

[a] multiplicity as observed in the spectrum
[b] estimated values due to overlap of signals
[c] second order spin system with approximate coupling constants

The suggested structures for **40b** and **40c** were determined via analysis of their allyl proton and carbon NMR data. Selective NOE's between the allyl protons and the proximate i-Pr spins readily allow the distinction between the endo and exo-isomers **40a** and **40c**, respectively. The diastereomer **40b** is assigned a syn/anti allyl structure. This decision arises from:

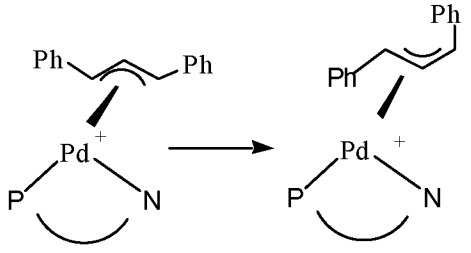

40a/c **40b**

a) a TOCSY measurement which indicates the three allyl spins.

b) a C,H-correlation to confirm the appropriate ^{13}C chemical shifts.

c) a P,H-correlation to locate the allyl proton pseudo-trans to the P-atom.

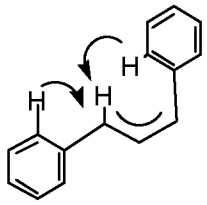

d) NOE's which confirm that two of the three allyl proton spins are cis.

e) the absence of the usual anti/anti NOE found in syn/syn isomers and

f) the observed NOE's between the anti proton and two sets of allyl phenyl protons.

There are no ^{1}H NMR data for **40d**, partially because of its limited abundance. Possibly **40d** is phosphine oxide, based on the ^{31}P chemical shift.

In contrast to the observations for **38** and **39**, a ^{31}P 2-D phase sensitive NOESY revealed exchange peaks between **40a** and **40c** (whose ^{31}P signal is somewhat broadened, see **Figure 3.19**). An analogous ^{1}H exchange spectrum is shown in **Figure 3.20**. The exchange is specific with, e.g., the terminal allyl proton pseudo-trans to the P-donor in **40a** exchanging with the terminal allyl proton pseudo-trans to the N-donor in **40c**, i.e.:

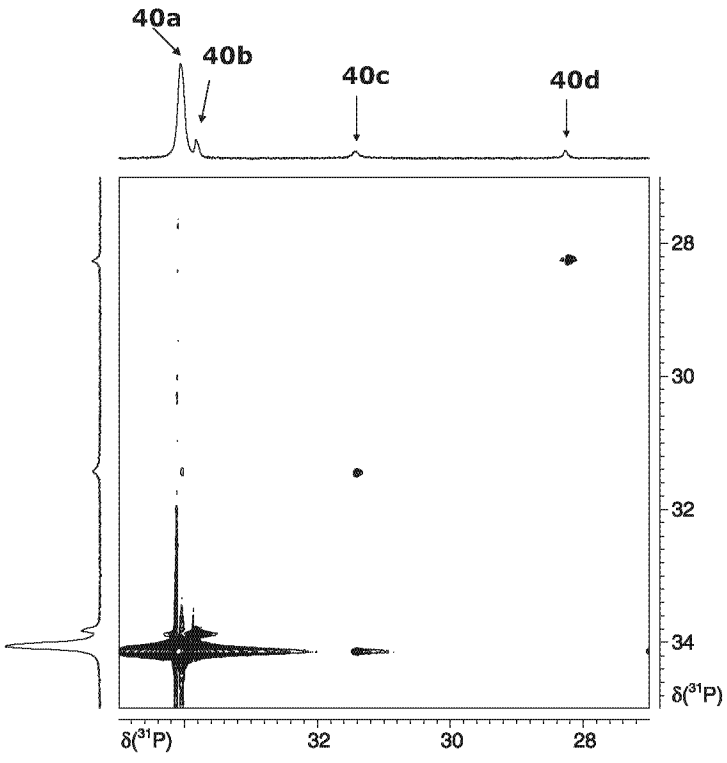

Figure 3.19. ^{31}P-^{31}P exchange spectrum revealing exchange between **40a** and **40c**.

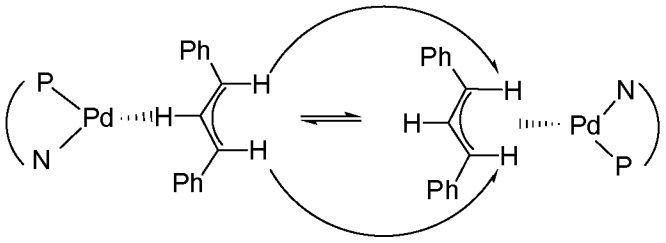

fragments indicating which protons are in exchange

This type of dynamic behaviour has been observed previously[56] and is thought to stem from a selective η^3-η^1 isomerization process (in conjunction with several additional steps). **Figure 3.20** also reveals very broad exchange peaks, connecting **40a** to an isomer of very low concentration. Analysis of these very weak and broad signals at ambient temperature, and 193K, confirms that it represents a fifth compound with the expected 3 allyl ^{1}H resonances.

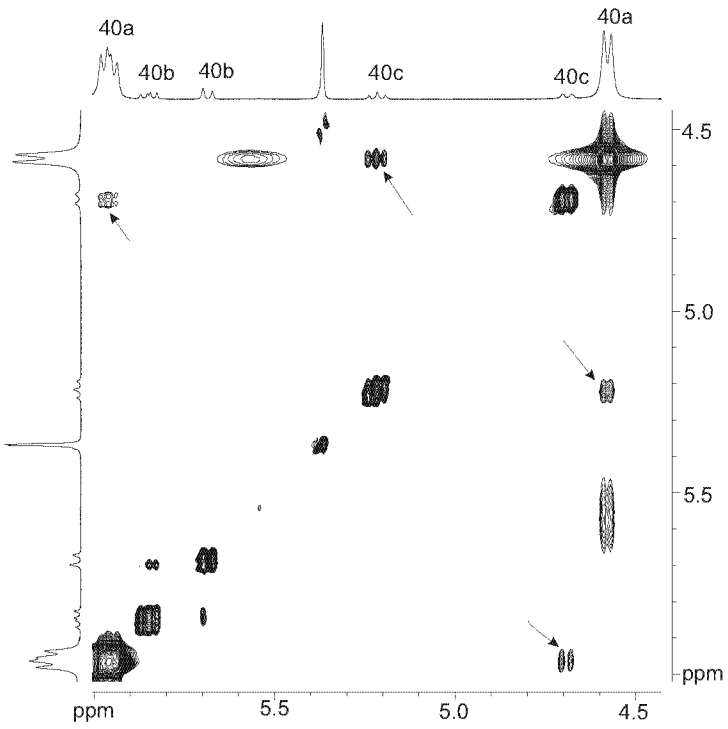

Fig. 3.20 section of the ^{1}H NOESY for **40** showing selective exchange between **40a** and **40c** as indicated by the arrows (CD_2Cl_2, 500 MHz)

Perhaps the most interesting NMR detail concerns the ^{13}C chemical shifts of the allyl-carbons in **38-40** and a summary of these is given in **Table 3.12**. There is now a modest ^{13}C literature for Pd-1,3-diphenylallyl complexes[57-59]. Normally, one expects a substantial difference between the two

terminal allyl carbon positions since the trans influence of a P-donor is usually much larger than that for an sp^2 N-donor[57]. The ^{13}C values for the two terminal allyl carbons **38-40**, support this view (ca δ = 103-106 for the C-atom pseudo-trans to P and δ = ca 65-68 for the C-atom pseudo-trans to N).

Table 3.12 ^{1}H and ^{13}C chemical shifts for the allylic positions in **38-40**[a]

compound	**Pos.**	δ **^{1}H** in ppm	δ **^{13}C** in ppm
38a	C1L	4.52	67.6
	C2L	6.30	108.0
	C3L	5.85	102.9
38b	C1L	4.62	82.6
	C2L	6.54	109.9
	C3L	5.63	89.7
39a	C1L	4.49	67.4
	C2L	6.33	108.7
	C3L	5.91	102.4
39b	C1L	4.55	82.0
	C2L	6.51	110.1
	C3L	5.54	89.2
40a	C1L	4.58	65.5
	C2L	6.35	109.0
	C3L	5.96	105.2
40b	C1L	5.69	72.2
	C2L	5.86	105.0
	C3L	6.61	94.6
40c	C1L	4.69	85.6
	C2L	6.37	109.0
	C3L	5.22	86.5

[a] data for complexes **38**[51] and **39**[29] from references

Moreover, this difference in trans influence propagates itself in substantially different Pd-C bond lengths, as determined by X-ray crystallography[29, 51, 60, 61]. Interestingly, for diastereomer **40c**, *there is almost no difference between the two terminal allyl chemical shifts,* δ = 86.5 and δ = 85.6, see **Figure 3.21**. *This equalising effect is*

unprecedented in Pd-coordination chemistry. It implies that the presumed built-in electronic difference, i.e., one carbon more electrophilic than the other, which normally leads to preferred attack of the nucleophile pseudo-trans to P-donor[52], has more or less disappeared (see fragment **A**). If these ground state data reflect the reaction coordinate, in any way, then the expected selection will vanish (or be strongly reduced). No relative kinetics for the disappearance of the individual diastereomers could be obtained; however, given that there is a modest amount of **40c** present, it is possible that its unexpected electronic structure makes a contribution to the reduced ee.

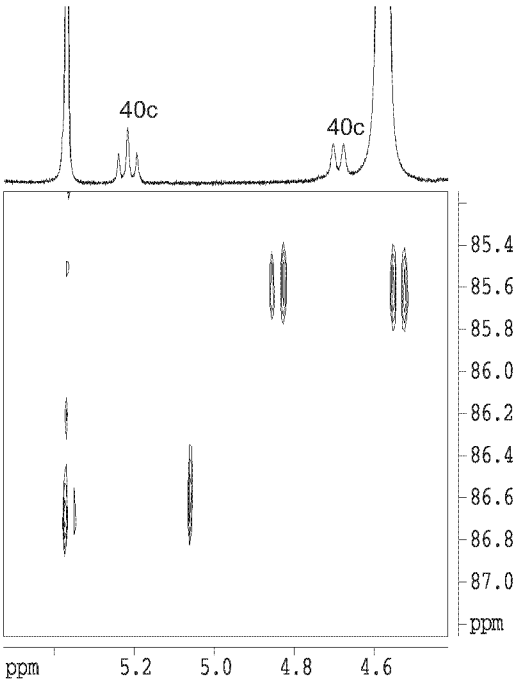

Figure 3.21 section of the $^{13}C,^{1}H$ correlation for **40** showing the two terminal allyl carbons for **40c** (CD_2Cl_2, 500 MHz)

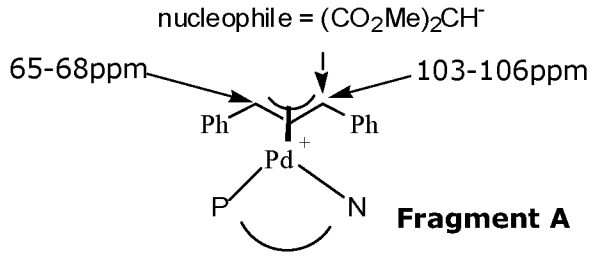

Fragment A

It is pertinent to note that, based on the observed ^{13}C chemical shifts of the allyl-carbons in **40c**, it would seem that the N-donor is unusually strong, and not that the P-donor is unusually weak. The chemical shift of ca 86.5 ppm for the carbon pseudo-trans to the P-donor is slightly smaller than that for observed for [Pd(η^3-PhCHCHCHPh)(dppe)$^+$ shown[58].

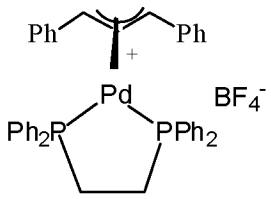

δ = 90.1 for the terminal allyl carbons

[Pd(η^3-PhCHCHCHPh)((R,S) Josiphos)]$^+$, δ = 96.4, 82.0 and 90.2, 89.6 for the exo and endo isomers and [Pd((η^3-PhCHCHCHPh)(S,S-Diop)]$^+$, δ = 95.2, 92.9, represent further examples[62] in which chemical shifts close to 86.5 ppm are observed. Routine values for a terminal allyl carbon of the η^3-PhCHCHCHPh, pseudo-trans to an sp^2 N-donor should be of the order of 65-75 ppm[63].

If compound **40b** arises via an η^3 to η^1 isomerization of a syn/syn isomer, then a consistent mechanism is shown in **Scheme 3.23**. This three-step mechanism consists of the η^3 to η^1 step, followed by rotation around an allyl C-C bond and reformation of the η^3 allyl ligand. We do not know if the allyl is exo or endo in **40b**.

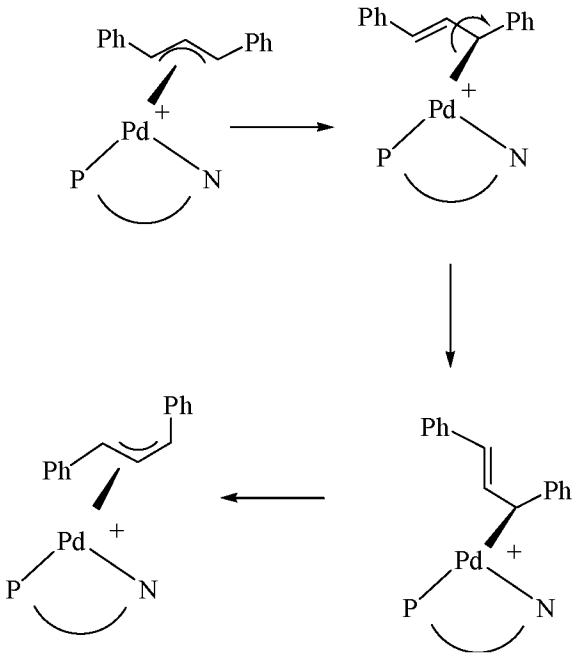

40b

Scheme 3.23. Showing the formation of isomer **40b**.

Possibly, the bulky *meta t*-butyl groups cause the C-P-C angle associated with the two P-phenyl substituents to "open", thereby moving these substituents forward towards the complexed allyl ligand. These increased steric effects result in a weakening of the Pd-C(allyl) bond cis to the phosphorus (and thus trans to the N-donor), with the apparent result that the

oxazoline nitrogen seems more labilising than normal. This explanation is also consistent with the observed structure (and postulated mechanism for the formation) of isomer **40b** i.e., steric effects and not electronic effects control the isomerization. Moreover, these steric effects may induce both the observed dynamics and, consequently, the larger number of observed isomers, all of which can contribute to loss of ee in the allylation.

The use of *t*-butyl groups in compound **37**, although quite effective in the Heck and other enantioselective reactions, has not produced the desired catalytic results in the allylation of eq. **3.3.1**. Nevertheless, the data described above indicate that remote substitutions in seemingly "innocent" positions, can lead to a cascade of small structural changes which afford both novel and unexpected organometallic chemistry.

3.4 Concluding Remarks:

This chapter report the various bonding modes exhibited by the MOP class for e.g., as a chelating P,C σ-donor (complexes **5**, **6**, **11**, **22** and **24**), or as a phosphine, π-olefin chelate (compounds **7**, **18**, **23** and **25)** and reasonably enough, as a P,O chelate via the O atom of the methoxy group, as in **12**. It was found that more than one naphthyl double bond can be involved as seen in **7** and **18**.

In the monodentate Phosphoramidite class, a new bonding mode was seen. Further, the 3,5-meta dialkyl effect is studied for both MOP and P,N-Oxazoline auxiliaries and found that the effect is seen in both the ligands.

3.5 Bibliography:

[1] B. M. Trost and M. L. Crawley, *Chem. Rev.* **2003**, *103*, 2921-2943.

[2] L. S. Hegedus, *Transition Metals in the Synthesis of Complex Organic Molecules*, University Science Books, Mill Valley, California, **1994**.

[3] G. Zeni and R. C. Larock, *Chem. Rev.* **2004**, *104*, 2285-2309.

[4] J. Tsuji, *Palladium Reagents and Catalysis*, John Wiley & Sons, Chichester, **1996**.

[5] G. Helmchen, *J. Organomet. Chem.* **1999**, *576*, 203-214.

[6] R. Noyori, *Asymmetric Catalysis in Organic Synthesis*, John Wiley and Sons, Inc., London, **1994**.

[7] T. Hayashi, *J. Organomet. Chem.* **1999**, *576*, 195-202.

[8] R. Noyori, *Angew. Chem.Int. Ed. Engl.* **2002**, *41*, 2008-2022.

[9] T. Hayashi, *Acc. Chem.Res.* **2000**, *33*, 354-362.

[10] P. Kocovsky, S. Vyskocil and M. Smrcina, *Chem. Rev.* **2003**, *103*, 3213-3245.

[11] F. Diederich and P. J. Stang, *Metal -Catalyzed Cross-Coupling Reactions*, WILEY-VCH, Weinheim, **1998**, p. 516.

[12] B. M. Trost and D. L. van Vranken, *Chem. Rev.* **1996**, *96*, 395.

[13] D. Zim and S. L. Buchwald, *Org. Lett.* **2003**, *5*, 2413-2415.

[14] T. Shimada, K. Mukaide, A. Shinohara, J. W. Han and T. Hayashi, *J Am. Chem Soc.* **2002**, *124*, 1584-1585.

[15] X. P. Wang, X. Li, J. Sun and K. Ding, *Organometallics* **2003**, *22*, 1856-1862.

[16] P. Kocovsky, A. V. Malkov, S. Vyskocil and G. C. Lloyd-Jones, *Pure and Applied Chemistry* **1999**, *71*, 1425-1433.

[17] J. W. Faller and N. Sarantopoulos, *Organometallics* **2004**, *23*, 2008-2014.

[18] P. Dotta, *Ph.D thesis, ETH Dissertation number 15543* **2004**.

[19] P. Dotta, P. G. A. Kumar, P. S. Pregosin, A. Albinati and S. Rizzato, *Organometallics* **2003**, *22*, 5345-5349.

[20] P. S. Pregosin and R. W. Kunz, *^{31}P and ^{13}C NMR of Transition Metal Phosphine Complexes*, Springer Verlag, Berlin, **1979**.

[21] H. O. Kalinowski, S. Berger and S. Braun, *^{13}C-NMR Spektroskopie*, Georg Thieme Verlag, Stuttgart, **1984**.

[22] B. E. Mann and B. F. Taylor, *^{13}C NMR Data for Organometallic Compounds*, Academic Press, London, **1981**.

[23] L. Xu, Q. Shi, X. Li, X. Jia, X. Huang, R. Wang, Z. Zhou, Z. Lin and A. S. C. Chan, *Chem. Comm.* **2003**, 1666-1667.

[24] E. Pretsch, J. Seibl and W. Simon, *Strukturaufklarung organischer Verbindungen*, Springer-Verlag, Berlin, **1986**.

[25] P. Dotta, P. G. A. Kumar, P. S. Pregosin, A. Albinati and S. Rizzato, *Organometallics* **2004**, *23*, 4247-4254.

[26] P. Leoni, M. Pasquali, M. Sommovigo, A. Albinati, P. S. Pregosin and H. Rüegger, *Organometallics*, **1996**, *15*, 2047-2052.

[27] T. J. Geldbach, D. Drago and P. S. Pregosin, *J. Organomet. Chem.* **2002**, *643*, 214-222.

[28] G. Trabesinger, A. Albinati, N. Feiken, R. W. Kunz, P. S. Pregosin and M. Tschoerner, *J. Am. Chem. Soc.* **1997**, *119*, 6315-6323.

[29] K. Selvakumar, M. Valentini, P. S. Pregosin, A. Albinati and F. Eisentrager, *Organometallics* **2000**, *19*, 1299-1307.

[30] P. Dotta, P. G. A. Kumar and P. S. Pregosin, *Magn. Reson. Chem.* **2002**, *40*, 653-658.

[31] P. Dotta, P. G. A. Kumar, P. S. Pregosin, A. Albinati and S. Rizzato, *Organometallics* **2004**, *23*, 2295-2304.

[32] T. Hayashi, M. Kawatsura and Y. Uozumi, *J. Am. Chem. Soc.* **1998**, *120*, 1681-1687.

[33] P. Dotta, P. G. A. Kumar, P. S. Pregosin and A. Albinati, *Helv. Chim. Acta* **2004**, *87*, 272-278.

[34] M. Kollmar and H. G., *Organometallics* **2002**, *21*, 4771-4775.

[35] E. Martinez-Viviente, H. Ruegger, P. S. Pregosin and J. Lopez-Serrano, *Organometallics* **2002**, *21*, 5841-5846.

[36] P. G. A. Kumar, P. S. Pregosin, J. M. Goicoechea and M. K. Whittlesey, *Organometallics* **2003**, *22*, 2956-2960.

[37] G. C. Ll oyd-Jones, S. C. Stephen, M. Murray, C. P. Butts, S. Vyskocil and P. Kocovsky, *Chem. Eur. J.* **2000**, *6*, 4348-4357.

[38] P. Dotta, ETH Dissertation 15543.

[39] A. Pfaltz, *Acta Chimica Scand.* **1996**, *50*, 189-194.

[40] W. S. Knowles, *Acc. Chem. Res.* **1983**, *16*, 106.

[41] E. N. jacobsen, Pfaltz, A., Yamamoto, Y., *comprehensive asymmetric catalysis, Springer, Berlin* **1999**.

[42] B. L. Feringa, *Acc. Chem.Res.* **2000**, *33*, 346.

[43] D. Huber and A. Mezzetti, *Tet. Asymm.* **2004**, *15*, 2193-2197.

[44] P. S. Pregosin, E. Martinez-Viviente and P. G. A. Kumar, *Dalton Trans.* **2003**, 4007-4014.

[45] D. Huber, Kumar, P. G. A., Pregosin, P. S., Mezzetti, A., *in preparation* **2005**.

[46] M. Eberstadt, G. Gemmecker, D. F. Mierke and H. Kessler, *Angew. Chem.* **1995**, *107*, 1813-1838.

[47] G. Helmchen and A. Pfaltz, *Acc. Chem. Res.* **2000**, *33*, 336-345.

[48] D. Flubacher and G. Helmchen, *Tet. Lett.* **1999**, *40*, 3867-3868.

[49] N. S. Goulioukina, T. M. Dolgina, G. N. Bondarenko, I. P. Beletskaya, M. M. Ilyin, V. A. Davankov and A. Pfaltz, *Tet. Asymm.* **2003**, *14*, 1397-1401.

[50] A. Togni, U. Burckhardt, V. Gramlich, P. S. Pregosin and R. Salzmann, *J. Am. Chem. Soc.* **1996**, *118*, 1031-1037.

[51] K. Selvakumar, M. Valentini, M. Worle, P. S. Pregosin and A. Albinati, *Organometallics* **1999**, *18*, 1207-1215.

[52] C. Breutel, P. S. Pregosin, R. Salzmann and A. Togni, *J. Am. Chem. Soc.* **1994**, *116*, 4067.

[53] G. Trabesinger, A. Albinati, N. Feiken, R. W. Kunz, P. S. Pregosin and M. Tschoerner, *J. Am. Chem. Soc.* **1997**, *119*, 6315.

[54] M. Tschoerner, P. S. Pregosin and A. Albinati, *Organometallics* **1999**, *18*, 670-678.

[55] K. Selvakumar, M. Valentini, P. S. Pregosin, A. Albinati and F. Eisentraeger, *Organometallics* **2000**, *19*, 1299-1307.

[56] P. S. Pregosin and R. Salzmann, *Coord. Chem. Rev.* **1996**, *155*, 35-68.

[57] J. M. Brown, D. I. Hulmes and P. J. Guiry, *Tetrahedron* **1994**, *50*, 4493-4506.

[58] R. Malet, M. Moreno-Manas, F. Pajuelo, T. Parella and R. Pleixats, *Magn. Reson. Chem.* **1997**, *35*, 227-236.

[59] M. Moreno-Manas, F. Pajuelo, T. Parella and R. Pleixats, *Organometallics* **1997**, *16*, 205-209.

[60] P. Braunstein, C. Graiff, F. Naud, A. Pfaltz and A. Tiripicchio, *Inorg. Chem.* **2000**, *39*, 4468-4475.

[61] P. Braunstein, F. Naud, A. Pfaltz and S. J. Rettig, *Organometallics* **2000**, *19*, 2676-2683.

[62] P. S. Pregosin and M. Valentini, *Enantiomer* **1999**, *4*, 529-539.

[63] B. Åkermark, B. Krakenberger, H. S. and A. Vitagliano, *Organometallics* **1987**, *6*, 620.

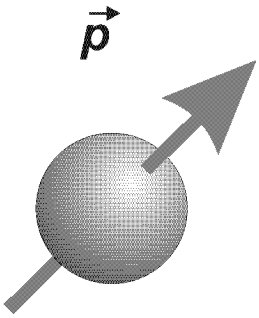

Appendices

Appendices

The Appendices presented below serve as a support to the chapters discussed earlier and/or some of the additional experiments which were carried out at a later stage.

Appendix 1- Pd(II)-acetonitrile complex with two MOP's

Monodentate chiral auxiliaries, MOP (or its analogues), **1-4**.

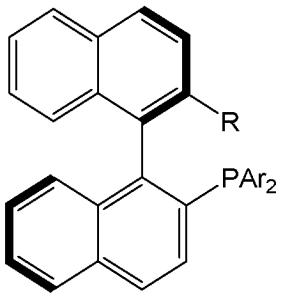

Ar = Ph(**a**), 3,5-di-*t*-butylphenyl(**b**), 3,5-dimethylphenyl(**c**)

1, R = H

2, R = OMe

3, R = CN

4, R = OH

Synthesis and bonding in $[Pd(CH_3CN)(2a)_2](BF_4)_2$, 5.

Scheme 1

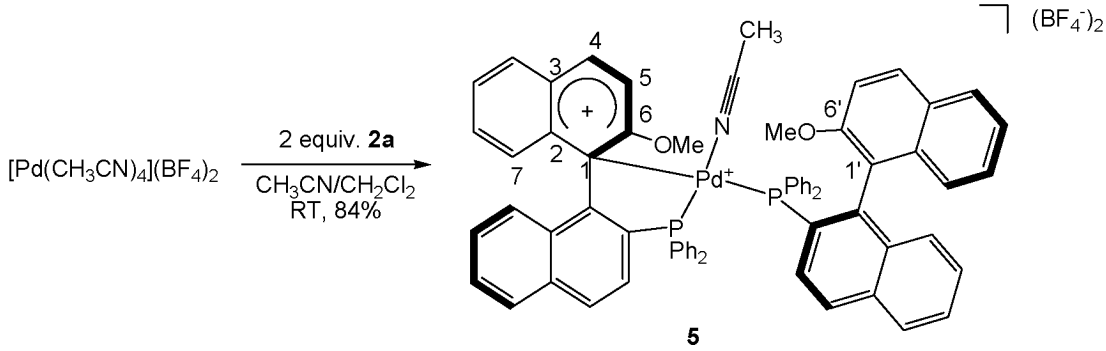

5

Synthesis of the target complex[1] **5** was achieved using $[Pd(CH_3CN)_4]$ $(BF_4)_2$ and two equivalents of ligand **2a** (MeO-MOP) as shown in **Scheme 1**. The ^{31}P and ^{1}H NMR spectra at room temperature were broad indicating a dynamic character of the complex **5**. Cooling to 183K led to sharpening of the signals. Two sharp ^{31}P singlets at δ= 40.1ppm and 47.2ppm were obtained which

showed no further coupling. The ^{1}H NMR spectrum was sufficiently resolved to determine the presumed structure of the complex.

The proposed structure for complex **5** was based on

(1) $^{13}C,^{1}H$ HMBC spectrum in which there was a correlation from H-5 and H-7 to C-1, δ= 99.4ppm, which indicates a weak Pd,C σ-bond[1] for one MOP backbone. The remaining MOP carbons show normal ^{13}C chemical shifts.

(2) Absence of the coordination of the methoxy group to the metal i.e., no difference in ^{13}C chemical shifts of the two MeO-groups in the backbone.

(3) PGSE diffusion data confirms that two MOP's were coordinated.

(4) High frequency shift of the ^{1}H CH_3 signal from the bonded acetonitrile (δ= 1.08ppm).

(5) ^{19}F-^{1}H HOESY measurements confirming the contacts from the anion to the complexed acetonitrile.

The broad signals at room temperature can be due to the following exchange process i.e., coordination of the ipso carbon from two MOP backbones,

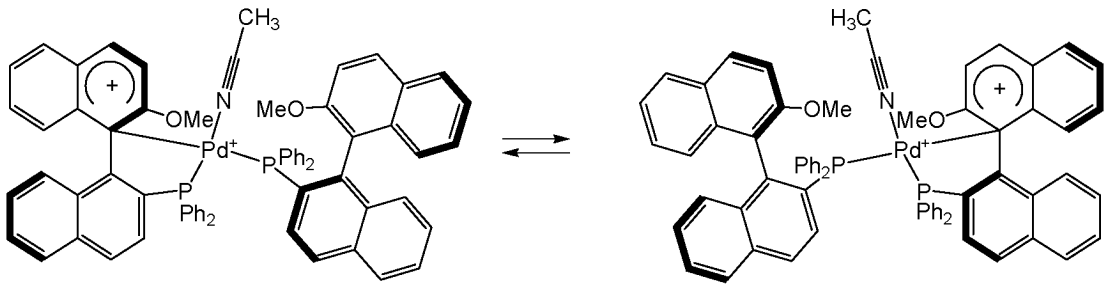

Figure 1 shows the $^{31}P,^{1}H$-correlation spectrum at 183K. The contacts from both the monodentate and chelated MOP to the complexed acetonitrile are clearly visible. Also seen is the contact to the methoxy group of the chelated phosphine. Figure 2 shows the $^{13}C,^{1}H$ HMBC-Spectrum for **5** where H-4 (and H-4') sees the carbon

adjacent to the methoxy group, C-6 (and C-6') via a long range correlation (183K). Note that the chemical shift for C-6 is shifted to low frequency indicating a distribution of positive charge. On inspection of Table 1, one can indeed recognize that the positive charge is distributed evenly in the metal-chelated aromatic ring. **Scheme 2** shows the difference in coordination chemical shifts for the monodentate *vs* the chelated MOP backbone.

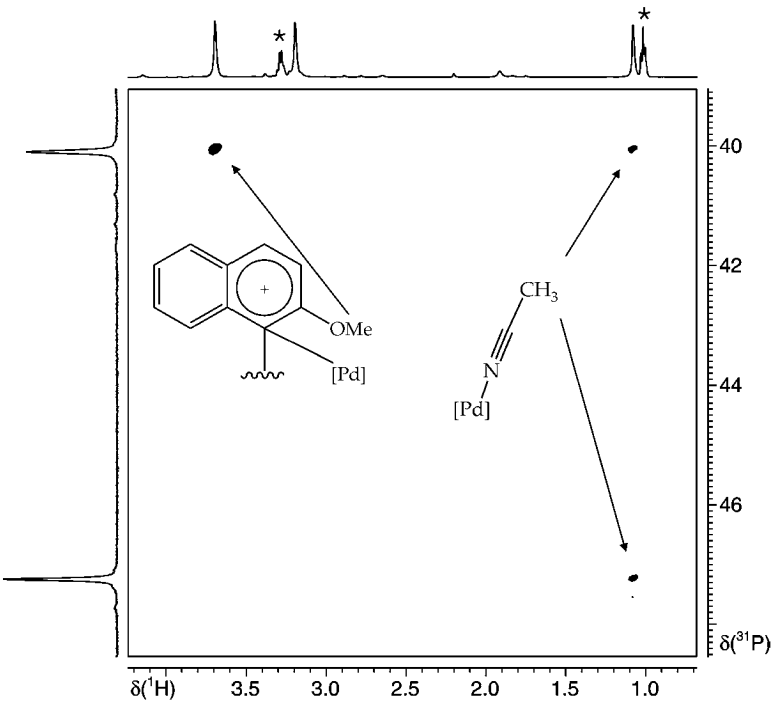

Figure 1. $^{31}P,^{1}H$-correlation spectrum for **5** showing contacts from both 31P signals to the methyl group of the complexed acetonitrile. Also seen is the correlation from one of the ^{31}P to the methoxy group of the MeO-MOP backbone which shows a Pd,C chelation. (*= ^{1}H-Signal from Ether). (500 MHz, CD_2Cl_2, 183 K)

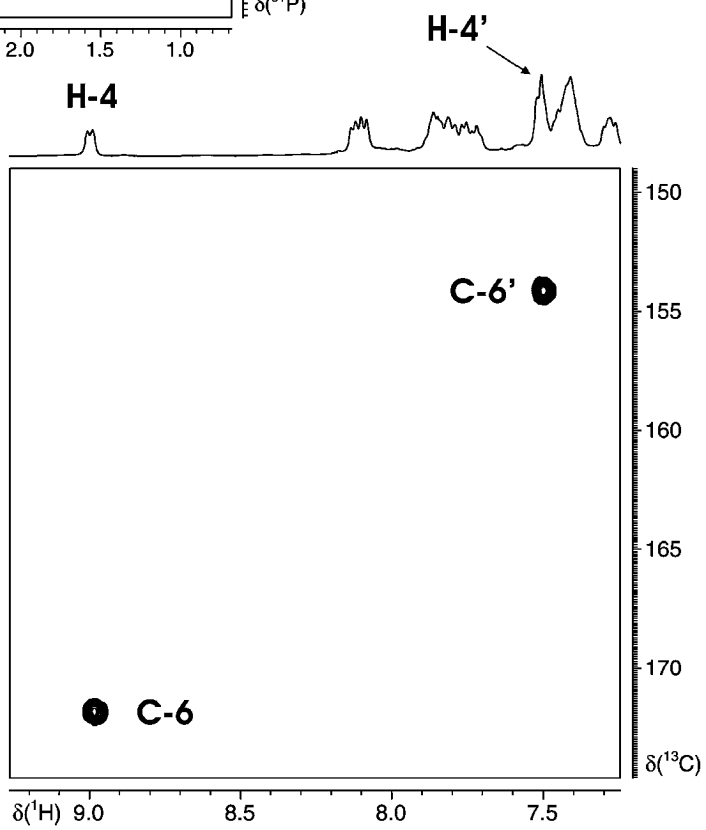

Figure 2. $^{13}C,^{1}H$ HMBC-Spectrum for **5** showing contacts from H-4 to C-6 in two different MOP backbone. (500 MHz, CD_2Cl_2, 183 K)

Table 1. ^{13}C chemical shifts for complex **5** (500 MHz, CD_2Cl_2, 183K)

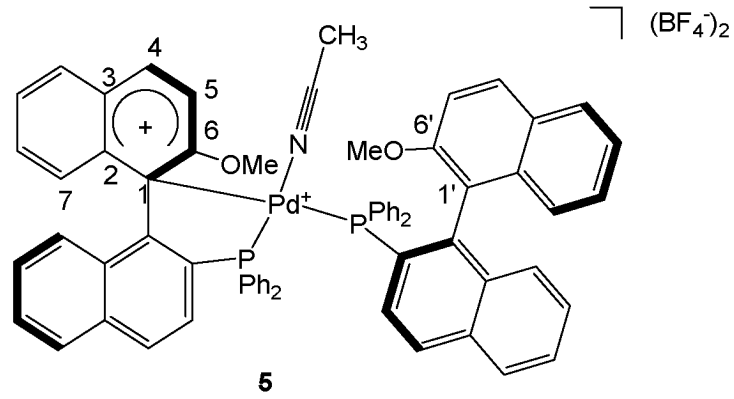

5

Position	δ ^{13}C in ppm	Position	δ ^{13}C in ppm
1	**99.5**	1′	116.2
2	141.2	2′	133.0
3	130.3	3′	128.3
4	148.4	4′	131.9
5	115.4	5′	111.9
6	**171.8**	6′	154.1
OCH_3	58.5	OCH_3′	55.8

Table 1 also shows the chemical shift of the methyl group of MeO from the two MOP ligands. The ^{13}C chemical shift of the methoxy group has not varied much upon chelation, implying that it has not much role except for sharing a meager amount of positive charge. **Scheme 2** shows that the *ortho*- and *para*-positions to the chelated ipso carbon are sharing the major chunk of positive charge relative to *meta*-carbons.

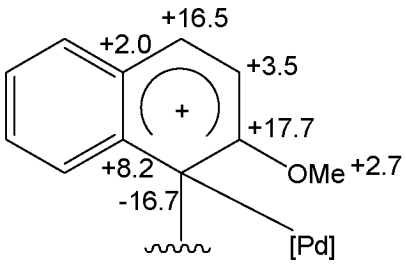

Scheme 2. Difference in ^{13}C chemical shifts (in ppm) for the complexed MOP-Ligand in **5**. $\Delta\delta$= δ(chelated MOP) - δ(monodenate MOP)

The absence of $^{2}J_{(P,P)}$ in the ^{31}P spectrum led to the confusion of whether there were two MOP's on the metal center, which led to carrying out the diffusion measurements.

PGSE diffusion measurements[2-4] confirmed our conclusion that MOP's were indeed coordinated to palladium metal. **Table 2** shows the diffusion coefficients (in m^2s^{-1}) for the complex **5** as well as those for the model complexes **6** and **7**, in dichloromethane solution measured at room temperature.

Table 2. Diffusion Coefficients in m^2s^{-1} and hydrodynamic radii in **Å.**

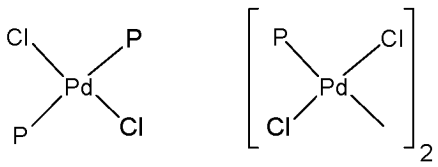

6 **7**

P =MeO-MOP

Compound		D (x 10^{-10})	r_h(Å)
6	Cation	7.37	7.3
7	Cation	6.92	7.7
5	Cation	6.43	8.3
	Anion	9.34	5.7

The D-values for complex **5** are now so big that it even exceeds the size of the *trans*-$PdCl_2$. The hydrodynamic radius for the anion is also big enough to be considered as resulting from some ion-pairing. The bigger size of the cation can be accounted for a formation of a bridged complex, which could not be proven. Further, in dichloro-methane, one can expect the cationic complexes to demonstrate significant ion-pairing as has been reported earlier. To test this hypothesis, $^{19}F,^{1}H$ HOESY correlation[4] was measured at room temperature (**Figure**

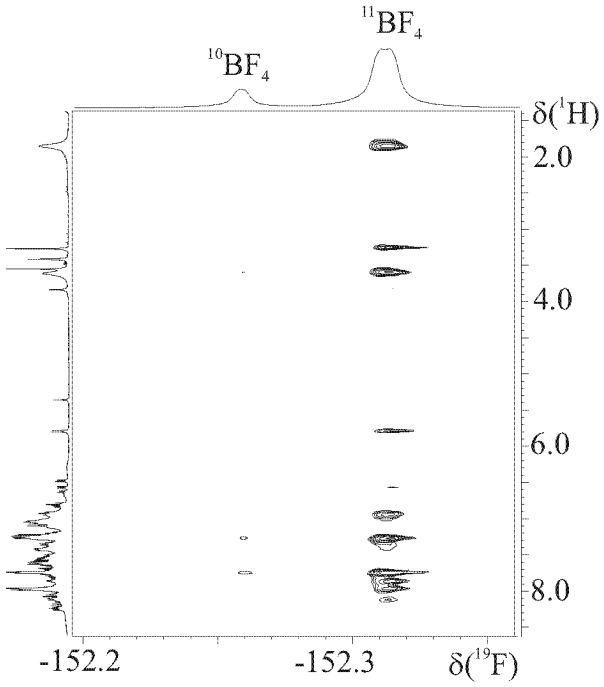

Figure 3. $^{19}F,^{1}H$-HOESY spectrum for complex **5**.

3). As there might be an exchange between the free and bound acetonitrile, the HOESY spectrum shows selective contacts to both the bound and free acetonitrile, plus contact to the methoxy group and some aromatic protons. It was not able to localize the anion in a specific position; anyway this experiment confirmed the Pd-bound acetonitrile.

In conclusion, an interesting bonding mode is seen where one among two chelating phosphines exhibits a weak σ-bonding to the palladium. The presence of two phosphines on the metal is proven by PGSE and HOESY measurements.

Appendix 2- Diffusion studies on Co(I)-MeO Biphep Complex:

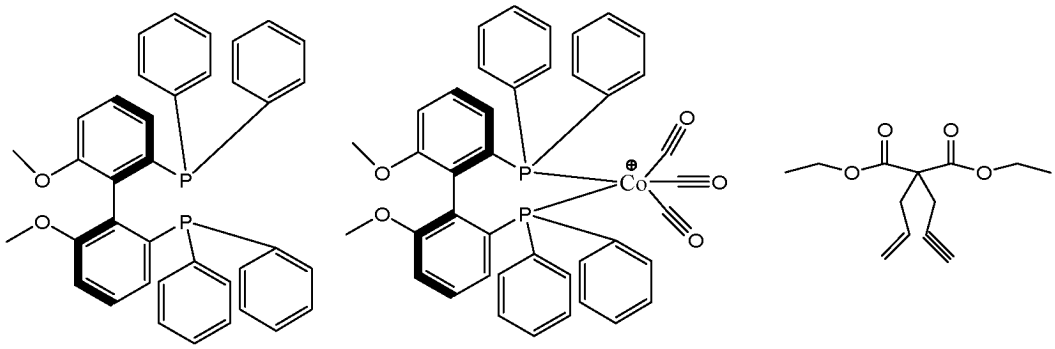

6 **7** **Substrate**

The cationic cobalt(I) carbonyl complex, **7**, was found to be a highly active enantioselective catalyst precursor in the Pausan-Khand reaction[5]. However, there seemed to be a difference in the catalytic activity upon changing of the anion. This led to the PGSE investigation of the anion dependence.

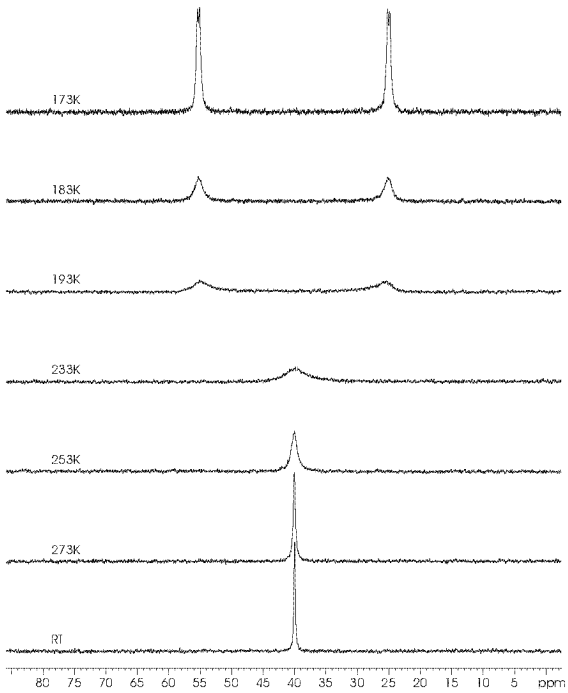

Figure 4. ^{31}P spectrum for complex **7**.

The coordinated phosphines were detected via low temperature ^{31}P measurements. At 173K the signals become sharp enough to reveal the $^{2}J_{P,P}$ splitting (**figure 4**). **Table 3** shows the relevant self-diffusion coefficients (in CD_2Cl_2 and $CDCl_3$) for the ligand **6**, complex **7** and the change resulting upon addition of the substrate. The hydrodynamic radius for the cation is similar on changing the anion from BF_4 to CF_3SO_3. Because the anion signal was very broad (even at 173K), an estimation of the D-values failed. An experiment was

done to check if the substrate coordinates to the metal centre (as thought to be in the catalytic cycle), however, it was observed that there was not much difference in D-values with and without substrate. Further, for one of the protons a surprising D-value of 6.43 was observed, which corresponds to a radius of 8.3Å, the structure could not be assigned due to overlap of signals. Furthermore, the ratio of r_h-values for the complex **7** in different solvents affords a value of ca. 1.26 (7.7/6.1), which is in agreement for a structure of double the molecular volume. This implies that the complex can exhibit different structure on variation of the solvent.

Table 3. List of D- and r_h values (2mM).

Compound	**Solvent**		**D**	**r_h (Å)**
6	CD_2Cl_2	cation	9.40	5.7
[**7**] BF_4	CD_2Cl_2	cation anion	8.76 broad	6.1
	$CDCl_3$	cation anion	5.36 broad	7.7
[**7**] CF_3SO_3	CD_2Cl_2	cation anion	8.78 broad	6.1
	$CDCl_3$	cation anion	5.45 broad	7.6
[**7**] BF_4 + Substrate	CD_2Cl_2	cation substrate	8.89 15.02	6.0 3.6
[**7**] CF_3SO_3 + Substrate	CD_2Cl_2	cation substrate Unknown	8.56 14.54 6.43	6.3 3.7 8.3

Appendix 3- Diffusion Studies on Ru(II)-d^{t}bpe complex

In a continuation of our earlier discussion (Section 2.3) on aqua complexes of Ru-bisphosphine cations[2], Whittlesey and coworkers[6] found that the thermolysis of solid [Ru(d^{t}bpe)(CO)$_2$Cl$_2$] (**8**, d^{t}bpe = ^{t}Bu$_2$PCH$_2$CH$_2$P^{t}Bu$_2$) under vacuum affords the five-coordinate complex [Ru(d^{t}bpe)(CO)Cl$_2$] (**9**), which was shown by X-ray crystallography[6] to contain a weak remote agostic interaction. Reaction of **9** with AgOTf/H$_2$O yields the tris aqua complex [Ru(d^{t}bpe)(CO)(H$_2$O)$_3$](OTf)$_2$ (**10**), which has been structurally characterized[6] and probed in solution by pulsed-gradient spin echo (PGSE) NMR spectroscopy.

Table 4. Diffusion Constants[a,b] and Radii[c] for **8**, **9** and **10**.

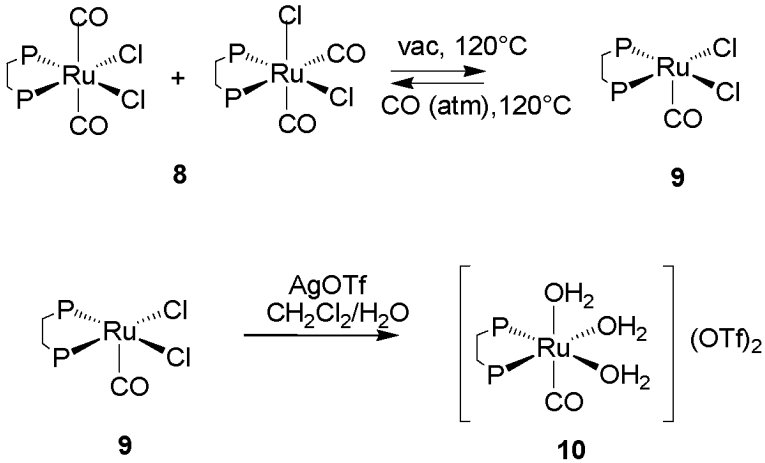

Compound	Fragment	T (K)	D^b	r_h(Å)
8		300	10.55	5.1
		223	2.84	5.4[d]
		223	2.85	5.4[e]
9		223	2.23	6.8
10	cation	300	8.78	6.1
	anion	300	8.88	6.0

[a] All measurements are for 2 mM solutions. Cations were measured by ^{1}H and anions using ^{19}F. [b] *D* values are given in units of 10^{-10} m^2 s^{-1}. [c] The viscosities used in the calculations are as follows: CH_2Cl_2, 0.405 (300 K); 1.071 (223 K). [d] d_3 = 75 ms. [e] d_3 = 50 ms.

Pulsed gradient spin-echo (PGSE) diffusion studies performed on the tris-aqua complex **10** show that it behaves very similarly to the dppe analogue[2] **4b** (Chapter 2, Section 2.3) in solution (**Table 4**). Diffusion constants of 8.78 x 10^{-10} m^2s^{-1} and 8.88 x 10^{-10} m^2s^{-1} were recorded for the cation and anion respectively in CD_2Cl_2/water solution; these almost identical values can be rationalized by either ion-pairing or hydrogen bonding of the anion to the coordinated water ligands. As the experiments were necessarily performed in the presence of excess water to help stabilize **10**, ion pairing would be less likely due to water solvation leaving us to favor the hydrogen bonding explanation.

Table 4 shows the observed *D*-and r_h values for the mixture of *cis* and *trans* isomers of **8**, at both ambient temperature and 223K; as expected, both sets of data are consistent with the properties of a mononuclear complex. Interestingly, complex **10** has a larger volume compared to **8**, which might be accounted for hydrogen bonding (see section 2.3). The low temperature diffusion measurements[7] were repeated with different mixing times to exclude the probability of convection. Complex **9** was structurally characterized to be a monomeric unsaturated species[6], however, the diffusion values do not agree with this structure. On comparing the *D*-values (223K) for the *cis*/*trans* mixture of [Ru(d^tbpe)$(CO)_2Cl_2$], **8** with that for [Ru(d^tbpe)$(CO)Cl_2$], **9**, shows that the latter is diffusing at a much slower rate (See **figure 5**). The ratio of the *D*-values (2.84/2.23) = 1.27 is in excellent agreement with a structure which has *ca.* double the molecular volume[8] of **8** i.e. this indicates

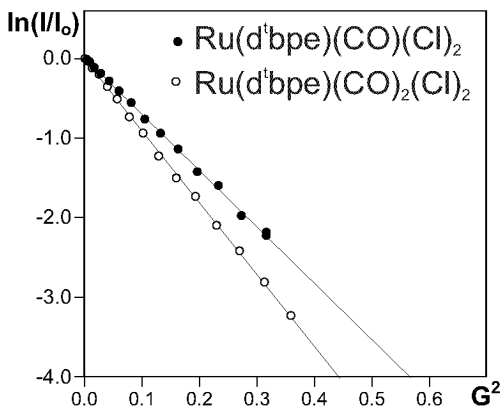

Figure 5.Slopes for complexes **8** and **9**.

that upon dissolution, **9** exists as a dimeric species (i.e, $[Ru(\mu\text{-}Cl)Cl(CO)(d^tbpe)]_2$) and is not the monomeric coordinatively unsaturated species which has been structurally characterized[6].

In conclusion, PGSE method has helped to distinguish the solution structure from that of the X-ray, thus unfolding new avenues in structural characterization.

Appendix 4- Diffusion studies on Ru(II)-BINAP complex

In a continuation of the previous discussion on PGSE applications in detecting hydrogen bonding effects (Chapter 2, section 2.3), several Ru(II)-BINAP model complexes (Section 2.2.1) were used in a comparison with the newly prepared Ru(II)-complexes, **11a,b**. These new dinuclear Ru(II)-arene phosphine complexes exhibited various H-bonding interactions in the solid-state[9]. This led us to study the hydrogen bonding effects via PGSE methods[4].

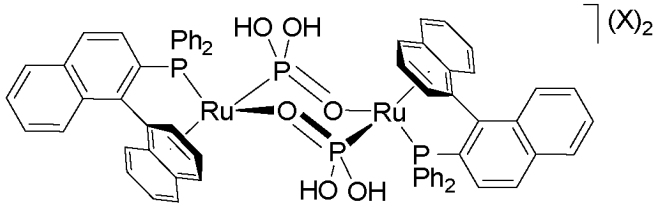

11, X= OTf, **a**; X =BArF, **b**

Table 5. Diffusion data for the di-nuclear Ru(II) complexes **11a**, **11b** and the model complex **12** (CD_2Cl_2, 2 mM) + **Figure 6.** Slopes for **11a** and **11b**.

Compound		D	r(Å)
11a (CF_3SO_3)	cation	7.33	7.3
	anion	7.63	7.0
11b (BArF)	cation	5.27	10.2
	anion	6.56	8.2
12a(X=CF_3SO_3)	cation	7.73	6.9
	anion	10.46	5.1
12b (X=BArF)	cation	7.71	6.9
	anion	8.05	6.6

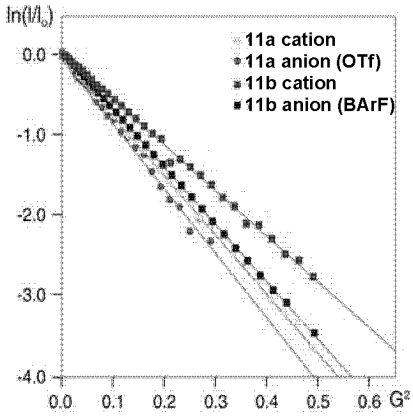

Table 5 and **Figure 6** show the ^1H PGSE data for the cations of **11a** and **11b** together with the corresponding ^{19}F derived data for the anions.

For the di-nuclear complex **11a**, the almost equivalent D values for the cation, 7.33 x10^{-10} m^2sec^{-1} and anion 7.63 x10^{-10} m^2sec^{-1},

support significant (but not 100%) H-bonding of the $CF_3SO_3^-$ anion to the OH-groups of the cation. The observed 7.63 D-value (the units will now be omitted for clarity) for the $CF_3SO_3^-$ anion is relatively small and indicates much slower than normal translation. A typical D-value for this anion in dichloromethane for a 1:1 salt would be much larger, e.g., the 10.46 value given in Table 5 for model compound [RuCl(*p*- cymene)(Binap)](CF_3SO_3), **12a**[2].

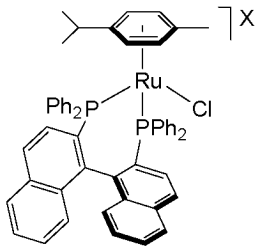

12

a, X = $CF_3SO_3^-$, **b**, X = $BArF^-$

As mentioned dichloromethane promotes some ion pairing e.g., in **12a**[2], the hydrodynamic radius, 5.1 Å, derived from the 10.46 D-value is too large for an isolated triflate anion. The D-value for the cation in the $BArF^-$ salt, **11b**, 5.27, is very much smaller in magnitude than the 7.33 value given for the cation in **11a**. This slower rate of diffusion for the cation of **11b** with $BArF^-$ is again consistent with markedly reduced translation due to the ion-pairing of two relatively large $BArF^-$ anions. Since the 6.56 D-value for the $BArF^-$ (via ^{19}F PGSE) is not identical to the value for the cation, 5.27, the ion pairing is not complete. For comparison we show the D-value, 8.05, for [RuCl(*p*-cymene)(Binap)](BArF), **12b** in Table 5, and note that the 6.56 value in **11b** is, indeed, much smaller.

In conclusion, it was shown via diffusion measurements that in **11a**, the triflate anion is H-bonded via hydrogen bridges to the hydroxyl-groups and that, in the $BArF^-$ salt, **11b**, the ion pairing is important, but not complete.

Appendix 5- Diffusion studies on Ionic Liquids

The use of ionic liquids as alternative solvent, especially in biphasic catalysis, continues to attract interest in the chemical community.[10-12] Many catalysts are efficiently immobilised in these liquids, allowing for facile catalyst recycling.[13] Addition of co-solvents may, however, be required for a number of purposes: (i) to help dissolve a catalyst (ii) to decrease the viscosity (iii) to induce phase separation between the ionic liquid and the substrates/products and (iv) facilitate catalyst activation.[14]

The continued interests on the solvent effects (chapter 2) lead us to the study of the effect of co-solvent on ionic liquid diffusion. The diffusion characteristics of the tetrafluoroborate and (to a lesser extent) hexafluorophosphate 1-butyl-3-methylimidazolium salts[15, 16], $[C_4C_1im]BF_4$ and $[C_4C_1im]PF_6$, was chosen as representative models for the pulsed gradient spin-echo (PGSE) NMR measurements.[2, 4]

Table 6 shows the self-diffusion coefficient values, D, for the cations (via ^1H) and anions (via ^{19}F) in the neat ionic liquids (using THF-d_8 capillary), $[C_4C_1im]BF_4$ and $[C_4C_1im]PF_6$, as well as the diffusion data arising from their dilution in either CD_3OD or CD_2Cl_2. The measured D-values for the neat ionic liquid $[C_4C_1im]BF_4$, 0.158 and 0.146, for the cation and anion respectively, suggest almost equivalent rates of translation and an extremely large average hydrodynamic radius. Clearly the average radius, r_H for the $[C_4C_1im]BF_4$ ionic salt, is in *the nanoparticle region*. For $[C_4C_1im]PF_6$, the D-values, 0.071 and 0.054 for the cation and anion respectively, are even smaller; however, after correcting for the rather different, measured viscosity (see table 6), the average hydrodynamic radius (and thus ionic volume) is somewhat smaller than for $[C_4C_1im]BF_4$.

Table 6. Diffusion data for the ionic Liquids

				D ($X10^{-10}$) m^2s^{-1}	r_H[a] (Å)	r_H[b] (Å)	η[c] (cP)
1	Neat ionic liquid $[C_4C_1im]BF_4$		cation	0.158	13.4		104.04
			anion	0.146	14.5		
2	0.55ml $[C_4C_1im]BF_4$	0.05 ml CD_3OD	cation	1.108	3.2	3.5	62.3
			anion	1.340	2.6	3.0	
3	0.1ml $[C_4C_1im]BF_4$	0.5 ml CD_3OD	cation	7.441	3.4	3.7	0.88
			anion	8.550	2.9	3.3	
4	0.01ml $[C_4C_1im]BF_4$	0.59 ml CD_3OD	cation	11.379	3.0	3.2	0.65
			anion	13.189	2.6	2.9	
5	0.55ml $[C_4C_1im]BF_4$	0.05 ml CD_2Cl_2	cation	0.698	4.3	4.7	72.8
			anion	0.770	3.9	4.4	
6	0.1ml $[C_4C_1im]BF_4$	0.5 ml CD_2Cl_2	cation	5.814	4.0	4.6	0.94
			anion	5.965	3.9	4.4	
7	0.01ml $[C_4C_1im]BF_4$	0.59 ml CD_2Cl_2	cation	8.957	4.6	5.0	0.53
			anion	9.042	4.6	5.2	
8	Neat ionic liquid $[C_4C_1im]PF_6$		cation	0.071	9.5		326.0
			anion	0.054	12.5		
9	0.1ml $[C_4C_1im]PF_6$	0.5 ml CD_3OD	cation	7.535	3.2	3.5	0.90
			anion	8.105	3.0	3.7	

[a] Using factor 6 in Stokes-Einstein equation, [b] Using factor c = 5.5 for the cation and c = 5.3 for the anion in Stokes-Einstein equation[17, 18], [c] measured viscosity value

It is known from the PGSE literature[2, 4, 8] that methanol successfully solvates the ions of many salts, and that for BF_4^-, a typical radius would be ca 2.6 Å. In the presence of ca 10% methanol as a co-solvent, the D-values of the cation, 1.108, and anion, 1.340, for $[C_4C_1im]BF_4$ increase by a factor of 7-8, thus indicating a major structural change in the ionic liquid. Using the

measured viscosity of this new solution to calculate the r_H value shows that the aggregate structure has been more or less completely destroyed (The Connolly-Solvent volume, http://connolly.best.vwh.net/, of the cation is estimated to be 149Å^3, which gives a hydrodynamic radii of ca. r_H = 3.3 Å, and ca r_H = 2.7 Å for the BF_4 anion. Consequently, our calculated r_H values for the individual ions are reasonable). Further dilution, seems to have only a minimal effect on the sizes of the solvated ionic fragments.

The addition of dichloromethane, a solvent in which ion pairing is recognized to be more important,[4] results in a similar but modified picture. The addition of ca 10% solvent leads once again to a major reduction in the aggregation state of the ionic liquid. However, the average particle is larger than in methanol and the cation and anion appear to be translating at almost the same rates, which we take to be due to ion pairing. Entry 7 which shows ca. equivalent D-values, but relatively large r_H values suggests that, even in a relatively dilute dichloromethane solution there is strong ion pairing.

Although PGSE NMR diffusion measurements cannot distinguish between reduced translation due to either ion pairing or hydrogen bonding, clearly, in the presence of each of the co-solvents, there is a major change in the structure of the $[C_4C_1im]BF_4$ ionic liquid. However, ^1H, ^{19}F- HOESY experiments[2-4] do provide data with respect to placing the anion in three-dimensional space, relative to the cation. **Figure 7** shows a set of HOESY spectra for the neat ionic liquid $[C_4C_1im]BF_4$ as well as for the various dilutions in both solvents.

In pure $[C_4C_1im]BF_4$ there are strong contacts *to all of the cation protons*, and thus there is no selectivity. The anion is trapped in the aggregate and sees all of the various protons more or less equally. Moreover, ^1H NOESY experiments support this view in that one observes contacts from the N=CH-N proton, δ = 8.4, to the two

non-equivalent olefinic protons, δ = 7.28 and 7.33, in keeping with an inter-molecular contact On dilution a) the selectivity increases and b) all of the cross-peak intensities decrease and sections (E)-(G) in **Figure 7** show these effects nicely.

Figure 7. (A) Neat ionic liquid (IL) $[C_4C_1im]BF_4$ (B) 0.55 ml IL + 0.05 ml CD_3OD (C) 0.1 ml IL + 0.5 ml CD_3OD (D) 0.01 ml IL + 0.59 ml CD_3OD (E) 0.55 ml IL + 0.05 ml CD_2Cl_2 (F) 0.1 ml IL + 0.5 ml CD_2Cl_2 (G) 0.01 ml IL + 0.59 ml CD_2Cl_2

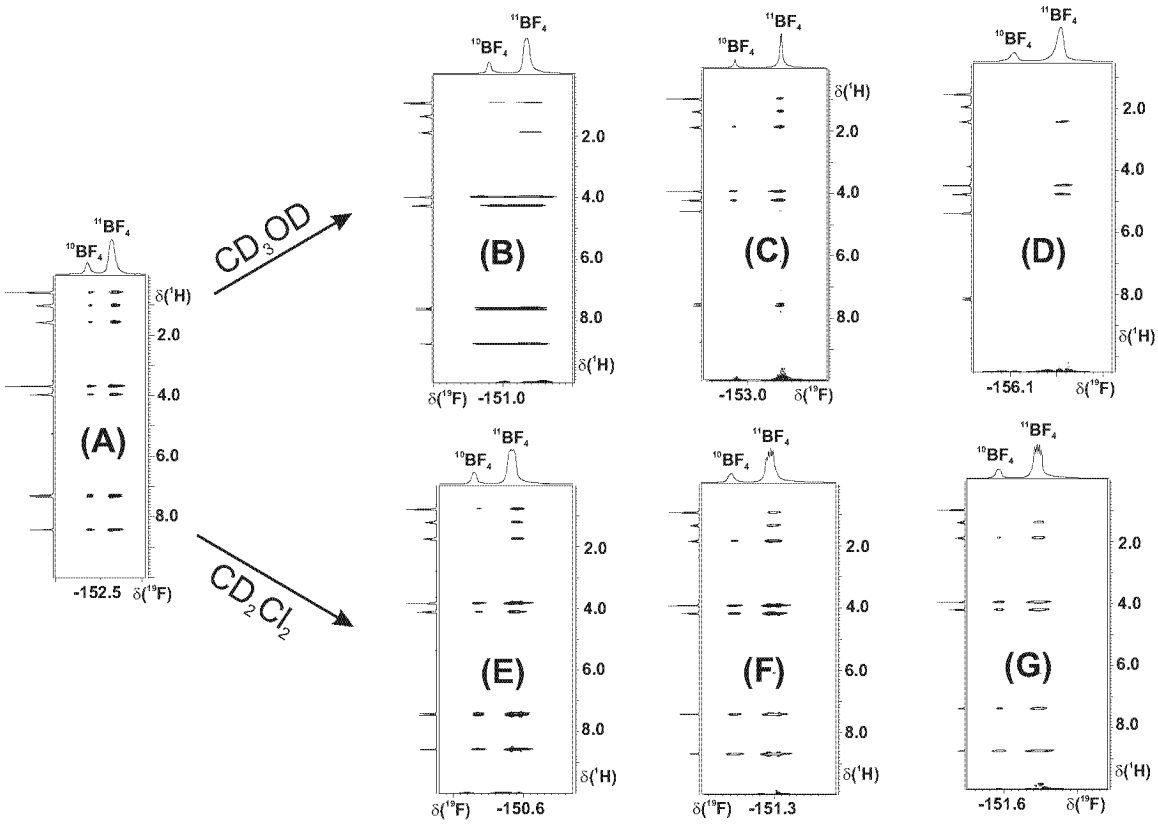

It has been suggested that hydrogen bonding forces are involved with this aggregation.[19] However, as the contacts to the N=CH-N proton are approximately equivalent to those arising from the two olefinic, N-methyl and N-methylene protons (see (B) and (E)), we discount selective hydrogen bonding as being the only major contributor and conclude that ionic interactions are primarily responsible for the observed HOESY effects. Accordingly one could tentatively assign a structural

A

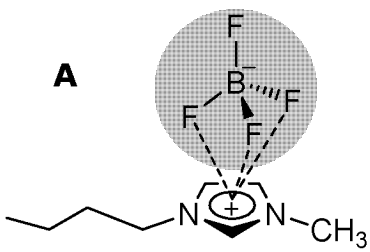

motif, **A** in which the BF_4^{-1} anion "hovers" above or below the imidazolium plane.

We note that, in deuterated methanol, the intensity of the imine proton (δ =8.4) slowly decreases due to slow exchange with the CD_3OD proton from the co-solvent and such exchange is well established.[20]

In Conclusion, the PGSE data clearly reveal that the ionic liquid exists as a relatively large, nanoparticle aggregate, which is substantially destroyed by the addition of co-solvent. The HOESY results reveal that, contrary to results from X-ray crystallography,[19] the anion does not occupy a specific position in this aggregate; however, in dichloromethane, where the PGSE data show almost complete ion pairing, there are strong, not very selective NOE contacts between the cation and anion. This eliminates hydrogen bonding as the primary source of the interaction between the cation and anion, as this would lead to selectivity in the HOESY contacts. These NMR data provide a new picture of the function of the co-solvent.

Two additional important implications may be derived from this study. First, the absence of selective contacts might find its expression in the often unexpectedly low melting points of ionic liquids. If on the one hand (diffuse) charge attraction is the dominant factor, but on the other hand, anions and cations cannot form a close packed structure due to their different size and shape, the crystallization energy will remain relatively low. Second, biphasic catalysis often suffers from slower reaction rates due to mass transfer limitations. As shown above, one needs only a relatively small amount of co-solvent to dramatically reduced aggregation within the ionic liquid. This might find its expression in significantly higher reaction rates.

References:

[1] P. Dotta, Kumar, P. G. A., Pregosin, P. S. and Albinati, A., *Unpublished results* **2004**.

[2] P. G. A. Kumar, P. S. Pregosin, J. M. Goicoechea and M. K. Whittlesey, *Organometallics* **2003**, *22*, 2956-2960.

[3] P. G. A. Kumar, P. S. Pregosin, M. Vallet, G. Bernardinelli, R. F. Jazzar, F. Viton and E. P. Kuendig, *Organometallics* **2004**, *23*, 5410-5418.

[4] P. S. Pregosin, E. Martinez-Viviente and P. G. A. Kumar, *Dalton Trans.* **2003**, 4007-4014.

[5] T. M. Schmid and G. Consiglio, *Tet. Asymm.* **2004**, *15*, 2205-2208.

[6] J. M. Goicoechea, M. F. Mahon, M. K. Whittlesey, P. G. A. Kumar, P. S. Pregosin, *Dalton Trans.* **2005**, *3*, 588-597.

[7] E. Martinez-Viviente and P. S. Pregosin, *Helv. Chim. Acta* **2003**, *86*, 2364-2378.

[8] M. Valentini, H. Ruegger and P. S. Pregosin, *Helv. Chim. Acta* **2001**, *84*, 2833-2853.

[9] T. J. Geldbach, F. Breher, V. Gramlich, P. G. A. Kumar and P. S. Pregosin, *Inorg. Chem.* **2004**, *43*, 1920-1928.

[10] J. Dupont, R. F. de Souza and P. A. Z. Suarez, *Chem. Rev.* **2002**, *102*, 3667-3691.

[11] P. J. Dyson, *Appl. Organomet. Chem.* **2002**, *16*, 495-500.

[12] M. Picquet, D. Poinsot, S. Stutzmann, I. Tkatchenko, I. Tommasi, P. Wasserscheid and J. Zimmermann, *Topics in Catalysis* **2004**, *29*, 139-143.

[13] D. Zhao, Z. Fei, T. J. Geldbach, R. Scopelliti and P. J. Dyson, *J. Am.Chem. Soc.* **2004**, *126*, 15876-15882.

[14] C. Daguenet and P. J. Dyson, *Organometallics* **2004**, *23*, 6080-6083.

[15] J.-F. Huang, P.-Y. Chen, I. W. Sun and S. P. Wang, *Spec. Lett.* **2001**, *34*, 591-603.

[16] A. Noda, K. Hayamizu and M. Watanabe, *J. Phys. Chem. B* **2001**, *105*, 4603-4610.

[17] I. Fernandez, E. Martinez-Viviente and P. S. Pregosin, *Inorg. Chem.* **2004**, *43*, 4555-4557.

[18] D. Zuccaccia, S. Sabatini, G. Bellachiom, G. Cardaci, E. Clot and A. Macchioni, *Inorg. Chem.* **2003**, *42*, 5465-5467.

[19] P. Koelle and R. Dronskowski, *Eur. J. Inorg. Chem.* **2004**, 2989.

[20] S. A. Katsyuba, P. J. Dyson, E. E. Vandyukova, A. V. Chernova and A. Vidis, *Helv. Chim. Acta* **2004**, *87*, 2556-2565.

Experimental Part

All the NMR experiments discussed in this thesis were measured on Avance Bruker instruments 250, 300, 400 and 500. The NMR spectrum for ^{31}P, ^{1}H, ^{13}C, ^{19}F, ^{195}Pt nuclei were acquired using a 5mm BBO probe. The ^{1}H, ^{19}F-HOESY measurements were carried out using a 5mm TXI four channel probe on the Avance 400MHz machine. The temperature for all the experiments was monitored using a built-in BVT unit in Bruker console.

The NMR parameters used were standard 1D/2D programs offered by Bruker X-WinNMR software.

The PGSE measurements, to calculate the self-diffusion coefficients (D) values, were performed on the Bruker Avance 300 and 400MHz spectrometer equipped with a microprocessor controlled gradient unit and a multinuclear BBI probehead with an actively shielded Z-gradient coil. The sequences used were the standard Stejskal-Tanner (see Chapter 1) via a Stimulated-Echo pulse sequence. The shape of the gradients was rectangular and its strength varied automatically in the course of the experiments. The calibration of the gradients on each spectrometer was carried out by means of a diffusion measurement of HDO in D_2O (D_{HDO}= 1.9 X $10^{-9}m^2s^{-1}$).

For the ^{1}H and ^{19}F measurements, δ (p_{16}) was set to 1.25-3.5ms and Δ was between 30 and 170ms (Standard parameters d_2 = 1ms, d_4 =15ms, d_3 =150ms, p_{16} =1.75ms for a 2mM sample). The gradient strength was usually incremented in steps of 3 or 4%, so that 15-25 points could be used for regression analysis. The number of scans per increment varied between 8 and 64, depending on the concentration, spectrometer and nucleus. For ^{19}F, T_1 was always determined before the measurement, and the recovery delay set to $5T_1$. For ^{1}H, this delay was always set to 5s. Typical total

experiment times were 0.5-2h for ^{1}H and 2-4h for ^{19}F measurements.

The ^{1}H, ^{19}F HOESY measurements were carried on a 400MHz Bruker Avance spectrometer equipped with a doubly tuned (^{1}H, ^{19}F) TXI probe. A mixing time of 600ms was used. The T_1 values for ^{19}F were calculated using Bruker Xwin-NMR software and d_1 was set to $5T_1$ accordingly. The concentration of the sample used was 10mM; the number of scans 64 and the number of increments in the F1 dimension 512.

Curriculum Vitae

Anil Kumar Payyadi Govardhan

I was born in a small village near Chickmagalur (India) on 26th of February 1977. I had my primary, secondary and college education during the period 1982-1994.

7/94 - 4/97	B.Sc degree in Physics, Chemistry and Mathematics Bangalore University, India
7/97 – 8/99	M.Sc degree in Inorganic Chemistry Bangalore University, India
8/99 – 12/00	Research Assistant in B. M. S. College of Engineering AICTE Project, Bangalore, India
01/01 – 12/01	NMR Project Assistant in S.I.F department Indian Institute of Science, Bangalore, India
01/02 – 03/05	Ph. D thesis at the ETH Zurich under the supervision of Professor Paul S. Pregosin on applications of NMR in homogeneous catalysis